Naval Research Reviews

Office of Naval Research
Three / 1989
Vol XLI

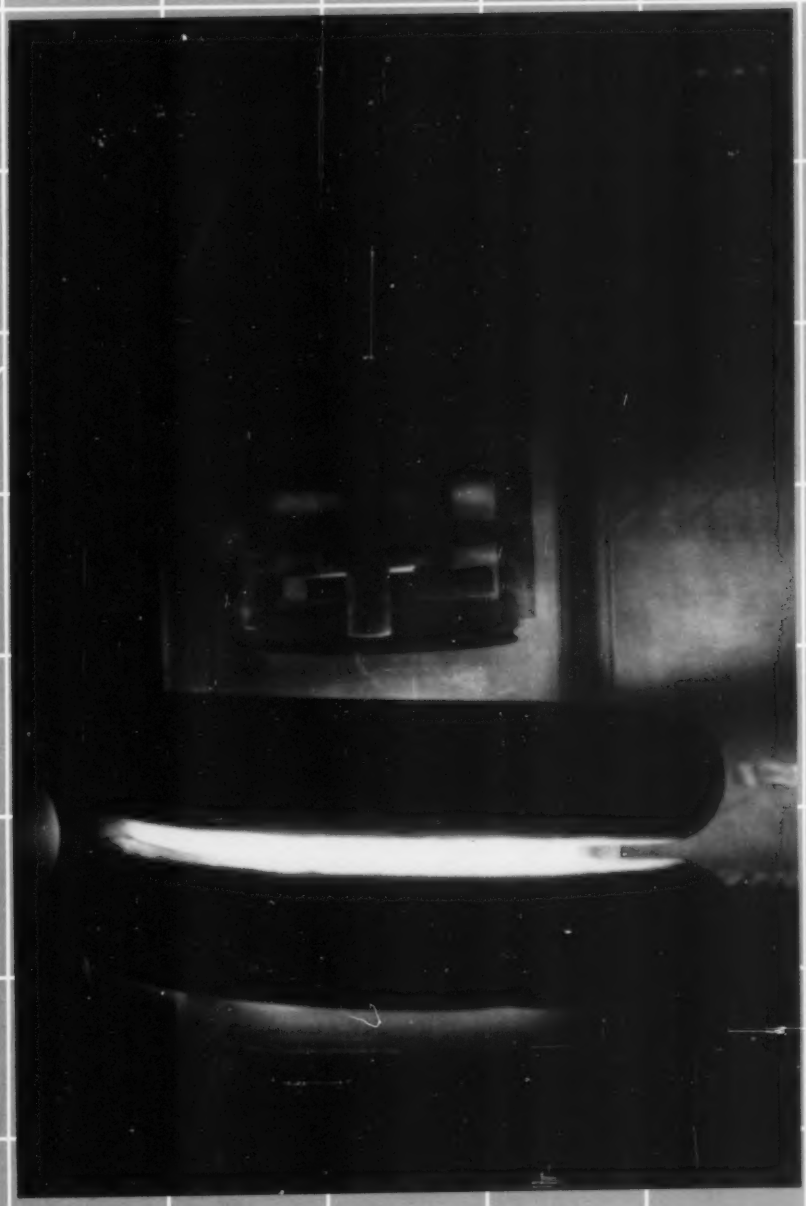

Parallel Computers

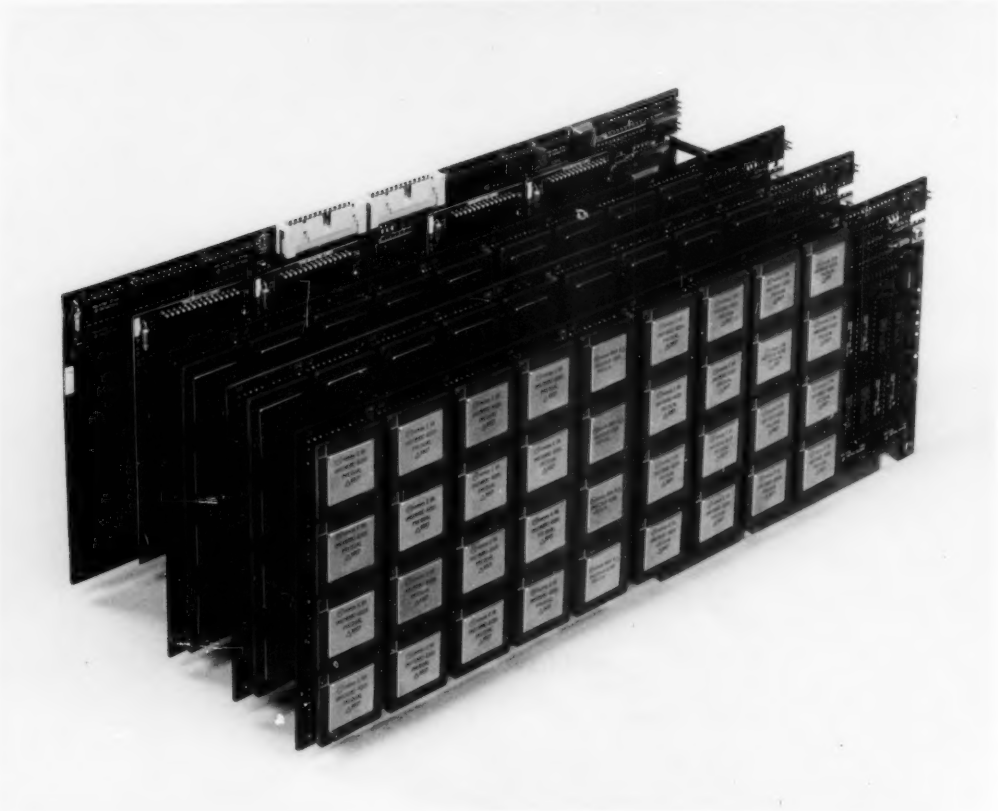

Scientists at the Naval Ocean Systems Center are exploring the design of massively parallel computers for the real-time processing of sensor data. They designed an IBM-AT board containing 32 transputers (a British-made high-performance RISC CPU specifically designed for parallelism). A unique feature of this approach is that the interconnect topology between all of these processors is variable under software control via four crossbar-switch chips. Therefore, algorithms can be easily run on different architectures (i.e., ring, mesh, line, hypercube, tree) to explore efficiency issues. The four-board set in the photograph contains a hundred transputers, each one capable of over 10 million instructions per second and 1.5 million floating-point operations per second. This combination of high performance, reconfigurration flexibility, and low cost is well suited to challenging problems in image processing, multi-target tracking, data fusion, radar processing, and underwater acoustic surveillance.

Naval Research Reviews

Office of Naval Research
Three / 1989
Vol XLI

Articles

3
Superconducting IR Focal Plane Arrays
by Fred W. Quelle, Jr.

9
Research In Advanced Electronic System Reliabilty
by C. Lau, C. Hu, E. J. McCluskey

21
Advanced Composites For Strategic Defense Initiative Systems
S. G. Fishman, J. A. Cornie, K. M. Prewo, R. K. Viswanadham, J. S. Epstein

36
Imploding Krypton Gas Puff Plasma As A Potential Source For X-Ray Lasers
J. Davis

46
Artifact Diamond Its Allure and Significance
Max N. Yoder

50
The Oxygem Heat Engine Based On Solid Electrolytes
A. V. Joshi, N. Weber, J. Nachlas

Departments

20
Profiles in Science

58
Research Notes

CHIEF OF NAVAL RESEARCH
RADM John R. Wilson, Jr., USN

DIRECTOR
Dr. Fred Saalfeld

DIRECTOR OF PUBLIC AFFAIRS
CDR Thomas E. Connor

CHIEF WRITER/EDITOR
William J. Lescure

SCIENTIFIC EDITORS
Dr. Robert J. Nowak
Dr. J. Dale Bultman
Dr. Albert W. Green
Mr. Steven W. Payne

MANAGING EDITOR
Marc J. Whetstone

ART DIRECTION
Typography and Design
Desktop Printer, Arnold, MD

About the Cover

Plasma-assisted chemical vapor deposition is a technique widely used in the growth of diamond and related refractory semiconductor films. To prevent particulate contamination, the growing surface is suspended upside down with film growth accruing on the lower surface. The upside down approach is also useful in that unwanted convection currents and their resulting turbulence are reduced as the byproducts of the film growth typically contain simpler (lighter) molecules which exit the growth reactor above the growing surface and do not intermix with the upward-flowing feed gases. The plasma reactor pictured is located at the Research Triangle Institute.

Naval Research Reviews publishes articles about research conducted by the laboratories and contractors of the Office of Naval Research and describes important naval experimental activities. Manuscripts submitted for publication, correspondence concerning prospective articles, and changes of address, should be directed to Code OPARI, Office of Naval Research, Arlington, VA 22217-5000. Requests for subscriptions should be directed to the Superintendent of Documents, U.S. Government Printing Office, Washington, DC 20403. *Naval Research Reviews* is published from appropriated funds by authority of the Office of Naval Research in accordance with Navy Publications and Printing Regulations. NAVSO P-35.

Introductory Remarks by Dr. Duston and Dr. Saalfeld

Dr. Dwight Duston

Director, Innovative Science and Technology
Office of the Strategic Defense Initiative Organization

Five years ago, the Strategic Defense Initiative Organization was established to spearhead one of the most ambitious research and development programs of the twentieth century...the search for defenses against the threat of ballistic missiles. The Innovative Science and Technology (IST) Office within SDIO was established soon after to fund novel approaches and explore new concepts in strategic defense. Today, with a program that sponsors over 40 basic research projects in a wide variety of disciplines and technologies and with an annual budget exceeding $150 M, the IST Program supports over 600 principal investigators at universities, small businesses, national and government laboratories, and in large industry.

The Office of Naval Research has played a key role in the growth and continued success of the IST Program. Through its talented corps of scientific officers, over half of IST's 40 projects are technically managed by ONR. The Science & Technology Agents, or STA's, have the responsibility for receiving and reviewing proposals, initiating procurement actions, managing individual research projects on a day-to-day basis, and providing technical and programmatic information on a regular basis to the IST staff members.

While this may sound very rigorous and procedural, the relationship between IST and ONR has proven to be anything but. Both organizations have strived to form a strongly synergistic interaction. The technical opinion of the ONR STA counts heavily in the IST decision-making process. The relationship is more collegial than managerial. This unique environment that exists between agencies has shown to be a profitable one for both SDIO and the Navy. Programs leverage off of each other, stronger interaction and collaboration occurs between both groups of researchers, and, in many cases, Navy and SDI programs have very similar goals and requirements. This will be evident as you read through some of the articles contained herein.

The SDIO Innovative Science and Technology Office is very proud of its association with the Office of Naval Research, a thriving cooperative effort between the Department of Defense's oldest and youngest basics research organizations! As the first five years of this cooperation come to a close, IST looks forward to a future of successful and rewarding interaction between us.

Dr. Fred Saalfeld

Director, Office of Naval Research
Office of the Chief of Naval Research

When the Innovative Science and Technology (IST) Office of the Strategic Defense Initiative Organization was established five years ago, to pursue the basic research programs of the organization, the Office of Naval Research (ONR) was there to lend a hand. Today ONR and IST are partners in basic research, benefiting IST's mission to develop a non-nuclear defense against ballistic missiles, and helping ONR's mission to prepare for the Navy of the future.

ONR is the oldest federal agency funding basic scientific research. For 43 years it has attracted distinguished scientists, primarily from the universities, to participate in research programs and provide the basis for our future technology. Seventeen of ONR's existing and long established programs were vital to IST's major research interests in: high speed computing; sensing, discrimination and signal processing; space power and power conditioning; directed and kinetic energy concepts; materials and structures; and propulsion and propellants. For these programs, IST and ONR have joined forces.

In this issue of Naval Research Reviews, we offer articles describing six ONR and IST's cooperative programs. Fred Quelle in *"Superconducting IR Focal Plane Arrays"* discusses some major problems confronting the development of semiconducting IR focal plane detectors, and how new technology based on superconductivity may overcome them. Clifford Lau and colleagues in *"Research in Advanced Electronic System Reliability"* describes research to develop a scientific understanding of the factors impacting the lifetime reliability of microelectronic systems, including Very Large Scale Integration (VLSI) technology and submicron devices. Steven Fishman and co-authors in *"Advanced Composites for Strategic Defense Initiative Systems"* couples micromechanics, materials science, chemistry, and physics to explore the influence of atomic scale processes of composite materials on their bulk macroscopic behavior. Jack Davis in *"Imploding Krypton Gas Puff Plasmas as Potential Source for X-Ray Lasers"* considers using pulsed power generators to drive a configuration of coaxially cylindrically symmetric krypton gas puff plasmas to conditions conductive to achieving gain in several lasing transitions of neonlike krypton. Max Yoder in *"Artifact Diamond: Its Allure and Significance"* discusses how alternative materials, such as tetrahedrally bonded carbon films for microelectronic components, can enhance system performance in a high-stress space environment. A. Joshe describes in *"The Oxygen Heat Engine Based on Solid Electrolytes"* a promising thermoelectric energy conversion concept which converts heat to electricity directly at high efficiency.

ONR often gets research started in critical fields without having to carry the total support burden. The joint and/or comanaged programs with IST, described here, are examples of such management. ONR is proud of its productive relationship with SDIO-IST. We look forward to continuing cooperative programs providing the finest scientific research for our national defense and the advancement of human knowledge.

Superconducting IR Focal Plane Arrays

Fred W. Quelle, Jr.
Office of Naval Research

Abstract

This article discusses a number of the major problems confronting the development of present day semiconducting IR focal plane detectors for large array space based applications, shows that an entirely new detector technology based on superconductivity may circumvent many of these difficulties, provides detailed data on the characteristics of these devices and outlines the development program underway to exploit this new technology.

Introduction

Present Semiconductor Focal Plane Arrays

Present infrared focal plane array technology involves the assembly of elements consisting of a high impedance semiconducting detector followed by a semiconductor amplifier, into a two dimensional detector array whose outputs are muxed together to produce an analog signal. This signal corresponds to the sequential interrogation of the infrared energy falling on each of the individual detector elements. Usually the detectors are fabricated in a two dimensional array on one substrate and the amplifier and muxing circuitry in a corresponding two dimensional array on a second substrate. Each of the detector and amplifier elements on these two arrays are then connected together by means of strategically placed indium bump bonds sandwiched between the two substrates.

Even with the benefit of today's modern large scale integrated circuit technology, it is a nontrivial task to fabricate large arrays of semiconducting elements on a single substrate having uniform electrical characteristics with no or at worst only a few bad elements. The highly precise impurity compensation and doping of the semiconductor substrate that is re-

quired in order to construct these devices makes it difficult to achieve high yields and further dictates constraints on minimum component size. For this reason it is difficult to construct the required semiconductor amplifier and readout circuitry in much less than a 100 micron square. Thus for focal plane arrays that are appreciably larger than 100x100 elements, it is necessary to assemble a mosaic of detector arrays.

System Implications Of Present Devices

In addition to the above fabrication problems, the semiconductor electronics associated with the focal plane array dissipates a substantial amount of power. The Strategic Defense Initiative (SDI) has used a figures of ~10 microwatts per pixel in designing their systems although currently used devices have significantly greater power dissipations. Even using the SDI figure of 10 microwatts per pixel says that a 1000x1000 array will have a heat dissipation from its electronics of 10 watts. Since noise considerations require thermal imaging detectors to be cooled to between 40 and 100° Kelvin (depending on the application), this power dissipation produces a serious refrigeration problem. To make matters worse, the large number of data lines required to bring the analog signal information from the focal planes to the high temperature processing electronics, conduct significant amounts of thermal energy down to the focal plane. The drive electronics associated with these lines produce additional heat dissipation. All of this energy must also be removed by the refrigerator. Figure 1 gives SDI projections of the weight and electrical power requirements for several types of refrigeration systems as a function of refrigeration power. From this, the serious systems implications resulting from the use of semiconducting IR focal plane array readout electronics should be apparent.

Potential Of Superconducting Devices

Since noise considerations require thermal imaging IR focal plane arrays to be cooled to relatively low temperatures, the possibility of replacing the semiconducting amplifier circuitry with essentially dissipationless superconducting electronics is appealing. Such an approach could reduce the power dissipation of the electronics by more than two orders of magnitude. Even if the lower temperatures necessary for the superconducting electronics were to increase the weight and power requirements of the refrigeration equipment needed to provide a given amount of cooling power by as much as an order of magnitude, we would still be an order of magnitude ahead of the game because of the much lower cooling power requirement. Furthermore, if on chip low dissipation electronics were to be available, it would be possible to do A/D conversion and more processing on chip and come out of the low temperature focal plane array with a single digital output

Figure 1

SDI projections of the weight and electrical power requirements for several types of refrigeration systems as a function of refrigeration power.

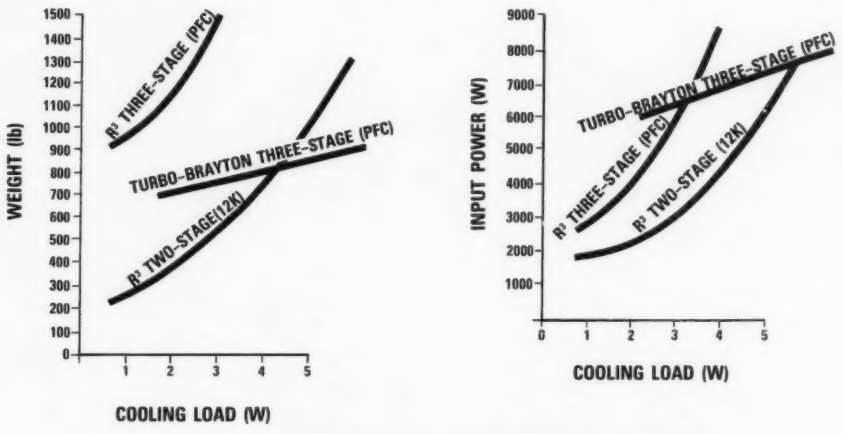

- ASSUME ONLY LAST STAGE LOAD IS VARIED
- OPERATION OF TURBO-BRAYTON AT >2W IS IMPRACTICAL DUE TO INEFFICIENCIES

Figure 2

A band gap situated symmetrically about the Fermi level.

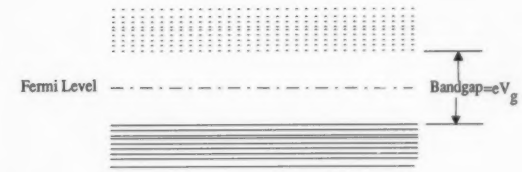

stream sent up an optical fiber. This would avoid much of the thermal conduction heating produced by large numbers of analog signal lines.

Superconducting SQUID amplifiers are inherently extremely low noise devices. They have been shown to have noise levels as much as two orders of magnitude below that of comparable semiconducting devices. It remains to be proven whether practical superconducting electronic circuits will exhibit this much of an improvement over the present semiconducting electronics used in focal plane arrays; however, it is reasonable to assume that a significant improvement in noise characteristics will be achieved by employing superconducting electronics.

Because of the inherently simple nature of monolithic superconducting electronics (wires and insulators placed on a glass or quartz substrate as opposed to carefully doped semiconductors) very high production yields can be achieved. This technology can readily be scaled to dimensions of many inches and is intrinsically capable of producing large uniform arrays having few if any bad elements. In addition, the smaller size of superconducting electronic circuits (few microns as opposed to many 10's of microns for semiconductor circuits), permits much more sophisticated processing to be carried out in a given area on the focal plane.

With all of these advantages, there is still a serious problem. Superconducting electronics are basically low impedance devices that cannot be directly driven by high impedance semiconductor detectors unless impedance transformation circuitry is used. Passive impedance transformation would require a transformer with a high turnsratio and thus is not very practical for this application. Alternatively, the use of a semiconductor transimpedance amplifier to match the impedance would sacrifice most of the gain which we are attempting to achieve with the superconducting circuitry. What is needed is a low impedance optical detector whose sensitivity is at least competitive with present semiconducting detectors. Since we have already justified committing ourselves to superconducting cryogenic temperatures to support superconducting electronics, it is reasonable to consider whether a practical superconducting optical detector can be developed.

Superconducting Optical Detectors

At the time the search for a superconducting optical detector was begun, no one had previously attempted to make such a detector. High temperature superconductors had not been invented. Furthermore, the high optical reflectivity characteristic of metallic superconductors suggested that even if we were able to produce a reasonably sensitive optical detector, it's quantum efficiency would be low due to the high reflectivity. Most workers in the superconductivity field were extremely pessimistic regarding the practicality of developing such a detector.

Possible Superconducting Optical Detectors

The resistivity of a simple superconductor below its transition temperature is zero and remains there until the temperature is raised up to the transition temperature at which time its resistance rapidly rises to the normal resistance of the material. In principal one could attempt to bolometerically use this rapid change in resistance to detect optical radiation. For metallic superconductors this transition occurs within 1 or 2 millidegrees Kelvin so while dR/dT may be phenomenally large, maintaining a large array of detectors in this few millidegree window is impractical. Some of the new high temperature ceramic superconductors have a broader transition region; however, since their transition temperature is well above the transition temperature of the metallic superconductors that currently have to be used for the electronics, they would be incompatible with our present superconducting electronics. Thus using the superconducting to normal transition as a conventional bolometric detector does not appear to be a viable candidate for use with presently available supercon-

Figure 3

Two superconductors which are separated by a thin insulating layer.

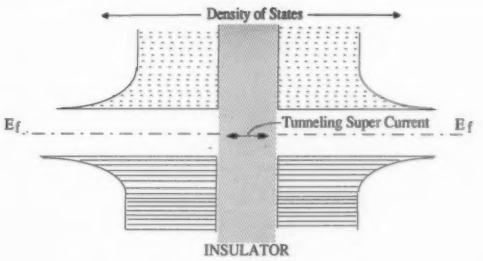

ducting electronic circuits. Some time in the future, if we should be successful in fabricating practical superconducting electronic circuits from high temperature superconductor materials, this issue may have to be reevaluated.

The Physics Of Josephson Optical Detectors

Superconductors have characteristics which to some extent are analogous to a semiconductors. The supercurrent in a superconductor is due to the correlated motion of Cooper pairs located at the Fermi level in the superconductor. This correlated behavior also gives rise to a forbidden region of energy states (ie. a band gap) situated symmetrically about the Fermi level as illustrated in Figure 2. As in the case of a semiconductor, above and below this band gap there is a very high density of states. In typical metallic superconductors this bandgap is of the order of a few milli-electron volts as opposed to bandgaps in semiconductors which typically are of the order of an electron volt.

Josephenson devices consists of two superconductors which are separated by a thin insulating layer as shown in Figure 3. When no potential is placed across the Josephenson device, the two sets of supercurrent states located at the Fermi level in each of the two respective superconductors are just opposite one another and tunneling through the thin insulating layer gives rise to a substantial supercurrent through the device. When a bias potential is placed across the Josephenson device, the tunneling current ceases until the bias is sufficient to bring one of the filled bands to an energy level opposite the large number of empty states in the other electrode. (See Figure 4.) Tunneling of carriers through the thin insulating layer then begins again giving rise to the current voltage characteristics illustrated in Figure 5. The bias potential across the Josephenson junction at which the sharp increase in current through the junction occurs is a very precise measure of the superconducting band gap. Thus a Josephenson device can be used to very accurately determine the superconducting band gap.

Figure 4

When a bias potential is placed across the Josephson device, the tunneling current ceases until the bais is sufficient to bring one of the filled bands to an energy level opposite the large number of empty states in the other electrodes.

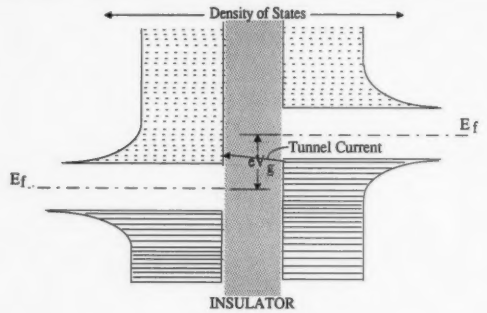

Figure 5

Tunneling of carriers through the thin insulating layer then begins again giving rise to the current voltage characteristics illustrated here.

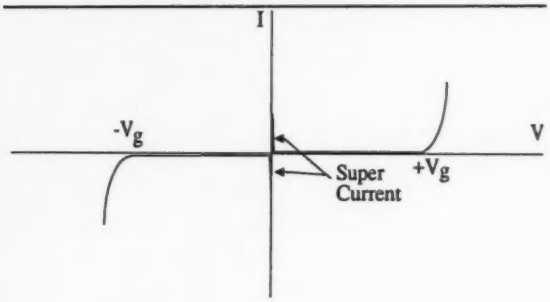

The width of the superconducting band gap in a superconductor below its transition temperature is related to the density of Cooper pairs in the superconductor both of which go to zero when the temperature of the superconductor is raised to the transition temperature. This temperature dependance of the bandgap is illustrated in Figure 6. Thus an optically induced thermal change in the temperature of a superconductor will result in a change of its superconducting band gap. Cooper pairs can also be broken through direct interactions with incident photons or electrons giving rise to a second mechanism known as pair breaking for modifying the bank gap of a Josephenson junction. both of these phenomenon could give rise to a change in the superconducting bandgap and thus an optical sensitivity in Josephenson devices. Previous experience with superconductors, which in retrospect were thermally well coupled to the low temperature substrate or bath, lead us to focus primarily on the pair breaking phenomena in our attempts to develop an optical sensitive superconducting device.

Practical Detector Embodiments

In discussing possibilities for designing a superconducting optical detector with various members of the superconducting community in 1984-5, Arnold Silver of TRW was the first to come up with a potentially viable solution. He felt that the most serious problem would be the high reflectivity of the

superconductor. He therefore proposed to absorb the infrared photons in a semiconductor substrate material such as GaAs. On the back side of the substrate he would place a Josephenson Junction. The absorbed photon would create an electron hole pair in the semiconductor and by means of a potential placed across the semiconductor he proposed to accelerate the electron and propel it into the Josephenson Junction. (See Figure 7.) Silver felt that the electron would have an energy of the order of 1000 times the bandgap energy and thus was bound to significantly modify the properties of the Josephenson Junction but there was no basis on which to calculate the efficiency of such a process. The only thing one could do was to try it and see whether and how well it worked. TRW was given a small contract and began work in March of 1985. Unfortunately, problems of fabricating Josephenson devices on GaAs substrates while maintaining appropriate electrical properties in the GaAs proved to be a more substantial task than originally envisioned. After overcoming numerous technical problems data now indicates that current gains (change in Josephenson current per electron injected from the semiconductor) in excess of 140 have been achieved. This current gain is in principal noise free in the same way that the current gain in a photomultiplier tube is noise free; however, detailed measurements to verify this have yet to be completed. This injected current can be gaited so that it is dumped into the Josephenson junction just at the time the circuit is being read out. Such an approach could considerably enhance sensitivity and signal to noise ratios in large focal plane arrays.

In the mean time Sadig Faris of HYPRES was aware of Japanese work on BaPbBi which appeared to exhibit a relatively good photo response. BaPbBi did not appear to offer exciting possibilities for fabricating large arrays of uniform optical detectors, so Faris proposed to see whether he could achieve similar results in Nb and NbN. He felt that the high optical reflectivity problem could be overcome by anti-reflective coatings on the superconductor. He was given a small contract in August 1985 to begin exploring these possibilities. The HYPRES work, which only involved laying down Josephenson Junctions on SiO_2 substrates, proceeded more rapidly than the TRW program and within a year they were measuring responsivities (R) of 3-8000 volts/watt for 10x10 micron junctions. Spectral response has been observed to be reasonably uniform from the visible out to 20 microns.

Characteristics of Present Devices

After demonstrating reasonable responsivity, the next step was to measure the noise equivalent power (NEP=Vn/R). For this, semiconductor amplifiers having input noise voltages (Vn) of $3\eta V/\sqrt{Hz}$ have been initially used since they did not require the development of a squid amplifier. Amplifier noise in all cases dominated the output even when a 200 element series array of superconducting Josephenson junctions was

Figure 6

Temperature dependence of the bandgap.

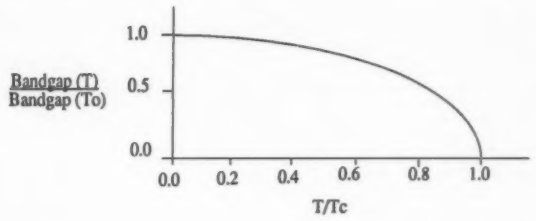

used in an attempt to overcome the amplifier noise. Nevertheless, NEP's=$3x10^{-13}W/\sqrt{Hz}$ have been obtained for 10x10 micron junctions. For a 1x1 micron detectors, which are quite practical to fabricate, the change in bandgap with intensity will be the same as for the larger junction but the power intercepted by the detector will be two orders of magnitude lower. Thus it will have an NEP=$3x10^{-15}W/\sqrt{Hz}$! If pixels larger than 1x1 micron are required, a series of 1x1 micron detectors would be used to fill the pixel area thereby boosting the output signal by N the number of elements in the series array. If when superconducting amplifiers are employed, the dominant noise turns out not to be amplifier front end noise but rather detector noise, this series arrangement would cause the detector noise to go up by only $\sqrt{N}$.

It was initially believed that pair breaking was the source of the optically induced change in the superconducting bandgap of measured by the Josephenson Junctions. For the TRW devices in which the Josephenson Junction is placed on a high thermal conductivity GaAs substrate this is still the correct interpretation. The HYPRES devices have usually been fabricated on lower thermal conductivity glass substrates. In this case it has recently become apparent that the change in bandgap due to the optically induced heating of the Josephenson junction appears to be an order of magnitude greater than the contribution due to pair breaking. When the HYPRES devices are placed on Si substrates or immersed in liquid helium this enhanced thermal effect disappears and we are left with only the response due to pair breaking. The thermal time constant for these devices on glass are in the submillisecond range and thus provide reasonable response times for a focal plane array. There are obviously many parameters that need to be explored in order to optimally exploit this phenomena. Since these devices function thermally, the optical reflectivity problem can now be solved by coating them with an appropriate absorbing material. A properly designed black coating should yield a factor of 2 or more increase in the above NEP's.

Figure 7

Accelerating the electron and propelling it into the Josephson Junction.

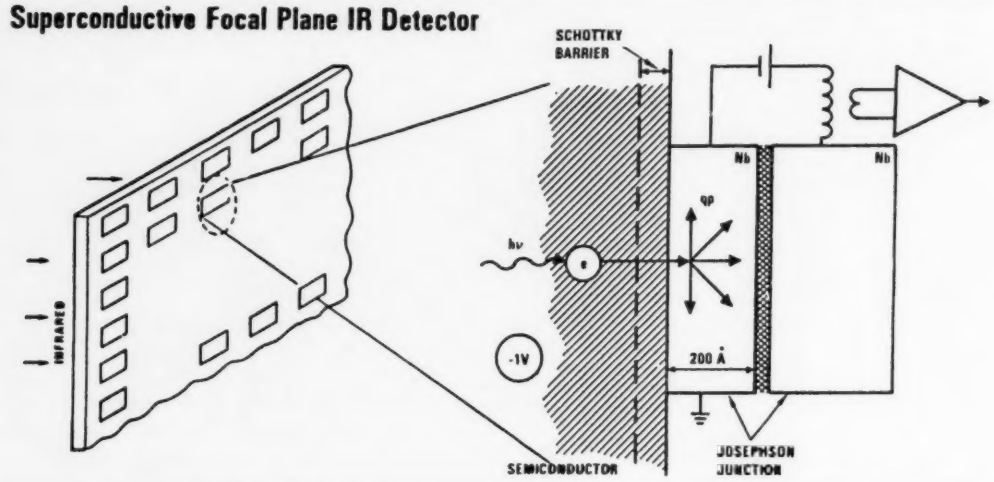

Further Development and Characterization Of Detectors

The major thrust of these programs during the coming year will be to install low noise superconducting amplifiers and begin to explore the fundamental noise limits with these devices. To date there is little information on which to base speculations of what those limiting noise mechanisms will be or the limiting sensitivity that they will provide. Based on the presently available data obtained using semiconductor amplifiers and knowledge of the improvements in noise characteristics that have generally been associated with superconducting circuits, it is anticipated that significant improvements in sensitivity will be forthcoming.

Superconducting Focal Plane Arrays

Superconducting Version Of Present Focal Plane Arrays

Next year, small arrays, 4x4 and 8x8, will be fabricated and tested. After that the next step will be to devise appropriate integrated superconducting amplifying, muxing and readout electronics and to devise ways to monolithically integrate all of this circuitry on a single substrate. Hopefully, this can be accomplished with circuitry having a heat dissipation of the order of .1 microwatt per pixel. It is not unreasonable to contemplate fabrication of large superconducting focal plane arrays having multi-inch dimensions using presently available superconducting fabrication techniques. The implications of this to IR focal plane array technology could be revolutionary.

Development Of Additional Onchip Processing

A major payoff for incorporating low heat dissipation superconducting electronics into focal plane arrays is that heat generation will no longer be the primary limiting factor on how much processing can be done on chip. A/D conversion is a task which can readily be accomplished with superconducting circuitry. Furthermore, digital processing associated with such things as target motion, etc. can be handled on chip. All of this digital output can be muxed into a single electrooptic modulator modulating a fiberoptic light beam to communicate with the outside world. It is anticipated that all of this can be accomplishable at a small fraction of the power dissipation of present day semiconducting focal plane arrays.

Biography

Dr. Fred Quelle is a scientific officer for the Applied Physics Field Division of the Office of Naval Research, Boston. His publications and research have been primarily in the fields of lasers, electro-optics, and detectors.

Research In Advanced Electronic System Reliability

C. Lau, Office Of Naval Research
C. Hu, University Of California, Berkeley
E. J. McCluskey, Stanford University

Abstract

Reliability of microelectronic chips and systems is becoming an increasingly important factor in the quality of electronic systems as the scale of integration continues to increase while device geometry continues to shrink to smaller dimensions. In the case of Strategic Defense Initiative (SDI) systems, designed-in reliability is imperative because of the criticality of the electronic systems and the impossibility of maintenance and repair in space. Microelectronic systems for sensors, signal processors, and supercomputers must be able to operate without human intervention for an extended period of time in a very harsh space radiation environment. Four specific areas of research in the reliability/survivability of very large scale integration (VLSI) circuits have been identified as critical to the success of future microelectronic systems for SDI application. These are fault tolerant systems and architectures, thin dielectric insulator films, contact/interconnect metal electromigration, and radiation hardening. Research has increased our understanding of the physics of dielectric breakdowns and wearouts and the mechanism of charge trapping in thin gate oxides and the understanding of the electromigration process in thin-film metals. Research in system reliability will continue to develop multiple fault models and methods for self-testing, error detection, and error control. Because reliability is a system-level issue, hierarchical methodology must be developed that spans reliability research in solid state materials, devices, circuits, macrocells, chips, packaging, boards, subsystems, and systems.

Introduction

Although not often explicitly stated, reliability has always been a major concern of electronic system designers. Reliability was very important in the days of vacuum tubes. Because of the deterioration of the heating filament and the electron emitting cathode, a vacuum tube typically changed its characteristics such as transconductance over a period of time, and lasted only for a few years. In fact, the very first digital computer built with vacuum tubes and mechanical relays did not become operational until the tubes could function reliably. Thus circuit designers had to design systems with a large set of varying devices, and had to consider reliability in the design.

Since the invention of the transistor, the reliability picture began to change. The transistor, once perfected, proved to be extremely reliable. Since there was no heating element or cathode, the transistor could virtually last forever, except for the gradual wearout of the solid state material. Thus systems built with transistors and solid state devices could last for over a decade without deterioration in performance.

The integrated circuit (IC) was made by putting many transistors monolithicly on the same substrate. For small scale integration circuits (SSI), with hundreds of devices on a chip, the reliability was not too different from discrete transistors except for the fact that there was greater power dissipation and consequently greater temperature rise on the chip. In other words, SSI integrated circuits, once tested to be working properly, could last for years without failure. Meanwhile the

scale of integration continued to increase and the device geometry shrank to ever smaller dimensions. Today it is not uncommon to see very large scale integration (VLSI) circuits containing a million devices at one micron geometry. There is every reason to believe that this trend to increase the scale of integration will continue.

As device geometry shrinks to submicron size and the scale of integration goes beyond VLSI, the reliability picture again begins to change. The once reliable discrete transistor is now so small that any slight change in the characteristic of the silicon material would cause it to fail. Furthermore, in digital circuits with hundreds of thousands of gates, the failure of a single device would cause the entire VLSI chip to fail. Thus as microelectronics become more and more complex, there are serious concerns about the reliability of the VLSI chips and systems. There are several factors which contribute to these concerns.

Scaling

All insulating materials breakdown if given a sufficiently high electric field. So it is true with the gate dielectric in Complementary Metal Oxide Semiconductor (CMOS) technology. All gate dielectrics in today's CMOS VLSI circuits are silicon oxides (SiO_2), which break down at about 10 MV/cm in a few seconds. Breakdown occurs at a lower electric field if the field is applied for a longer period of time and if latent defects are present. As the device geometry shrinks to below a micron, the thickness of the gate dielectric also shrinks to about a hundred angstroms. If the supply voltage remains at 5 volts, the electric field at the gate is 5 MV/cm, which is near or above the practical breakdown strength of SiO_2. The electric field along the electron path in the silicon near the drain also becomes quite high. This high field can create "hot electrons", which can damage the Si/SiO_2 interface and cause the transistor performance to degrade with time. These are the primary reasons for the push to lower the supply voltage to about 3 volts for submicron circuits.

Complexity

As the scale of integration continues to increase, more and more devices are being put on a chip. One reason is that it is more efficient utilization of silicon to put related circuits on the same chip. Another reason is that circuits on the same chip can run at a higher clock speed than off-chip circuits because of shorter interconnect distances with lower resistances and capacitances. Off-chip driver circuits are typically large and consume more power, and are to be avoided. Unfortunately in digital circuits without any designed-in fault tolerance, if one of the devices fails the entire chip is useless. With that many devices on a chip, the possibility that one of them will fail is not minuscule.

Speed

There is a continuing demand for faster and faster chips. For civilian application, the clock speed on many microprocessor chips have been pushed from a few megahertz (MHz) to as high as 20 MHz in the last few years. The clock speed on the DoD Very High Speed Integrated Circuits (VHSIC) phase 1 program is 25 MHz for 1.25 micron technology. For the VHSIC phase 2 program, the on-chip clock is to be 100 MHz for the 0.5 micron technology. But as the clock frequency increases, there is greater susceptibility to coupling between wires on the chip. At high frequencies, the short wires would behave like antennas and radiate out electromagnetic (EM) energy. This EM radiation gets picked up by the wires in its vicinity. This coupling contributes to greater noise on the chip. At the same time as the devices become smaller, there is a need for greater precision in the threshold voltages. Thus the noise margin, or the ability of the device to withstand noisy signal without falsely switching states, is lowered and causes the chip to be susceptible to errors.

Process Variations

As the devices become smaller and the chips get bigger, the fabrication and manufacturing process is also getting more complex. Increasingly exotic devices are invented in that endless pursuit for performance and reliability. For example, lightly doped drain (LDD) devices are widely used to alleviate the concentration of electric fields near the drain areas of Field Effect Transistors (FET), and vertical trench isolation techniques have been tried to prevent the coupling of closely located devices. Multilevel metalizations are also used to more efficiently utilize the silicon areas on the chip and to reduce the overall size of the chip. But multilevel metals require more masking layers and thus further increase process complexity. As the devices are so small, the process parameters must be strictly controlled to maintain the uniformity of the fabricated devices. Any deviations from the designed parameters and geometry can result in a bad chip. For example for 1 micron geometry, if the fabricated MOSFET channel length is 0.2 micron longer than the design value, the circuit will probably fail the speed specification. On the other hand, if the channel length is 0.2 micron shorter, the circuit may fail after a short service time due to hot carrier induced degradation. Furthermore, when the FET channel length is below a micron, the smallest particle can contaminate the process and cause the fabricated device to fail. Thus the control of purity of the chemicals, gases, water, and clean-room air is becoming increasingly critical to the yield and reliability of the fabricated VLSI chips.

Material Defects

All bulk materials contain defects regardless of the great care that is put into its preparation. As devices get smaller, the smallest defect in the silicon material or metalization can cause malfunction in the devices and circuits. At the same time, as the VLSI chips become bigger, it becomes critical to reduce the number of defects per area since the yield is exponentially lowered as a function of the chip size for a given defect density. However, in spite of significant research efforts, it is extremely difficult to grow silicon crystals without any defects. The best silicon substrates still may contain as many as five defects per centimeter square. This would result in very low yields (<1%) for extremely large chips (1 cm^2). Furthermore, even if the chip is tested to have functioned properly initially, latent defects may cause reliability problems later on in the chip's lifetime.

SDI/IST Program

Reliability is important to military electronic systems. The Navy ships and aircrafts must be able to sense the threat environment, develop defense strategies, and utilize its weapons to negate that threat. The weapon systems and its electronics must work when it is needed in the battle environment. There is no second chance. Compounding the reliability problem is that the military environment is much more severe in terms of temperature ranges, shock and vibration, humidity, and most importantly radiation. In fact the radiation requirements, such as total dose, dose rate, and single event upsets are getting harder and harder to meet.

For strategic defense systems, the reliability of VLSI chips and systems is particularly important. The importance of reliability of electronic systems to the Strategic Defense Initiative (SDI) is outlined in the Fletcher reports.[1,2] VLSI chips and systems are undoubtedly the underlying technology that makes large-scale strategic defense system possible, including sensors, signal processors, and supercomputers for battle management. Because of the criticality of SDI systems, the electronics must operate continuously and particularly at time of high demand. The lifetime of space-based systems must be ten to twenty or more years. Unfortunately, maintenance and repair are virtually impossible for space-based electronic systems. Thus designed-in reliability is imperative for these very complex electronic systems. Additionally, the massive nature of SDI systems (thousands of sensors and parallel computers) would require generic reliability techniques to make it affordable. It is with these considerations that the Innovative Science and Technology (IST) office of the SDI Office initiated a research program on Reliable/Survivable Advanced Electronic Systems in 1985.

The objective of this research program is to develop the scientific understanding of factors that impact the lifetime reliability of microelectronic systems, and to develop the methodology for the design of highly reliable/survivable advanced electronic systems. The program is in direct support of virtually every aspect of the SDI program, particularly in the areas of sensors, signal processors, and battle management. From the very start, it is recognized that VLSI reliability is a very complex problem. The approach is to develop a methodology of hierarchial reliability, spanning from the purity of starting silicon materials to the design of reliable systems, as shown in Figure 1. The methodology must ensure that errors that are not detected at a lower level should be detected at a higher level. For example, error detection and correction circuits must be included at the microcell level to correct for faults that may go undetected at the circuit level or the device level. Similarly self-testing and reconfiguration schemes should be developed at the system level to ensure total system reliability. However due to funding limitations, it is not possible to fund all areas of research. Four areas of VLSI reliability have been identified as critical to the success of future VLSI chips and systems for SDI application: (1) Systems and architectures for fault tolerance; (2) Thin dielectric insulator films; (3) Contact/interconnect metal electromigration; and (4) Radiation effects on VLSI devices and circuits, and the associated radiation hardening techniques.

Figure 1

Hierarchial Reliability

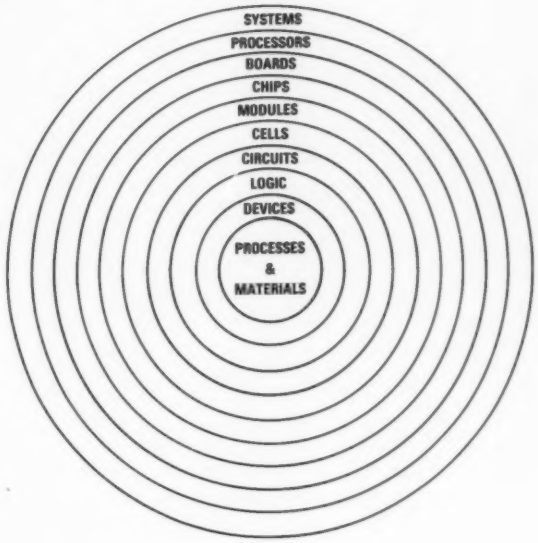

Technology Reliability Issues

Due to the limited space we will only discuss the technology reliability issues relating to metal-oxide-semiconductor (MOS) technology — the workhorse of VLSI. The need for increased circuit density and speed has driven down the lateral dimension of the transistor (the channel length) and the vertical dimension of the transistor (the gate oxide thickness). This scaling results in larger transistor currents, which are responsible for the improved circuit speed.

	Oxide thickness	Channel length	Operating voltage	Current per mm
1972	1200Å	7 μm	5V	15mA
1977	700Å	4 μm	5V	50mA
1982	250Å	2 μm	5V	200mA
1987	200Å	1 μm	5V	400mA
	150Å in DRAM			
	80Å in EEPROM			

After such aggressive reductions in oxide thickness and channel length, without a corresponding decrease in the operating voltage, and such a large increase in current density it is no surprise that we are now faced with three serious threats to IC reliability: oxide integrity, channel hot-electron induced device degradation, and metal electromigration. A fourth reliability concern is the radiation effects.

For each reliability problem, research must be done to address the underlying physical mechanisms, testing methods, process improvements, and to improve the reliability prediction at the circuit design stage. In the next several sections we shall describe each of the four problems, examples of research accomplishments, and research that needs to be done.

Oxide Reliability

Although numerous models for breakdown have been presented, there has not been a strong consensus concerning the breakdown mechanism. Electric field or current enhancement at some weak spots due to sodium ion drift, or hole trapping, or electron trapping, or trap generation have been suggested as the causes of breakdown at various times in the past.

Recent research has uncovered strong evidences of hole generation and trapping in the oxide during high field stressing and the rates of hole generation and trapping are directly correlated with oxide lifetime[3]. Hole trapping in the oxide causes an increase in the electron tunneling (Fowler-Nordheim tunneling) current density, further increasing the rate of hole generation and trapping. This positive feedback loop leads to catastrophic breakdown[4].

The lifetime of a given oxide sample is a function of the applied electric field, a phenomenon known as time-dependent dielectric breakdown (TDDB). This makes it difficult to test the oxide reliability and determine a safe operating voltage for a given IC technology. Up to now, the standard practice is to assume

$$t_{BD}=Ae^{-\beta E_{ox}} \quad (1)$$

The time-to-breakdown, t_{BD}, is measured at a few large oxide field, E_{ox}, values and the test data are extrapolated according to Eq. (1) to determine the t_{BD} for the intended lower operating field.

The hole-induced-breakdown model described above has recently predicted a different relationship[4].

$$t_{BD}=Be^{G/E_{ox}} \quad (2)$$

Figure 2

Oxide lifetime before breakdown occurs, t_{BD}, is a function of the oxide field, E_{ox}. Lifetime at a low operating field is usually extrapolated from high field test data according to $t_{BD} \propto e^{-\beta E_{ox}}$. However, $t_{BD} \propto e^{G/E_{ox}}$, as predicted by a recent theory, is more accurate.

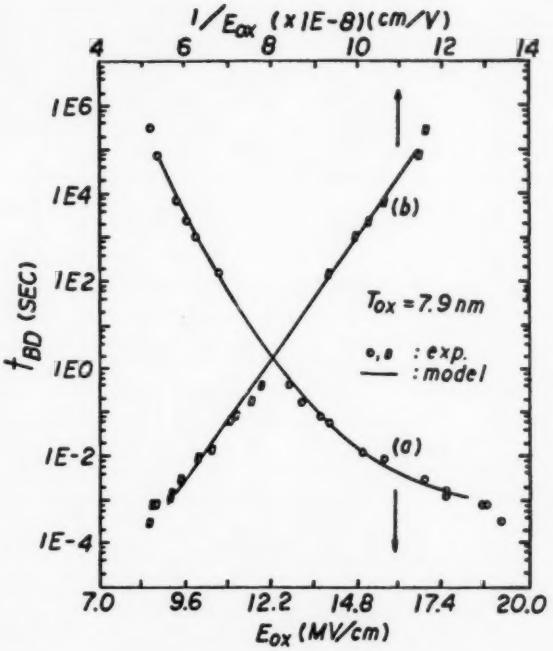

Figure 3

A method to determine the density of defects (thin spots) in oxide as a function of the defect severity, in terms of the "effective" thinning, was recently developed. This information allows one to predict the statistical rate of failure due to oxide breakdown.

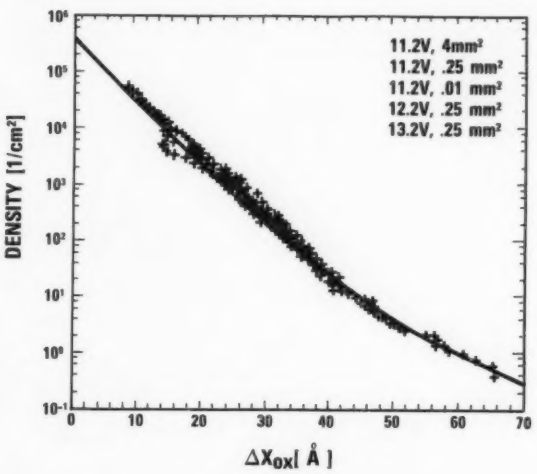

Figure 2 shows that Eq. (2) is a much more accurate model than Eq. (1).

Oxide failure in a large VLSI circuit always occurs at a single weakest spot. And the reliability of the circuit is determined by that single, randomly distributed "defect". It is, therefore, imperative to characterize these "defects". Recent research has developed a method to determine the defect density $D(\Delta X_{ox})$ as shown in Figure 3, where ΔX_{ox} is the effective thinning of the oxide at the defect points[5]. Once the defect density for a given oxide technology has been determined, the failure rate of a circuit containing any area of oxide can be predicted as a function of voltage and time according to Eq. (2).

A large portion of the defects is believed to be a direct result of the metallic precipitates in the silicon substrate that become incorporated into the oxide during thermal oxidation. Good pre-oxidation gettering has been shown to reduce the rate of early failures. A novel and interesting idea, recently verified experimentally, is that good CVD (Chemical Vapor Deposition) thin oxide may be more reliable than thermal gate oxide because the gaseous sources contain less metallic impurities than the silicon substrate[6].

These university research results need to be verified against high volume reliability testing typically performed in the industry. Temperature dependence needs to be added to the model. The mechanism for hole generation in oxide is not understood, especially for the case of low voltage operation.

Figure 4

Inset shows the LDD MOSFET structure, which will be standard for 5V submicron or micron MOS technologies. Peak channel electric field (a function of the n region doping concentration) is reduced in an LDD device and the hot-carrier limited device lifetime can be greatly prolonged.

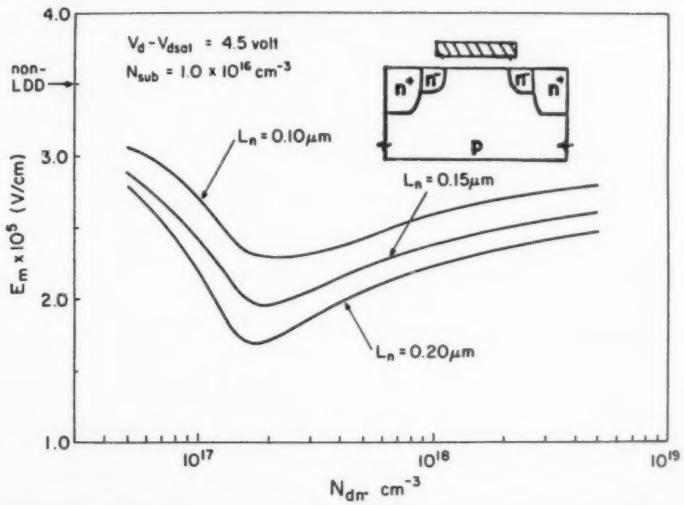

A close correlation between oxide reliability and radiation hardness is suspected, because both are linked to hole trapping, and should be investigated.

Hot Carrier Induced MOSFET Degradation

Near the drain junction in the MOSFET channel, there is a high field region, about 2000Å long, known as the pinch-off region. Field strength can reach $3X10^5$V/cm in 1.5 μm MOSFETs. At this electric field, electron temperature is 2500°K. High energy electrons can enter the oxide and become trapped or create acceptor-like interface traps and introduce interface trapped charge. The result is a decrease in device current and a drift in the threshold voltage and other device parameters[7]. This is known as hot carrier (electron) induced degradation. It is customary to consider the transistor to have failed when the current has decreased by 3% or 10%, or the threshold voltage has drifted by 10 mV or 100 mV.

The electric field strength can be significantly reduced, hence the device lifetime dramatically improved, by using the lightly doped drain (LDD) structure. An LDD structure is shown in the inset of Figure 4. Next to the heavily doped drain (and source) diffusion, a lightly doped region is introduced. This reduces the peak electric field in the same manner a decrease in doping concentration would reduce the peak field at a reverse biased p-n diode junction. Figure 4 shows the reduction in the electric field as predicted by an analytical model[8].

Testing and predicting device lifetime is greatly facilitated by noting that the hot electrons not only cause device degradation but also causes impact ionization. Impact ionization produces a small but easily measurable hole current that flows out of the substrate contact, known as the substrate current, I_{sub}. It was theoretically predicted and now well established that

$$\tau = 10^6 \left(\frac{I_{sub}}{W}\right)^{-3} \qquad (3)$$

where τ is the device lifetime in seconds; W is the device width in μ; and I_{sub} is in μA. This relationship is shown in Figure 5. Thus, τ, which may be longer than 10 years, can be estimated by making a single I_{sub} measurement or a few short accelerated lifetime tests.

Further research is needed to determine if device lifetime can be related to $I_{sub}(t)$ under switching voltage waveforms. If it can be related to $I_{sub}(t)$, we would be able to simulate $I_{sub}(t)$ at the circuit design stage and predict the device lifetime. If (and there are some evidences for this) it cannot, the reason needs to be understood and alternative means for lifetime prediction must be found. Another challenging research area is how to make the interface more resistant to hot carriers. Hydrogen-free oxide and oxynitride are good candidates for hot-carrier resistant dielectrics.

Figure 5

Hot-carrier limited device lifetime, τ, is a power-law function of the impact ionization generated substrate current, I_{sub}. W is the transistor width. At high voltage, for example, I_{sub} is large and τ is short. Such a plot allows one to extrapolate high voltage test data to determine the device lifetime at a lower operating voltage.

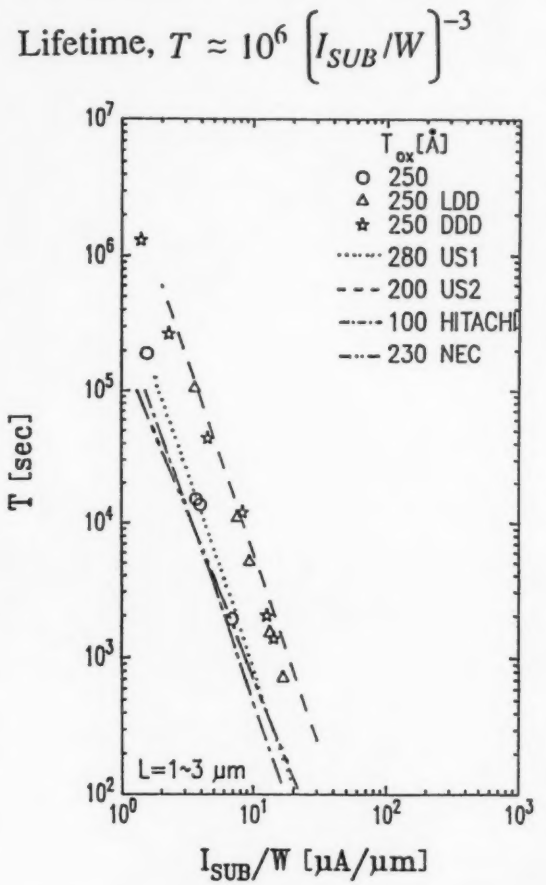

Metal Electromigration

Electrons can knock metal (principally aluminum in VLSI circuits) atoms out of their lattice sites. At very high current density ($>10^5 A/cm^2$) and over an extended period of time, voids and breaks in the metal line can develop. This is the basic electromigration problem. The mechanism is fairly well understood and the following mean-time-to-failure model is universally accepted for DC stressing

$$MTF = A J^{-n} \exp(E_a/kT) \quad (4)$$

where n is about equal to 2.

The remaining question is about pulse current stressing. In VLSI, current waveforms are highly peaked (CMOS inverters conduct current only during the short switching transients) at high clock frequencies (10-100 MHz). Should J in Eq. (4) be the average or the RMS current? Experimental results suggest that it is neither; MTF appears to be a complicated function of frequency and duty cycle. The effects of non-rectangular current pulse shapes are too intimidating to have been studied.

This complex behavior is recently explained[9] by a simple model. The metal vacancy density, n(t) is determined by the rate of vacancy generation, that is proportional to J(t), minus the rate of annihilation that is n/τ, where τ is the vacancy lifetime. The metal mass transport rate is proportional to the product J(t)n(t). Therefore, MTF is the time for the integral $\int J \cdot n \, dt$ to reach a certain constant.

Future research will have to address the question of bipolarity current stressing, i.e. to what extent does the current flowing in one direction repair the damage done by the current flowing in the other direction. There is also a large number of metal technology issues to be studied — copper doped aluminum, refractory metal, metal/semiconductor interface and metal/metal interface reliabilities.

Radiation Effects

There are three important radiation effects — total dose effect, dose rate effect, and single event upset (SEU). The total dose effect results from hole trapping in the oxide which causes the threshold voltage to drift until the circuit ceases to function to specification. Radiation hard processes have been developed to minimize this effect, but further research is needed. For example, some radiation hard processes attain the radiation hardness (unknowingly perhaps) by compensating the trapped holes with negative interface trap charges. Under certain conditions, such as at high temperature where holes can be thermally detrapped, this charge balance can be lost. Better understanding of the mechanisms and tempral dependence of electron and hole trapping, interface trap generation, electron and hole recombination, and interrelationships among these mechanisms is needed for a complete understanding of the total dose hardness. This significant overlap among radiation effects, hot electron effects, and oxide TDDB makes an unified study of these effects particularly useful and promising. New materials such as CVD oxide and new processes need to be investigated.

The basic mechanisms of SEU and the dose rate effect are known and somewhat similar. Simple models have been proposed for new phenomena such as funneling as due to α-particle or heavy ions have been proposed[10]. Charge collection may be minimized by using clever doping profiles, perhaps produced with high energy (MeV) ion implantation. CMOS offers additional opportunities to manipulate the device structure. To guide these development, better physical understanding and analytical models of charge collection in complex device structures are needed. Circuit configurations can be modified to reduce sensitivity to collected currents and charges. Several new SRAM cells have been proposed for this purpose. For designing more complex circuits, circuit simulators that can simulate the effects of, and predict the resistance to, pulse radiation and SEU would be extremely beneficial.

Table 1

Types of Tests

Production	Tests of manufactured parts to sort out those that are faulty
Wafer Sort or Probe	Test of each die while still on the wafer.
Final or Package	Test of packaged chips and separation into classes or bins (military, commercial, industrial)
Acceptance	A test to demonstrate the degree of compliance of a device with purchaser's requirements.
Sample	Test of some but not all parts
Go/No Go	Test to determine whether device meets spcifications
Characterization or Engineering	Test to determine actual values of device AC and DC parameters and the interaction of parameters. Used to set final specifications and to identify areas to improve process to increase yield.
Stress Screening (Burn-in)	Test with stress (high temperature, temperature cycling,vibration...) applied to eliminate short life parts
Reliability (Accelerated Life)	Test after subjecting the part to extended high temperature to estimate time to failure in normal operation
Diagnostic (Repair)	Test to locate failure site on failed part
Quality	Test by quality assurance department of a sample of each lot of manufactured parts. More stringent than final test
On-line or checking	On-line testing to detect errors that occur during normal system operation
Design Verification	Verifying the correctness of a design

Figure 6

Manufacturing Quality

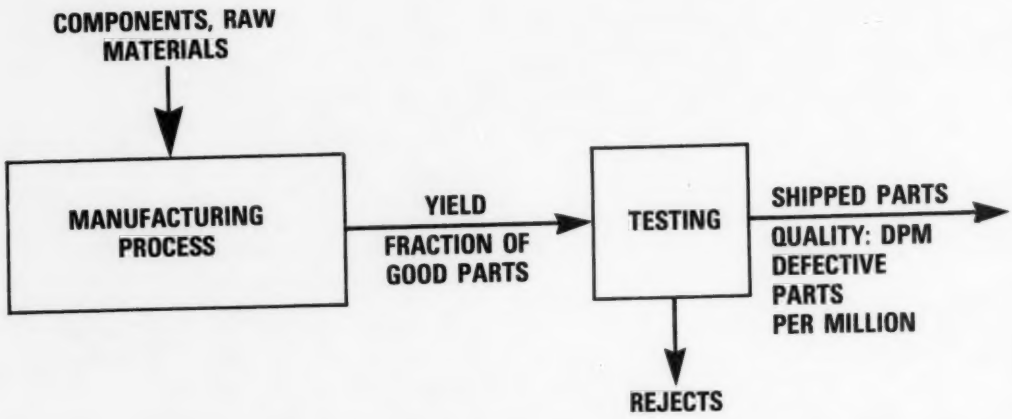

System Reliability Issues

Manufacture of an electronic system that can be *guaranteed* to operate correctly for a lifetime measured in years requires that:

1. The components from which the system is assembled are defect-free;
2. The assembly process is correct;
3. The reliability of the components is sufficiently high so that the number that fail during the system lifetime can be accurately bounded; and
4. The system includes facilities to detect the occurrence of a failure, isolate its effects, and reconfigure the system to exclude the failed device and replace its function.

In very general terms, two complementary techniques must be used to ensure that these requirements are satisfied: the manufacturing, assembly, and design must be as fault-free as possible, and adequate test procedures must be used to detect failures. Both techniques must be used since neither is sufficient by itself. Producing reliable components was discussed in the preceding section. This section discusses testing.

Manufacturing Test

The most important requirement in building a reliable system is to ensure that it is constructed of non-failed components. To do this, the manufacturing process should have the highest possible yield (ratio of good components to all components manufactured), and then should be followed by a thorough test procedure to eliminate any bad devices.

The current state-of-the-art in integrated circuit manufacturing is that the yield can be quite low (less than 50%) for aggressive designs using large die with many small-geometry devices. Even more conventional designs rarely have yields as high as 90%. A board assembled with 100 chips, each having a 10% probability of being bad, will have a probability of containing a failed chip of $1 - (.9)^{100} = 99.997\%$. Clearly this is unacceptable; the manufactured devices must be tested to increase the *quality level* (percentage of good chips) of the chips used in board assembly.

Present integrated circuit production test techniques have two major shortcomings:

1. One is the use of the single-stuck fault model to rate the effectiveness of a test procedure, even though it is clear that many of the defects that actually occur are not accurately represented by such a model; and
2. The other is the acceptance of a *fault coverage* (percentage of faults detected) less than 100%.

Fault coverage is discussed in the following subsection, followed by a discussion of fault models in the next subsections.

Fault Coverage: After a piece of equipment is manufactured or assembled, it may require testing before being sold or used. The need to test depends on: (1) the process yield, Y, the proportion of finished units that are not defective, and (2) the acceptable quality level, AQL, the planned minimum fraction of defective shipped units.

If, as is often the case, the process yield is lower than the AQL, defective units must be identified and removed so as to increase the percentage of good units (Figure 6). The procedure of identifying defective units is called testing (the process

of determining whether a piece of equipment is functioning correctly or is broken or faulty).

Testing done during manufacturing is called manufacturing or production testing. Testing is also done for other purposes or at other stages in a product's life. Table 1 lists some of these other types of tests.[11,12]

Test quality is usually measured by *fault coverage C*, the percentage of possible defects that are detected by the test procedure. The process yield and the AQL determine the required fault coverage. This dependence can be quantified by assuming a model for how manufacturing defects affect the process yield. The model used here[13, 14] is based on the two papers by Williams. It assumes that the causes of chip failure can be enumerated as n possible defects per chip, and that the test process can detect the presence of m out of all n possible defects. It is further assumed that the occurrence of each of the n defects is independent and equally likely with probability p. The quality level achieved by a test with fault coverage C for a process of yield Y is given by:

$$QL = Y^{1-C} \qquad (5)$$

This expression makes no assumptions about the range of values of the variables. Modern integrated circuit manufacturing typically requires quality levels of at least 99.99% (corresponding to fewer than 100 defects per million devices). If a high yielding process (Y > 90%) is assumed (since the required coverage will be higher for a poorer process), it is possible to rewrite the expression for QL as:[15]

$$1 - QL \approx (1 - C)(1 - Y) \qquad (6)$$

For a QL of 99.99% and a 95% yield, the required fault coverage, C, is 99.8%.

There is amazingly little empirical data on the relationship between fault coverage and quality level for integrated circuits. Only one experiment to relate test coverage and quality level in an actual IC process has been reported in the literature[16]. The chip designer's test patterns had a 96.6% fault coverage, but this test failed to discover 103 bad dies. Use of this test with 96.6% fault coverage would have resulted in an unacceptably low QL of 99.15% in manufactured ICs. Both the theory and the experiment lead to the conclusion that 96.6% fault coverage is inadequate.

In summary, the theoretical studies, as well as the one experiment that has been published, indicate that single-stuck production test fault coverages of greater than 99% are desirable for manufacturing high quality ICs.

It is both difficult and expensive to guarantee such high fault coverage. Design-for-testability techniques are used increasingly to enhance the fault coverage. But even with the inclusion of test scan paths high fault coverage is expensive. One technique that has been used successfully is to partition the chip and test combinational subcircuits exhaustively (apply all possible input patterns)[17]. This technique is very effective, but its use has been limited because of the difficulty of obtaining a viable partitioning. Research is on-going to develop automatic methods of partitioning designs.[18]

Even 100% single-stuck fault coverage may not be adequate to guarantee defect-free chips. Many failure modes are not correctly represented as single-stuck faults. Other fault models are discussed in the next subsections.

Complex Stuck Faults: Single-stuck faults may accurately represent physical failures in which a single circuit net is either open-circuited or is shorted to a power rail. If, as is often the case, more than one such fault occurs; a *multiple-stuck fault model* is required for accurate modelling. A *bridging fault model* is needed for those very common situations in which two signal nets are incorrectly interconnected. There is no disagreement about the occurrence of failures that require *complex stuck fault* models, multiple-stuck faults or bridging faults, to represent them accurately; but these models are never used in developing test patterns because there are so many such faults. In a circuit with n nets, there are approximately 2n single-stuck faults, 3^n multiple-stuck faults, and n^2 two-net bridging faults.

Both theoretical studies and experimental results have shown that single-stuck fault test sets detect many complex stuck faults. But recent studies have demonstrated that even test sets with 100% single-stuck fault coverage may have inadequate coverage of complex stuck faults[19,20]. Cost-effective techniques have been developed to augment single-stuck fault test sets to improve the complex fault coverage[19,20]. Modified exhaustive test techniques, called *pseudo-exhaustive tests*, have been described that provide guaranteed coverage of both single and complex stuck faults without the necessity of fault simulation to determine coverage[21].

Pattern Dependent Faults: There are other failure modes that cannot be represented as stuck faults since they do not result in incorrect interconnections, but rather introduce spurious circuit elements[22]. These failures are particularly pernicious since the element parameter values may depend on the chip temperature or supply voltage value and thus may appear to be temporary malfunctions. While stuck-fault test sets may fail to detect such failures, pseudo-exhaustive tests have been shown to be effective in discovering their presence. Research is continuing to quantize the coverage of such faults.

Delay Faults: Failures that alter component values without introducing extra components can cause the circuit to fail due to violation of timing parameters. Such failures are modelled as delay faults. They can be very difficult to detect since the parameter values can depend on temperature or supply voltage, and many signal paths must be tested to discover the presence of a localized delay fault. The develop-

ment of cost-effective test methods for delay faults is an area of intensive current research.

MOS Faults: The possibility of having failures in NMOS or CMOS circuits that convert a combinational circuit into a sequential circuit has been demonstrated and a great deal of effort has been devoted to developing test procedures for such faults. None of these procedures are cost-effective. Furthermore, it has been demonstrated that this is a class of failure that is better avoided by proper design (layout) methods[23].

Fault Tolerance

The most critical feature of systems that must continue to operate correctly after a failure has occurred is the ability to detect and localize the failed element. Many schemes for error-detection have been developed, but they are all based on the assumption that failures manifest themselves as either single-stuck faults or as unidirectional errors. There is general agreement that most operational failures are the result of temporary rather than permanent component failures. Recent experiments have demonstrated that temporary failures do not have the characteristics of stuck faults, but rather are delay or pattern dependent faults[22,24]. Research is underway to characterize the ability of standard error detector structures to detect such failures[25].

Summary

Since the initiation of the research program and particularly during this past year, significant accomplishments were made in terms of understanding the physics of failures in the devices and metals and developing design techniques to circumvent these failures. In this paper, we presented briefly the issues and some recent research results in technology reliability and system reliability. In other funded efforts, thin aluminum and aluminum-alloy films have been prepared and characterized by means of TEM, SEM, and optical microscopy. Low temperature deposition of multilayer oxynitride thin film has been demonstrated by means of remote enhanced plasma chemical vapor deposition (REPCVD) technique. Parallel test techniques have been developed for testing high density memories. Reconfiguration schemes have been developed to ensure graceful degradation and fault tolerance in processor arrays. High speed high reliability signal processing using logarithmic and residue number systems have been demonstrated in a new experimental computer architecture.

There are four major technology reliability concerns: oxide time dependent breakdown, hot carrier induced MOSFET degradation, metal electromigration, and radiation effects. For each of these four concerns we need to research these inter-linked subtopics — underlying physical mechanisms, testing methods, process improvement, and means of predicting reliability at the circuit design stage. At the present time, the basic underlying mechanisms are known and rudimentary testing methodologies, at least for DC stressing, for comparing technologies are available. How to analyze tests under realistic waveforms and how to use the data of simple tests to predict circuit reliability are the next research challenges. Computer aided design (CAD) tools will have to be developed to accomplish these research goals. There is still much promise in the search for improved processing technologies, material, and/or device structures to improve electronic component reliability by orders of magnitude.

In order to achieve high system reliability and availability it is necessary to screen out failed parts before assembling the system. This requirement mandates the use of extremely thorough IC test techniques that detect 100% of the failures that can be modelled as single-stuck faults as well as close to 100% as possible of failures requiring more complex fault models. This level of coverage will require the use of pseudo-exhaustive test techniques. CAD implementations of such techniques are currently being developed at the Stanford Center for Reliable Computing (CRC).

Continual system operation depends on the ability to detect failures during operation and to reconfigure the system. Present techniques for failure detection are of questionable value for non-single-stuck faults caused by temporary failures. Work is underway at CRC to develop both more accurate models and also improved error detectors for temporary failures.

It is clear that reliability is a very complex problem. For large-scale VLSI systems, reliability must start from the basic starting silicon materials, and going all the way to reliability at the system level. Since reliability is a system level issue, hierarchical reliability methods must be developed to solve the reliability problem. Reliability issues must be addressed throughout the manufacturing and operation of VLSI chips and systems at various levels, from silicon materials, fabrication process, devices, logic design, circuits, macrocell, chips, boards, subsystems, and systems. The reliability problem cannot be solved at any single level. For example, errors that are not detected and corrected at the gate level must be detected at the macrocell level. Any remaining errors must be detected and corrected at the system level.

The solution to the reliability problem lies in reliable devices, correct design, and thorough testing. Firstly, the system must be built with reliable parts since it is impossible to build a reliable system out of unreliable components. That is the reason so much research is concentrated on improving the reliability at the device and component level. Secondly, the design must be correct to make it possible to separate the fabrication flaws from potential design errors. Therefore, design techniques and CAD tools must be developed to insure the correctness of design before committing to silicon fabrication. Finally, the chip and system must include designed-in testability to allow for the thorough testing of the system to insure reliable operation throughout the system's lifetime.

Biography

Dr. Clifford Lau is a Scientific Officer in ONR in the Electronics Division. He received his Ph.D. in electrical engineering and computer science from the University of California at Santa Barbara in 1978 and has been with ONR since 1980. His current research interests include VLSI systems and computing architectures, VLSI reliability, signal processing algorithms and architectures, and neural networks.

Dr. Chenming Hu is Professor of Electrical Engineering and Computer Sciences at the University of California, Berkeley, where he received his Ph.D. degree in 1973. He was an Assistant Professor at M.I.T. from 1973 to 1976, and a manager of nonvolatile memory development at National Semiconductor in 1980-81 while on leave from U.C. Berkeley. His research interests include semiconductor devices and IC technology.

Professor E.J. McCluskey is Director of the Stanford Center for Reliable Computing and a Professor in both the Computer Science and the Electrical Engineering Departments. He has degrees from Bowdoin College and M.I.T. He worked at Bell Telephone Laboratories and Princeton University before moving to Stanford in 1966. He is President of Stanford Logical Systems Institute and Palo Alto Research Associates, companies providing consulting services in computer engineering especially testing and design-for-testability.

References

1. Fletcher, J. C., (Study Chairman), The Strategic Defense Initiative, Defensive Technologies Study, unclassified summary, Department of Defense, April 1984.

2. Fletcher, J. C. (Study Chairman) and McMillian, B. (Panel Chairman), "Battle Management, Communication, and Data Processing (U), "Report of the Study on Eliminating the Threat Posed by Nuclear Missiles (U), February 1984.

3. I.C. Chen, S. Holland, C. Hu, "Oxide Breakdown Dependence on Thickness and Hole Current," *Technical Digest of International Electron Devices Meeting (IEDM)*, 1986, pp. 660-663.

4. C. Hu (Invited Paper), "Thin Oxide Reliability," *Technical Digest of International Electron Devices Meeting (IEDM)*, 1985, pp. 368-371.

5. J. Lee, I.C. Chen, C. Hu, "Modeling and Characterization of Oxide Reliability," *IEEE Trans. on Electron Devices, Vol. 35 No. 12, Dec. 1988, pp. 2268-78.*

6. J. Lee, I.C. Chen, and C. Hu, "Comparison Between CVD and Thermal Gate Oxide Dielectric Integrity,"*IEEE Electron Device Letters*, Vol. EDL-7, Sept. 1986, pp. 506-509.

7. C. Hu (Invited Paper), "Hot Electron Effects in VLSI MOSFETs," *Technical Digest of Third International Symposium on VLSI Technology, Systems, and Applications*, 1987, pp. 79-84.

8. C. Hu, S. Tam, F-C Hsu, P.K. Ko, T.Y. Chan, and K.W. Kyle, "Hot-Electron-Induced MOSFET Degradation," *IEEE Trans. on Electron Devices*, Vol. ED-32, Feb. 1985, pp. 295-305.

9. B. Liew, N. Cheung, C. Hu, "Electromigration Interconnect Lifetime under AC and Pulse DC Stress," *1989 International Reliability Physics Symposium Proceedings*, April 1989, pp. 215-219.

10. C. Hu, "Alpha-Particle Induced Field and Enhanced Collection of Carriers," *IEEE Electron Device Letters*, EDL-3, Feb. 1982, pp. 31-34.

11. Healy, J.T., *Automatic Testing and Evaluation of Digital Integrated Circuits, Reston Publishing Co., Reston, VA, 1981*

12. Stevens, A.K., *Introduction to Component Testing*, Addison-Wesley Publishing Co., 1986.

13. Williams, T.W. and N.C. Brown, "Defect Level as a Function of Fault Coverage," *IEEE Trans. Comp.*, Vol C-30, No. 12, pp. 987-988, Dec. 1981.

14. Williams, T.W., "Test Length in a Self-testing Environment," *IEEE Design and Test*, pp. 59-63, Apr. 1985.

15. McCluskey, E.J. and F. Buelow, "IC Quality and Test Transparency," *IEEE Trans. on Ind. Electronics, Vol. 36, No. 2* May 1989, pp. 197-202.

16. Daniels, G. and W.C. Bruce, "Built-in self-test trends in Motorola microprocessors", *IEEE-D&T*, APRIL 1985

17. Gelsinger, P.P., "Built In Self Test of the 80386," ICCD 86.

18. Shperling, I. and E.J. McCluskey, "Circuit Segmentation for Pseudo-Exhaustive Testing via Simulated Annealing", *Int. Test Conf.*, Washington, D.C., pp. 58-65, Sept. 1-3, 1987.

19. Hughes, J.A., and E.J. McCluskey, "Multiple Stuck-at Fault Coverage of Single Stuck-at Fault Test Sets," *International Test Conference*, Washington, D.C., Sept. 8-11, 1986

20. Millman, S. and E.J. McCluskey, "Detecting Bridging Faults with Stuck-at Test Sets," *Stanford Center for Reliable Computing Technical Report*, 1987.

21. McCluskey, E.J., *Logic Design Principles*, Prentice-Hall, 1986.

22. Cortes, M. and E.J. McCluskey, "An Experiment on Intermittent-Failure Mechanisms," *International Test Conference*, Washington, D.C., Sept. 8-11, 1986

23. Zasio, J.J., "Non Stuck Fault Testing of CMOS VLSI," *Dig. COMPCON Spring 85*, San Francisco, CA, Feb. 1985.

24. Cortes, M., and E.J.McCluskey, "Modeling Power Supply Disturbances in Digital Circuits," Proc. *IEEE International Symposium on Solid State Circuits*, Anaheim, CA, Feb. 19-21, 1986.

25. Amer, H.H., M.L. Cortes, and E.J. McCluskey, "Robust Dynamic Recovery Mechanisms", *Proc., Int'l. Conf. on Computer Design*, Port Chester, NY, Oct. 1987.

Profile in Science

Sadeg M. Faris

Dr. Sadeg M. Faris is the President of HYPRES, Inc., Elmsford, New York. Before he founded HYPRES in 1983, he spent eight years at IBM in the Yorktown Heights, New York, research facility working on the development of a high-speed superconducting computer utilizing Josephson junction technology. Dr. Faris has invented memory cells, laser-programmable logic arrays, a sampling system that measures electrical and optical picosecond signals and a large variety of other superconducting devices. For these efforts, IBM awarded Dr. Faris seven Invention Achievement Awards. In 1983, he received IBM's "Outstanding Innovation Award" for his invention an development of a superconducting oscilloscope. His development of the QUITERON (three terminal superconducting device) was chosen by IBM as Invention of The Year in 1983. He holds fifteen patents and is the author of over forty publications in the science and technology of superconductivity and optics.

With Office of Naval Research support, Dr. Faris created the first manufacturing facility for the production of NbN integrated circuit chips. These chips will be used for the Navy's Digital Magnetometer project for ASW and other activities and HYPRES' own products which utilize inexpensive, reliable and compact closed-cycle refrigerators operating below 10°K.

Also with ONR support, Dr. Faris, demonstrated for the first time that superconducting sensors have higher sensitivities than conventional technologies. The superconducting sensors will be the major component of monolithic focal plane arrays which combine the sensor and other low-power dissipation, superconducting circuits for digital and analog processing. The focal plane arrays will exhibit higher performance, lower cost, more reliability and lower weight.

Advanced Composites For Strategic Defense Initiative Systems

S. G. Fishman
Office of Naval Research

J. A. Cornie
Massachusetts Institute of Technology

K. M. Prewo
United Technologies Research Center

R. K. Viswanadham
Martin Marietta Laboratories

J.S. Epstein
Georgia Institute of Technology

Future systems for the Strategic Defense Initiative have material requirements which are more severe than for other Department of Defense or industrial applications. These requirements include operation at extremely high temperatures, absolute dimensional stability during thermal cycling, high vibration damping, low weight, high strength and mechanical stiffness, and high reliability. Added to these is the necessity of being survivable in hostile environments (laser attack, particle impact), and of course, affordable to fabricate. Because of the variety of extremely stringent, often unique, combination of material requirements, the only solution for many of these applications are novel advanced composites, which can be tailored to provide the required properties for specific SDI applications.

Although, composite materials with high operating temperature potential have been under development for a number of years, there are major deficiencies in processing science and fundamental understanding of their mechanical behavior and environmental degradation mechanisms.

In the past, because of their great complexity, composites have largely been developed in an empirical manner. As a result of the great combination of fibers, matrices, and composite architectures possible, as well as the near-term need for these materials, such inefficient and expensive material development procedures can no longer be tolerated. With this in mind, the Strategic Defense Initiative Office of Innovative Science and Technology established a program to establish scientific understanding of the processing science, composite behavior mechanisms, and new measurement techniques necessary to make possible the innovative materials required for future SDI systems. The program was designed to address processing on a fundamental level, identify and correct lack of understanding in specific areas, and demonstrate innovative material concepts. A center for processing science of metal matrix composites and ceramic matrix composites, two of the most important classes of materials for SDI applications was established during fiscal year 1985 at the Massachusetts Institute of Technology. In addition, other investigations were initiated to generate basic understanding of composite science, develop novel property measurement methods, or demonstrate innovative materials, at university and industrial research laboratories. Descriptions of the center and some of the research being conducted in carbon reinforced glasses, intermetallic matrix composites, metal matrix composites, and on the development of new mechanical property measurement methods are presented herein.

A Center For The Processing And Evaluation Of Metal And Ceramic Matrix Composites,

Materials Processing Center, Massachusetts Institute of Technology

The great advantage of composite materials is the specificity of their properties, i.e., it is possible to engineer materials to a specific application. This advantage, however, has been a retardant to their application. With such freedom of design, it is not possible to accumulate a large data base. We may never have the production volume or the demand to produce such a data base for many systems. In the absence of a large data base, alternative methods must be found for predicting materials performance. Thus, the goal of the Center for the Processing and Evaluation of Metal and Ceramic Matrix Composites is the complete and fundamental understanding of the relationships between microstructures, properties and processing parameters of metal and ceramic matrix composites. With this understanding, these technologies can be economical as well as a technical reality.

The research topics sponsored by the SDIO/IST within the Center address issues pertaining to the successful introduction of metal and ceramic matrix composites into engineering structures. Individual research topics have been selected on the basis of their ultimate impact on important SDIO structural applications and in their conformance with the program's overall structure.

Figure 1

Specific Properties of A1 and Mg Matrix Composites

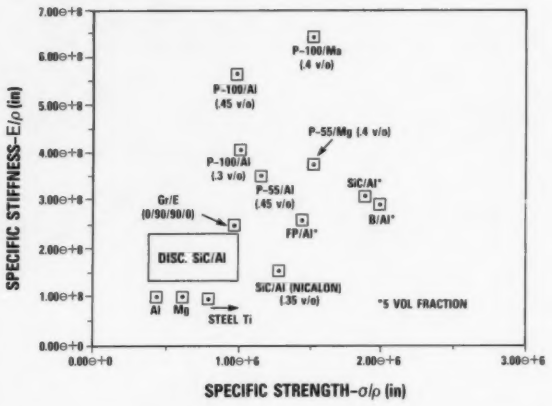

Metal and ceramic matrix composites have been simultaneously addressed throughout the program. The two areas differ slightly in their principal foci: metal matrix research emphasizes improvements of property levels; while ceramic matrix composite research is concentrated on improved reliability. Concerns for the matrix-reinforcement interface, processing and microstructural control are fundamental to both. Although each activity is unique in its approach and goals, certain activities and approaches are common to all. The

Figure 2

Central problem of metal matrix composites. Interfaces act as mechanical fuses to arrest impinging cracks by interface delamination.

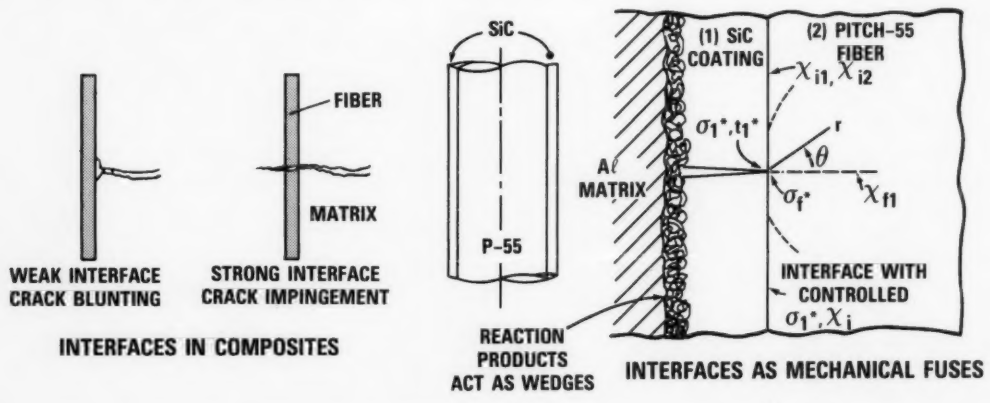

emphasis of the Center is on fundamental process understanding (i.e., understanding the relationships between processing, microstructure and materials properties).

Because of the low viscosity and short curing time (i.e., solidification time) of liquid metals as compared to resins and the net shape potential of casting technology, metal matrix composites are potentially less expensive to manufacture and more applicable to SDIO structural applications than resin matrix composites. That potential is being explored in the activities of the Center and the other programs associated with the Center.

The initial work has been with Al and Mg alloy matrices because of the structural efficiencies of composites of those materials as shown in Figure 1.

Carbon fiber (P-55) is being featured for most of the continuously reinforced studies. However, Al_2O_3 fiber in the form of Saffill™ and Fiber FP™ and SiC(AVCO SCS-2™) has been used in modeling studies. In the semi-solid slurry processing studies, SiC, B_4C and Al_2O_3 particulate materials have been used for either process development or process modeling.

Carbon fiber reinforced composites are difficult to fabricate in any but the most simple shapes by any process other than casting or liquid metal infiltration processing. Further, the minimum sections required for the gossamer structures that are needed for space structures can not be produced by any other method. However, implementation of casting technology has been hindered by a lack of understanding of processing fundamentals. These areas of needed knowledge include the following:

- Fluidity (fluid flow through a preform with or without accompanying solidification.
- macrosegregation.
- fiber wetting and interfacial reactions.
- the development of alloy microstructure during solidification fiber distribution

Figure 3

Matrix Transfer Molded Composite Pipe-Section

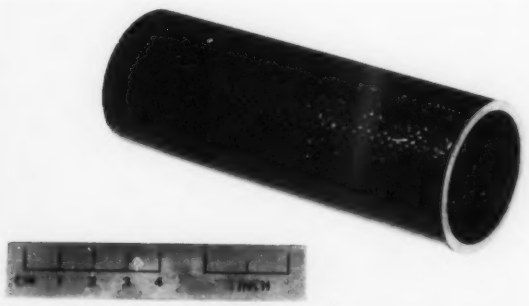

Figure 4

Composite Mirrors fabricated from Carbon Fiber Reinforced Glass

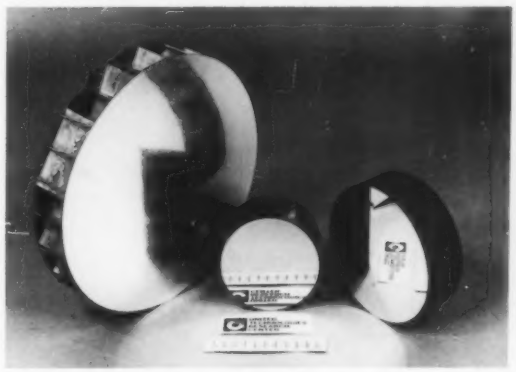

Continuously reinforced metal matrix composites represent the maximum potential for strengthening in directions of principal stresses. However, as much as a two-fold improvement in specific stiffness can be achieved isotopically with particulate reinforced metal matrix composites. The most economical method of producing discontinuously reinforced metal matrix composites is by solidification processing or, more specifically, semi-solid processing. As in pressure infiltration mentioned above, the performance has been less than potential because of processing defects. The principal defects are porosity introduced during the inclusion of particulates into the melt to form the semi-solid slurry and poor distribution of ceramic reinforcement arising from the movement or "pushing" action of the solidifying metal.

- The critical fundamental issues that must be addressed are:
- The development of solidification microstructure in the presence of particulates.
- interfacial reactions and wettability.
- particle pushing effects.
- modeling of stirring and mixing
- modeling of deformation behavior of semi-solid slurries

These issues are being addressed both fundamentally and practically. Fundamental studies are being conducted on the evolution of microstructure of Al-Cu-Mg and Mg-Al alloys with SiC and B_4C particulates respectively. Particle pushing effects are being explored in Al-Cu-Mg alloy/SiC systems. Mathematical modeling of semi-solid stirring and rheology of deformation studies are also underway. An extensive cross cutting study is also underway to explore the wettability in

Figure 5

Longitudinal and Transverse Strain Versus Applied Tensile load for 0°-43 V/o HMU/7740

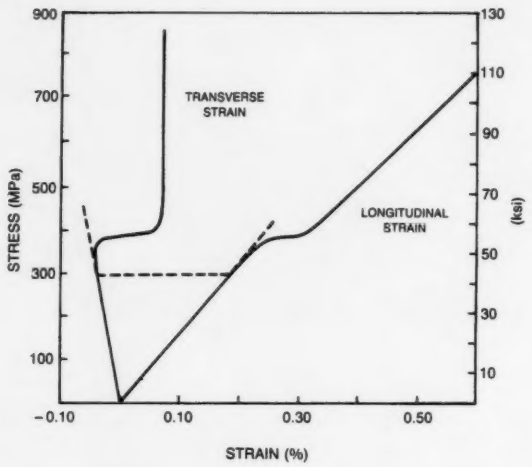

continuous and discontinuous systems as well as methods for treating fiber or particulate surfaces to improve wettability.

The properties of composites are determined by the nature of the interfacial region. The need to engineer the interface is common to both metal and ceramic matrix composite activities in the Center. There are at least three reasons for tailoring (engineering) the interfacial zone in metal matrix composites; 1) to control the fracture path, 2) to protect the fiber surface from degradation due to handling or from chemical interaction with the matrix during consolidation, and 3) to provide wettability for the ease of processing. Reasons 1 and 2 are general for metal and ceramic matrix composites; reason 3 is specific to solidification processing of metal matrix composites.

The Center's program is focused on tailoring the interface through use of Plasma Assisted Chemical Vapor Deposition (PACVD) This technique results in amorphous coatings with freedom to specify both coating modulus and residual stresses. The tailoring effort is backed by micromechanical analysis and measurement of specific properties of the interface as well as finite element elastic plastic analysis of fiber arrays.

The central problem of engineering interfaces in metal (and ceramic) matrix composites is the arrest of cracks at the interface. In one program at the Center a P-55 carbon fiber/pure Al composite has been chosen as a model system for engineering the interface. The problem of a reinforcing fiber coated with a brittle sacrificial layer in a ductile matrix is shown in Figure 2. A crack is shown to nucleate in the reaction zone between the matrix and the coating and impinges on the fiber/matrix interface. The stress $\sigma_{\theta\theta}$ atθ=0 probes the strength of the fiber while the same stress atθ=$\pi/2$ is responsible for interface separation. The radial shear stress $\sigma_{r\theta}$ at the interface (θ=$\pi/2$), on the other hand, probes the shear strength of the interface. Thus, two failure processes are possible upon interaction between impinging cracks and interfaces: 1) fiber fractures, or 2) fiber uncouples from the coating in shear or in tension.

Interfacial strength requirements for the protection of fibers by crack arrest at the coating/fiber interface are given in Figure 2. When the ratio of; interface cohesive strength to fiber strength is less than the ratio of evolving elastic crack tip stresses responsible for interface separation and fiber fracture (i.e., the ratio of $s_{\theta\theta}$ atθ=$\pi/2$ $s_{\theta\theta}$ atθ=0), the interface will separate in tension providing that the interfacial stresses are tensile. This condition leads to an upper bound for the interface cohesive strength. Likewise, when the ratio of interface shear strength to fiber strength is less than the ratio of $s_{r\theta}$ the interface (θ=$\pi/2$) to $s_{\theta\theta}$ atθ=0, the interface will separate in shear. This bounds the maximum interface shear strength. When the ratio of interface cohesive strength to interface shear strength is less than the ratio $s_{\theta\theta}/s_{r\theta}$ at the interface, tensile separation will be preferred. Also, the toughness of the interface should be less than toughness of the fiber or the coating for the crack to advance through the fiber.

Ceramic matrix composites have potential for a wide range of applications including components for advanced aerospace propulsion systems to laser hardening of space structures and orbital insertion and re-entry systems. Properties generally sought include strength, hardness, stiffness,

Figure 6

Effect of Vol% Fiber on Composite Stress-Strain Behavior

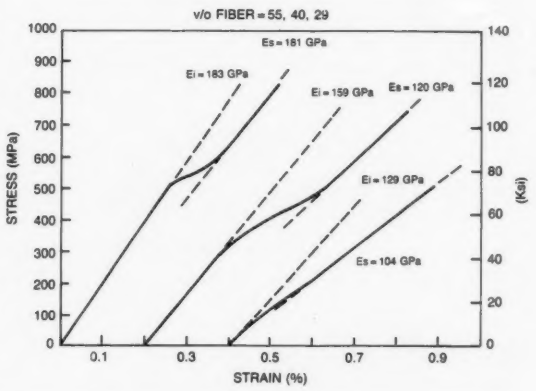

Figure 7

Tensile Fracture and Proportional Limit Strains for 0°-HMU/7740 ● = Filament Tows, O= 3000 Filament Tows

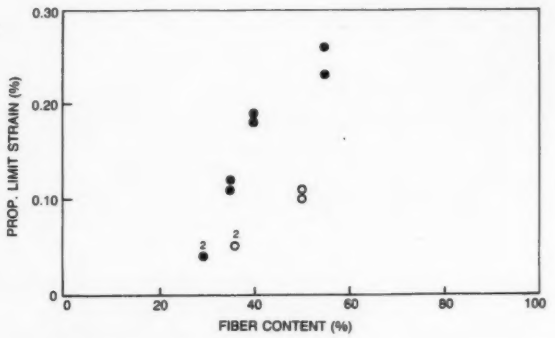

Figure 8

Fiber-Matrix Interfacial Shear Strength (τ_{max}) vs Composite Short Beam Shear Strength (SBSS) for 0°-HMU/7740 with Various Matrix Additives

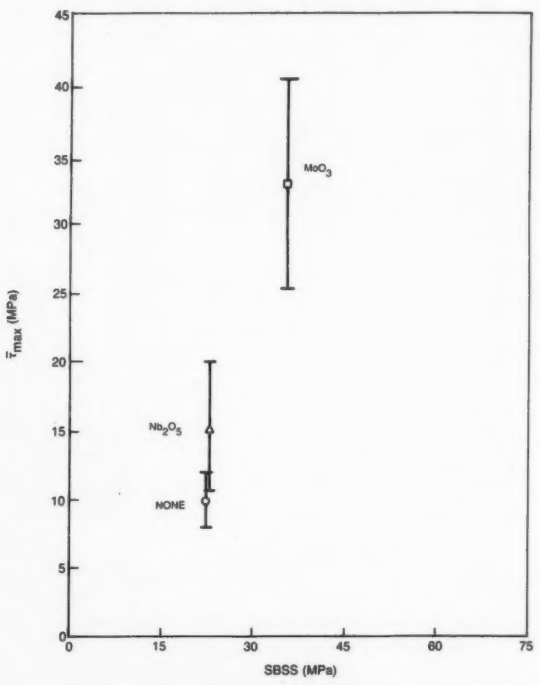

toughness, resistance to chemical attack, wear resistance, and reliability. Many applications require higher temperature capabilities than can be satisfied with alternative materials. The composite properties result directly from the properties of component materials, their bonding and the matrix/reinforcement architecture.

The initial investigations in the ceramic matrix composite section of the Center have been directed toward reaction bonded SiC(RBSC) and reaction bonded Si_3N_4 glass transfer molding (glass infiltration), and pre-ceramic polymer synthesis of B_4C for fibers and matrices. Work is also in process on the evaluation of BN, non-stoichiometric silicon carbide (SiC_{1-x}) deposited by PACVD on SiC fibers as well as the evaluation of the SCS-6 interface in Si_3N_4 and SIC systems.

Carbon Fiber Reinforced Glass For Space Based Applications.

The use of carbon fibers to reinforce glass matrices provides a unique opportunity to achieve composites that possess properties particularly well suited to space based applications. As in the cases of reinforced polymers and metals, the use of carbon fibers provides composites with the potential for high levels of stiffness, strength, and dimensional stability. The use of glass as a matrix material offers an opportunity to achieve superior long time durability and resistance to environmental effects. Glasses are not likely to outgas, are highly resistant to atomic oxygen, and are exceptionally resistant to elevated temperature exposure.

While a wide variety of ceramic matrices may also be considered as composite matrices, the use of glass provides the unique ability to fabricate composite articles of complex shape in a manner similar to that currently used for conventional thermoplastic matrix composites. An example of this capability is shown in Figure 3 where a thin walled, tube of woven carbon fibers in glass is shown. The tube was densified in a single operation with the actual matrix densification taking place in a matter of a few minutes. The resultant composite microstructure is fully dense. Significantly more complex shaped articles can also be fabricated as exemplified by the mirrors shown in Figure 4. These mirrors were fabricated with thin walled face and back plates encasing a lightweighted structural core. All elements of these mirrors were fabricated at United Technologies Optical Systems Division using carbon fiber reinforced glass. Their surfaces have been coated to provide the necessary reflectivity and they exhibit exceptionally high levels of dimensional stability.

While the above describes several important advantages for the carbon fiber reinforced composite system, it can also be said that the true performance potential for such a system has not yet been fully realized. It is only the first of a broad range of fiber reinforced ceramic matrix composites which can

Figure 9

Electron Microprobe Step Scan Analysis of Composites with Matrix Additives

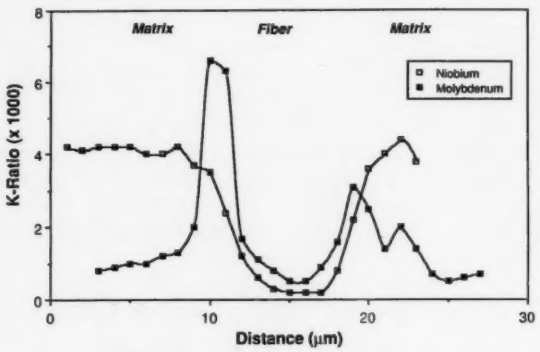

revolutionize the performance of space based structures. The SDIO sponsored research activity is intended to create a fundamental basis for the understanding and improvement of composite performance and to lead to concepts for composite enhancement, not only for carbon reinforced glass but also for other future forms of ceramic matrix composites.

The first issue addressed by this program is the unique stress-strain behavior of ceramic matrix composites. As illustrated in Figure 5 for unidirectional carbon fiber reinforced glass, the stress strain response to tensile loading is highly nonlinear. In addition, composite tensile strength is only 60% of that typical of polymer matrix composites. The nonlinear aspect of composite behavior is due to the microcracking of the glass matrix at a low value of strain and may prove to be the limiting factor in composite mechanical performance. The theory of Aveston, Cooper, and Kelly provides a basis for the determination of the level of strain at which microcracking is expected to take place. As shown in the following expression, increasing the volume percent of fiber in the composite should be effective in increasing this strain and as an additional benefit it should also increase composite stiffness.

$$\varepsilon_c = \left(\frac{12\,\tau\,\gamma_m\,E_f\,V_f^2}{E_c\,E_m^2\,r\,V_m} \right)^{1/3} \qquad (1)$$

ε_c = matrix failure strain in the composite
E = elastic moduli of composite, matrix, and fiber.
τ = interfacial shear strength.
V = volume fractions of fiber and matrix.
r = fiber radius
γ_m = matrix surface fracture energy

Creation of composites with increasing levels of fiber content have confirmed this dependence of microcracking strain on fiber content, Figures 6 and 7. The strain level was increased five fold with an increase in fiber content from 25 to 55%.

As can be seen in the above expression, the fiber-matrix interfacial shear strength is also an important factor in controlling microcracking. Increasing this level should enhance the microcracking strain and more importantly, it should increase composite shear strength as well. To demonstrate this, a series of unique glass compositions was created and used to react with the carbon fibers during composite fabrication. By these reactions it was possible to alter the nature of the fiber-matrix interface as confirmed by individual fiber-matrix debonding experiments. These have been related to composite shear strength with the result shown in Figure 8. As projected by the model, composite shear strength increased with increasing interfacial bond strength. Detailed chemical analysis of the interface region confirmed that reaction between the fiber and matrix (particularly in the case of the glass containing MoO_3) was the cause of this enhancement. Electron microprobe analysis indicated that the Mo had migrated to the interface region (Figure 9), while x-ray diffraction showed that significant amount of Mo_2C were created.

The tailoring of the fiber-matrix interface properties affects many aspects of glass matrix composite performance. In addition to increasing composite strength, it is also important to preserve the interface as a region for resistance to crack growth in these brittle fiber-brittle matrix systems. At the present level of strength, it is possible to demonstrate tolerance to impact damage similar to that typical of resin matrix composites. As shown in Figure 10, only local damage is incurred by projectile impact. This is unlike the case of monolithic ceramics where total structural failure (shattering) would occur.

Figure 10

Front Impacted Faces of Graphite Fiber Reinforced Composites

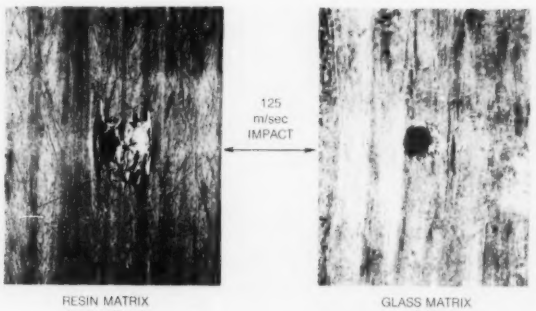

Figure 11

Microstructure of NiA1 Composites (a) 0% TiB_2 (b) 5% TiB_2 (c) 10% TiB_2 (d) 20% TiB_2

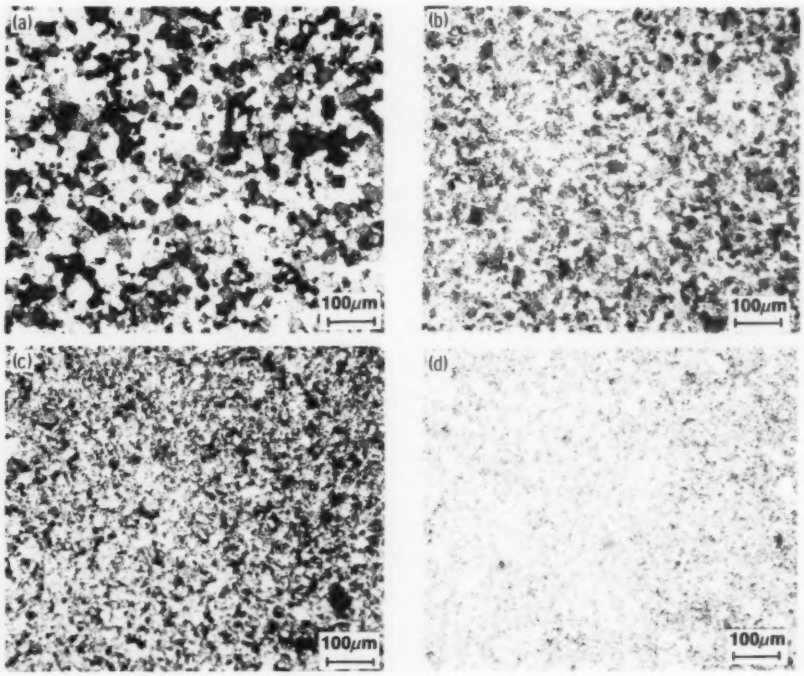

The current program is continuing to explore the fundamental mechanisms controlling ceramic composite performance so that systems exhibiting superior high temperature strength and stiffness may also be created to meet the needs in space based power, reentry, and other applications.

Nickel Aluminide/Titanium Diboride Composites

by XD™ Synthesis

Metal Matrix Composites are prime candidates for space applications in which high specific mechanical properties, high thermal and electric conductively, high vibration damping and, dimensional stability are important.

A new approach to forming metal matrix composites reinforced with XD™ particles not possible with standard metallurgical techniques, the XD™ process, has been under development at Martin Marietta Laboratories for the past several years. Under this program, an attempt is being made to apply the XD process to produce composites based on nickel

Figure 12

Transmission Electron Micrograph Showing TiB_2 Particles in NiA1 Matrix

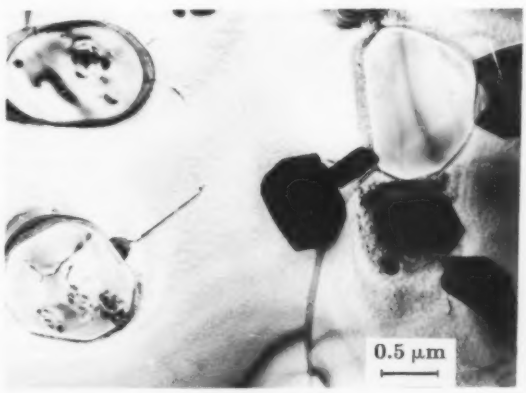

Figure 13

Room Temperature Hardness vs TiB_2 Volume Content

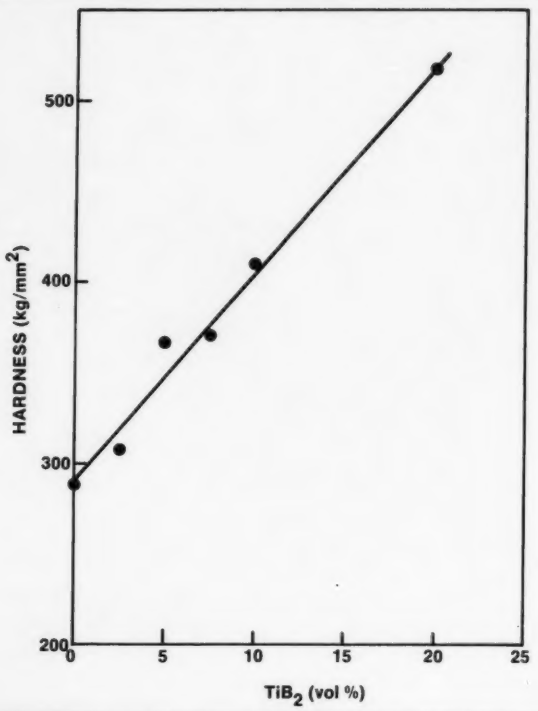

aluminides with enhanced high-temperature strength and low-temperature ductility.

Of the various nickel aluminides, NiAl has many attractive features, e.g., a very high melting point (1912 K)[2], high modulus (higher than that of steel)[3], low density (5.9 g/cm^3)[4] and excellent oxidation resistance [5,6]. Its major drawbacks are low strength at high temperatures and inadequate low-temperature ductility.[7] Although grain refinement may partially alleviate the ambient ductility problem[8] lack of adequate creep strength continues to be a disadvantage. The objective is to use XD™ synthesis to produce a dispersion of fine, discrete particles of a refractory second phase in this matrix, which will result in improved creep strength and enhancement[9] in toughness. An alternate approach to enhancing the high-temperature strength of NiA1 is to precipitate ternary compounds by adding group V elements.[10] However, because these dispersoids are produced by precipitation, they will be unstable at high temperatures. The present approach will not suffer from this limitation since the dispersoid can be preselected to be thermally stable and has the added advantage that the matrix as well as the dispersoid can be formed in a single step.

In the present investigation, NiAl with controlled volume fractions of titanium diboride ranging from 0.025 to as high as 0.5 was made. Titanium diboride is of interest because of its high modulus, low weight, and good thermal stability. Subsequent x-ray diffraction (XRD) and scanning electron microscopy (SEM) examination indicated that the thermal stability of TiB_2 in NiAl was excellent at least up to a temperature of 1500°C.

Figure 14

Flow Strength vs Strain Rate at 1200K

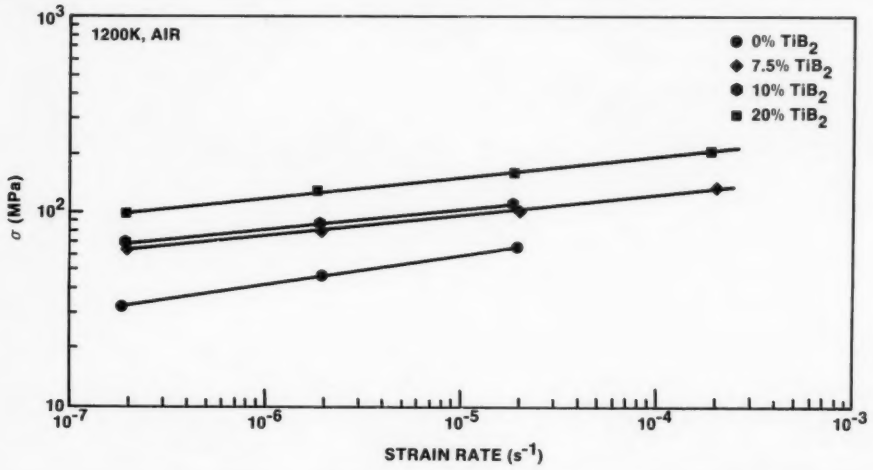

Figure 15

Flow Strength vs Strain Rate 1300K

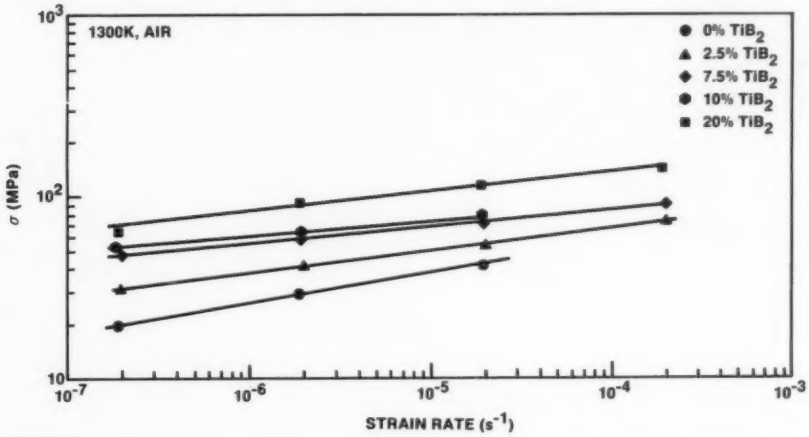

Figure 11 shows the microstructures of composites with 0, 5, 10, and 20 vol% tiB_2; small amounts of $A1_2O_3$ were present in all the samples. The average size of the TiB_2 particles was about 1 micrometer. Average grain size of the NiAl matrix decreased from about 30 micrometers in the 0 vol% material to about 8-10 micrometers in the 10 vol% material which should result in enhanced toughness. Further grain refinement for second-phase contents exceeding 10 vol% was found to be insignificant. A bright-field transmission electron micrograph from a composite with 5 vol%TiB_2 is shown in Figure 12. The TiB_2 particles appear to be well bonded to the matrix and show considerable substructure in the form of small angle boundaries, stacking faults and dislocation networks. The dark particles are $A1_2O_3$ measured densities for the various compositions agree well with calculated values, indicating adequate control on the amount of second phase. Room-temperature hardness measurements made on composites with 2.5, 5.0, 7.5, 10, and 20 vol% TiB_2 (Figure 13) show a systematic increase in room-temperature hardness with increasing TiB_2 content as expected.

The high-temperature deformation behavior of these composites was evaluated by measuring their stress-strain response in air at 1200 and 1300K and strain rates ranging from 2.0×10^{-7} to $2.0 \times 10^{-4} s^{-1}$. Their oxidation resistance was not adversely affected by the presence of TiB_2. Flow strength vs strain rate data for composites with 0, 2.5, 7.5, 10, and 20 vol% TiB_2 are shown in Figures 14 and 15. The flow strength of composites with 20 vol% TiB_2 is about three times higher than that of the base composition. All the materials exhibited the expected dependence of flow strength on strain rate. The strain-rate dependence of flow strength for the composites is less than that of the base material.

As mentioned earlier, a second important factor that limits the applicability of NiAl-based materials is lack of adequate low-temperature ductility. As tightly bound discontinuous and continuous composites have notoriously low fracture toughness, it is important to devise a manner to enhance the tough-

Figure 16

Damping Bahavior of Single-Ply (0°) P55/6061Al at Low Strain Amplitudes Indicating Little Strain Amplitude Dependence and Lower Damping than the 6061 Aluminum Matrix Alloy (Free-Free Flexure in Vacuum).

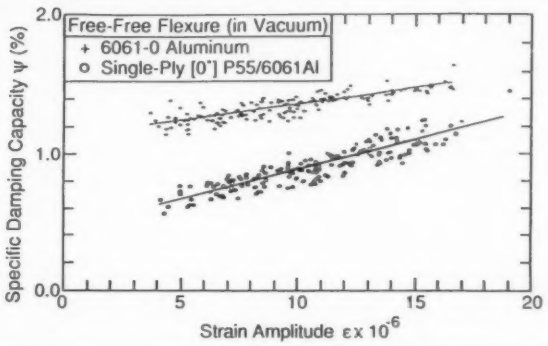
Free-Free Flexure (in Vacuum)
+ 6061-0 Aluminum
o Single-Ply [0°] P55/6061Al
Specific Damping Capacity ψ (%)
Strain Amplitude εx 10-6

ness in these composites. One possibility would be to use transformation toughening[11] of the NiAl matrix. A martensitic transformation occurs in NiAl at Ni-rich compositions and can be stress induced.[12] If this transformation can be made to occur at the tip of a crack, toughness could be improved. Room-temperature toughness might also be improved by incorporation of weakly-bonded whiskers in the NiAl matrix. Both approaches are being pursued. It is anticipated that future efforts in the development of these composites will be based on the use of TiB_2 for enhancement of high-temperature strength and the use of either transformation toughening or whisker-reinforcement for ambient toughening.

Damping Characteristics Of Metal Matrix Composites.

Primary concerns during acquisition, pointing and tracking (APT) maneuvers of large space structures (LSS) are to suppress vibration and achieve dynamic dimensional precision. Vibrational control can be achieved by various active control and passive damping measures. While the role of inherent material damping is frequently omitted in the active control analyses, it may provide a significant source of passive energy dissipation to ensure successful stabilization of large flexible space structures with fewer active controls.[13] Inherent material damping capacity of conventional structural alloys is very low. Preliminary damping measurements of structural materials such as continuous fiber-reinforced graphite-aluminum (Gr/Al) and graphite-magnesium (Gr/Mg) composites, which are important candidates for space applications, indicated that these metal matrix composites (MMC) exhibit high damping than their matrix alloys.[14] In the current SDIO/IST program, a systematic investigation is being conducted to understand fundamentally the damping mechanisms and subsequently develop an approach to enhance the damping capacity of Gr/Al and Gr/Mg composites. A unique and innovative approach using *in situ* characterization techniques is utilized to evaluate damping and to identify the sources of energy dissipation.

Initially, reliable test techniques were developed to obtain repeatable and reproducible data of unidirectional single-ply P55/6061 Al (Gr/Al) composites. Three different test techniques, free-free flexure, clamped-free flexure (cantilever beam) and tension-tension fatigue, were used. All flexural tests were conducted in vacuum because measured damping behavior can be severely affected by energy losses, particularly due to aerodynamic drag.[15] Both flexural and extensional mode tests were conducted at strain amplitudes from 1×10^{-6} to 800×10^{-6} within the frequency range 0.1 to 150 Hz. Like metallic materials, Gr/Al composites exhibited regions of strain amplitude independent and dependent damping. At low strain amplitudes levels ($\varepsilon < 10^{-5}$),the specific damping capacity, ψ, of Gr/Al composites was nearly independent of dynamic strain, and lower than the damping values of the aluminum matrix

Figure 17

Damping Behavior of Single-Ply (0°) P55/6061Al at Intermediate Strain Amplitude Dependent Behavior and Higher Damping that the 6061 Aluminum Matrix Alloy (Tension-Tension Fatigue).

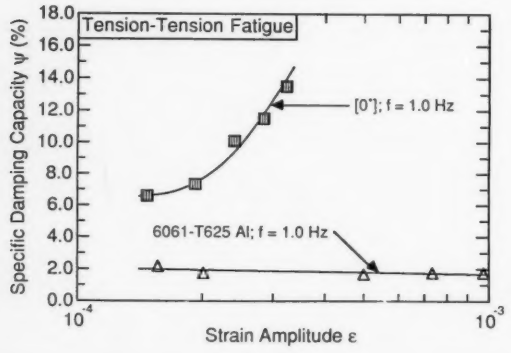

Figure 18

Comparison of Measured Damping Behavior versus the Behavior Predicted by the Micromechanical Model (J_2 Yield Criterion) for Single-Ply (0°) P55/6061Al Panels (Tension Tension Fatigue).

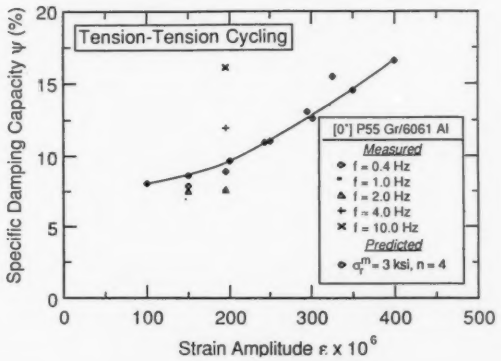

Figure 19

Granato-Lucke (G-L) Plot of Damping Data for Single-Ply (0°) P55/6061Al under Tension-Tension Fatigue Testing Indicating the Proper Strain Amplitude Dependence.

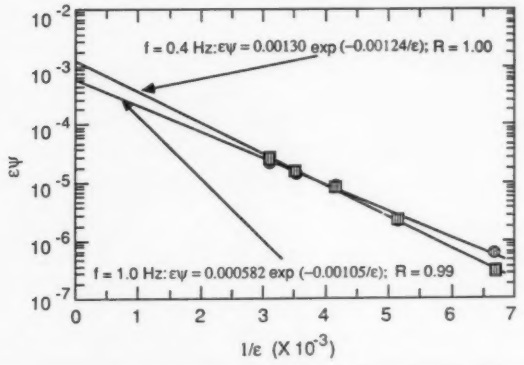

Figure 16. Damping behavior in this region can be explained using Hashin theory[16] which expresses the dynamic response to linear anelastic (or viscoelastic) composites in terms of their constituent fiber and matrix materials as shown below:

$$\psi_{11} = V_f\left(E_f/E_{11}\right)\psi_f + (1-V_f)\,(E_m)\,(E_f/E_{11})\psi_m \qquad (2)$$

where ψ_{11}, ψ_f and ψ_m are the axial specific damping capacity of the composite, fiber and matrix respectively, V_f is the fiber volume and E_{11}, E_f and E_m are the axial elastic moduli of the composite, fiber and matrix respectively. Generally, the damping contribution from Gr fiber is considered negligible as they are almost perfectly elastic. Using ψ_f of about 0.1% and ψ_m of 1.2%, equation 2 yields ψ_{11} of 0.41%, which is quite consistent with the measured value of 0.6% by the free-free flexure method. Energy dissipation at these low strain levels can be attributed to anelastic relaxation mechanisms involving atomic diffusion, dislocation relaxation (Bordoni Peak), dislocation resonance and the Zener thermoelastic effect.

At intermediate strain levels, the damping capacity increased with an increase in strain amplitude. Furthermore, the average for the composite was higher than the ψ value of the aluminum matrix, particularly in extensional mode Figure 17. Strain amplitude dependent damping response of these composites was examined in terms of both analytical micromechanical and microstructural models.

A micromechanical model was developed (based on the assumption that the energy dissipation is caused by local yielding of the matrix at intermediate strain levels) using the commonly known "J_2" yield criterion, i.e. effective damping energy depends upon distortional energy. This "J_2" damping is a nonlinear phenomenon and is affected not only by existing stress (strain) levels, but also by stress and thermal histories. It was observed that at any dynamic stress level, the predicted roman ψ values correlated reasonably well with the measured damping values (Figure 18), provided that contributions were included from residual stresses (present near the interfaces due to differential thermal contraction between fiber and matrix during consolidation). These results indicate that the residual stress state plays a significant role in the damping behavior of Gr/Al composites.

At the microstructural level, the strain amplitude dependent damping response was analyzed in terms of the Granato-Lucke (G-L) model.[17,18] According to G-L theory, dislocations breakaway from minor pinning beyond a critical strain amplitude, and damping arises from the resultant hysteresis in the dynamic applied stress vs. dislocation strain curve. The strain amplitude dependent damping component ψ_H can be expressed as $\psi_H = (C_1/E)\exp(C_2/E)$ where C_1 and C_2 are material constants related to microstructural parameters. Figure 19 show a G-L plot of Gr/Al test data, and the calculated mobile dislocation density from this analysis is of the order 10^{13} 1/m^2. Dense dislocation networks near the fiber-matrix interface in Gr/Al composites were also revealed during TEM examination that can be attributed to the differential coefficient of thermal expansion (CTE) between the fiber and matrix and the attendant residual stress state (Figure 20). Measured average dislocation densities of the order 10^{14} 1/m^2, obtained from various TEM images of inter-fiber matrix regions, is consistent with the mobile dislocation densities (10^{13} 1/m^2) predicted by G-L theory, suggesting that dislocation damping is the operative mechanism at intermediate strain levels.

Figure 20

TEM Image of Inter-Fiber Regions of Single-Ply (0° P55/6061Al Indicating Dense, Tangled Dislocation Substructures Near the Fiber-Matrix Interface.

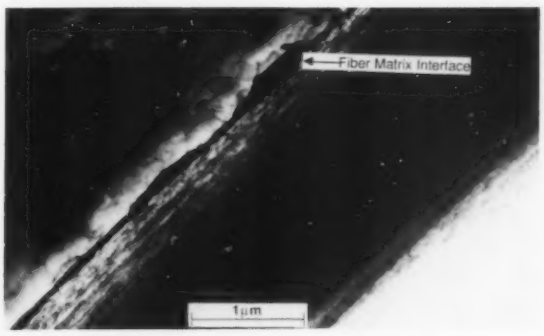

Damping test data analysis of Gr/Al composites showed that the matrix and attendant dislocation substructure near the fiber-matrix interfaces play a dominant role in energy dissipation mechanisms. Among metallic materials suitable for composite fabrication, cast megnesium alloys such as Mg-1%Zr, Mg-1%Mn and Mg-1%Si exhibit very high damping in the range $\psi \approx 50\% - 70\%$.[19] Subsequently, specimens fabricated from cast panels of P55/Mg-1%Mn and P55/Mg-1%Zr are being tested to examine their damping response. Preliminary test results indicate that these Gr/Mg composites exhibit higher damping than the aforementioned Gr/Al composites (Figure 21). From these damping results and microstructural examinations, it is believed that damping can be further enhanced by appropriate heat treatment to obtain the desired grain size and microstructure.

Submicron Moire Interferometry: A Revolutionary Tool To Investigate The Micromechanical Response Of New Generation Materials

Inherent to the concept of tailoring materials for a specific purpose is the ability to **quantitatively** understand the effects of such microstructural tailoring. The effects of tailoring a material spans orders of magnitude in effect - from neighboring local constituents such as fibers and interfaces at the micron level to gross structural level deformation at the centimeter level. This program is investigating the extension of an existing tool, Moire interferometry, into a revolutionary technique with an ability to visualize displacement fields over orders of magnitude yielding quantitative previously unseen phenomena from microstructural tailoring. The moire effect is observed when two superimposed repetitive patterns distort relative to one another and the distortion appears as a third pattern in space - a moire effect. Qualitatively, one terms the moire effect as **parallel optical data processing**. The moire effect is parallel due to the full field nature of the fringe pattern - it is not discrete. The data that is processed is the relative displacement between two gratings. The parallel nature of the moire effect is extremely powerful. If a grating is attached to a material such that it deforms with the material and is observed through an undeformed grating in space, the regions where material deformation becomes intense spatially becomes evident in the full field moire pattern. The grating attached to the material is the **active** grating and it samples the material surface deformation. The grating that is held constant in space is termed the **reference** grating and it computes the deformation field from the sampling, active grating. The computation speed is the speed of light. Quantitatively, each moire fringe is a **line of constant displacement** whose direction is perpendicular to the direction of the reference grating. The value of displacement associated with a moire fringe is simple:

$$U=N/F \qquad (3)$$

where U is the displacement value of the moire fringe,
N is the relative fringe order, typically from a datum.
F is the reference grating computational frequency (lines/inch, 1/in, or lines/mm, 1/mm)

It is evident then that the ability to sample material deformation is inversely proportional to the active grating frequency. The ability in accuracy of the computation is inversely proportional to the reference grating frequency. The upper limit of the mechanical moire line crossing effect is 1000 lines per inch (40 1/mm). This upper limit implies that the minimum deformation that could be detected on a material by a reference grating is 1/1000 of an inch (25 microns). More importantly the minimum spatial sampling that the active grating could sample is about 1/1000 of an inch. For new generation materials such as composites, the microstructural tailoring occurs on the micron level. Further the composites are extremely stiff. Important deformations occur in micron size regions with typically a few microns in total deformation over an entire sample. The mechanical moire effect is inadequate for this class of composites.

Moire interferometry eliminates both the low spatial sampling ability of the mechanical active grating and the low computational accuracy of the reference grating. In moire

Figure 21

Damping Behavior of As-Cast (0°) P55/Mg-1%Zr Exhibiting Higher Damping than P55/6061Al Composites (Clamped-Free Flexure in Vacuum).

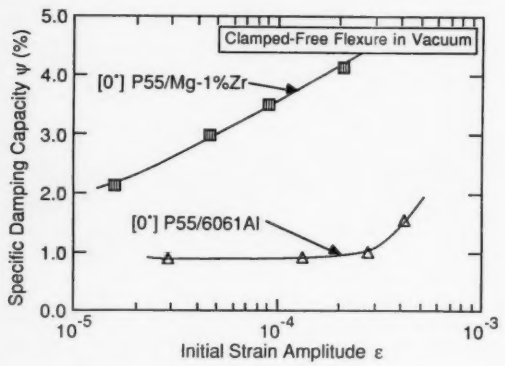

interferometry typical active grating frequencies are 30,000 lines/in (1200 1/mm) with computational reference grating frequencies of 60,000 1/in (2400 1/mm). Moire patterns are being produced that can sample spatial detail in materials as low as 1/1200 of a mm (0.8 microns) with a sensitivity to compute in-plane deformation as low as 1/2400 of a mm or 0.4 microns! By employing pulsed light sources we now have the ability to time sample transient deformation events as low as a millionth of a second (1 microsecond). What does this mean in physical terms? We now have the ability to look at the deformation fields from strong transient impacts in composite interfaces where high degrees of microstructural tailoring take place and where the subtle beginnings of material failure begin.

Moire interferometry achieves such high grating frequencies by using the interference that occurs between two coherent beams of laser light interacting at a relative angle. The two beam interference yields a grating - whose frequency can achieve half that of the frequency of light employed. For blue - green light this upper limit is about 100,000 1/in or 4000 1/mm! In moire interferometry the spatial grating is photographed and replicated onto the material. When the material is deformed in front of the two laser beam spatial grating moire patterns of extremely high sensitivity are produced. In addition, pulsed lasers may be employed to strobe light thus freezing transient deformation fields in advanced composites under impact. The laser pulse width is 20 billionths of a second (20×10^{-9} sec.) - fast enough to freeze stress wave displacement fields in composite interfaces traveling in excess of 8 km/s! We are now beginning to understand the fundamental mechanisms of transient impact delamination in composites.

In Figure 22 moire interferometry was utilized to study microplasticity occurring between bundles of 10 micron graphite fibers and the magnesium matrix of a metal matrix composite subjected to vibration in a three-point bending

Figure 22

Static Moire Interferometry — Single Cycle Hystersis Damage.

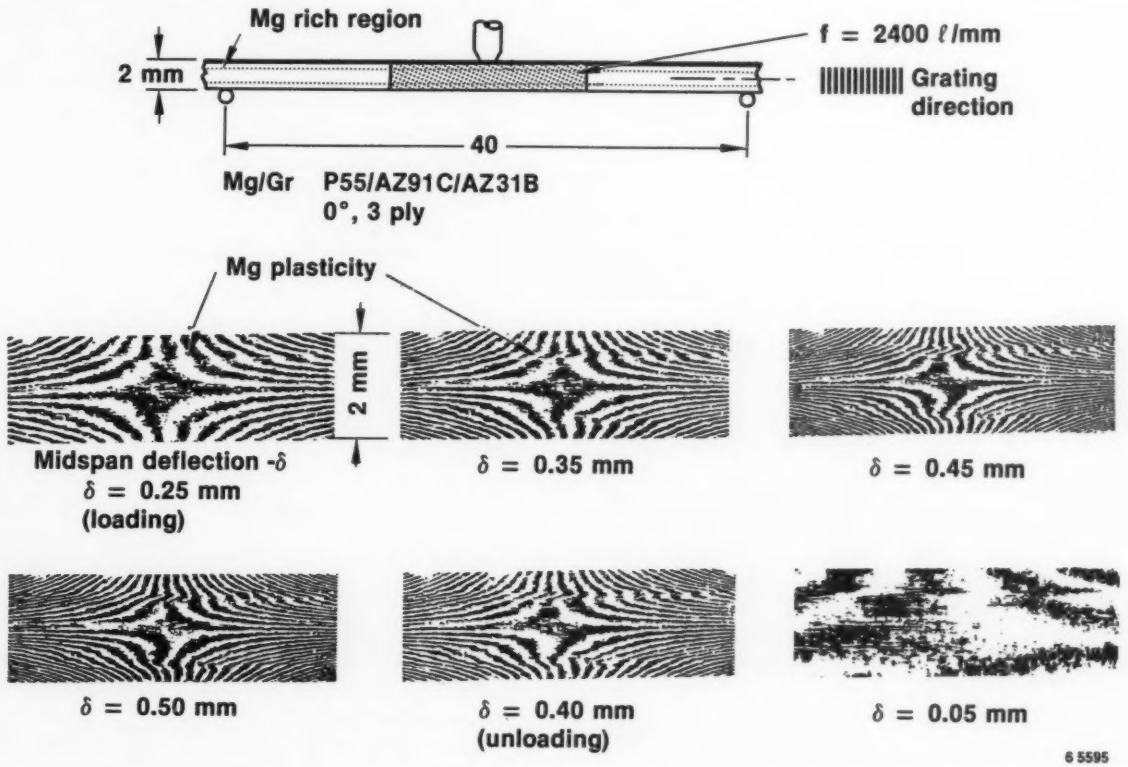

mode. The discontinuity appearing in the displacement field is the magnesium microplasticity occurring at the fiber bundle interface - a mechanism of material damping previously unseen. It is seen that the fringes really contain fine articulations. These fine articulations are individual 10 micron fibers shearing in the magnesium rich region that joins She larger bundles of 10 micron fibers.

Figure 23 details the dynamic aspects of moire interferometry. A graphite/epoxy composite is impacted to introduce transient waves parallel in the direction of the composite layering. This composite is composed of alternating layers of graphite fibers 90 degrees (perpendicular) to the impact direction and 0 degrees (parallel) to the impact direction. The Figure shows fringes of constant displacement spanning the specimen free edge. Each fringe is an increment of compressive displacement of 0.4 microns. Within each spanning fringe are fine articulations corresponding to the number of alternating 0 and 90 degrees layers. These articulations are due to the different speed of wave propagation between the 0 and 90 degree layers. Within the 90 degree layers the impact wave travels at 3 km/s. Within the 0 degree layers the impact wave travels at 8 km/s. The result is that these two different speeds meet at the interface causing a strong interfacial shear. Under stronger impacts delamination and spalling would occur.

Concluding Comments

Many of the future Strategic Defense Initiative systems are materials limited. These materials needs can best be met by tailor-making advanced composites, with properties optimized for specific applications.

The goal of the advanced composites program of the Innovative Science and Technology Office of SDI is to make possible new design options for design engineers developing systems for the Strategic Defense Initiative. The program approach is to demonstrate the feasibility of innovative composites and to establish a firm basis of scientific understanding of composite phenomena.

Figure 23

Dynamic Moire Interfermerometry — G/E Composite Stress Wave Behavior.

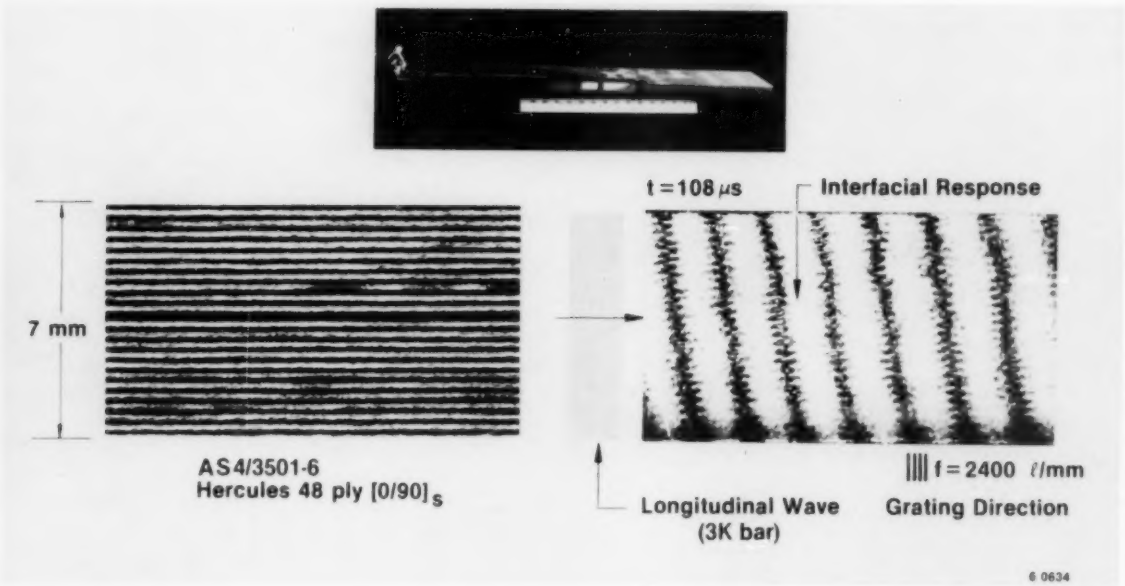

Biographies

Dr. Steven G. Fishman is Program Manager of Structural Materials at the Office of Naval Research, Arlington, Virginia. His papers and research have been in solid state diffusion, mechanical properties of composites and corrosion of metals. He is chairman of the ASM-AIME Joint Composites Committee.

Dr. James A. Cornie is Director of the Metal Matrix Composites Processing Center at the Massachusetts Institute of Technology, Cambridge, Massachusetts. He is a noted expert in composite processing and has conducted extensive research in liquid metal infiltration of fibrous preforms.

Dr. Karl M. Prewo is Manager of Materials Science at United Technologies Research Center, East Hartford, Connecticut. His research has been in the areas of ceramic composites and metal composites processing and mechanical properties. He is a member of the American Ceramic Society and a Fellow of the American Institute of Mining, Metallurgical and Petroleum Engineers.

Dr. R. K. Viswanadham is Group Manager, Metallic Materials, Multimetals Inc., Louisville, Kentucky. His research interests are in intermetalics processing and mechanical processing of metals.

Dr. Mohan S. Misra is Manager, Materials and Structures at Martin Marietta Aerospace, Denver, Colorado. He is involved in research in mechanical behavior of advanced composites and structural metals, He is a member of the American Society of Materials.

Dr. John S. Epstein is Assistant Professor at Georgia Institute of Technology, Atlanta, Georgia. His publications and interests are in the fields of interferometry, laser non-destructive evaluation methods and mechanical properties of materials.

References:

1. J. Aveston, G.A. Cooper and A. Kelly, "Single and Multiple Fracture," PP- 15-26 in the Properties of Fiber Composites, Conf. Proc. Nat. Physical Lab., IPC Science and Technology Press Ltd., Surrey, England, 1971.

2. M. Hansen and K. Anderko: Constitution of Binary Alloys, McGraw Hill, New York, NY, 1958, and the supplements by R.P. Elliott, 1965 and by F.A. Shunk, 1969.

3. M.R. Harmouche and A. Wofenden: J. Test. Eval., 1985, vol. 13, no. 6, P- 424.

4. A.J. Bradley and A. Taylor: Proc. R. Soc., Ser. A, London, 1937, vol. 159, p. 56.

5. E. Fitzer and P. Gerasimoff: Z. Metallk., 1959, vol. 50, p. 187, referenced by E.A. Aitken in Intermetallic Compounds, Ed. J.H. Westbrook, John Wiley, New York, NY, 1967, p. 507.

6. V. Imai and M. Kumazawa: Sci. Rept. Res. Inst. Tohoku Univ., 1959, vol. II, No. 4, referenced by E.A. Aitken in Intermetallic Compounds, Ed. J.H. Westbrook, John Wiley, New York, NY, 1967, p. 507.

7. E.M. Grala: Mechanical Properties of Intermetallic Compounds, Ed. J.H. Westbrook, John Wiley, New York, 1960, p. 358.

8. E.M. Schulson and D.R. Barker: Scr. Metall., 1983 vol. 17, p, 519.

9. J.C.M. Li and S.C. Sanday: Acta Metall., 1986, vol, 34, no. 3, p. 537.

10. M. Sherman and K. Vedula: J. Mater. Sci., 1986, vol. 21, p. 1974.

11. A.G. Evans and R.M. Cannon: Acta Metall., 1986, vol. 34, no. 5, p. 761.

12. S. Rosen and J.A. Goebel: Trans. AIME., 1968, vol. 242, p. 722.

13. H. Ashley: *On Passive Damping Mechanisms in Large Space Structures.* AIAA Paper No. 82-0639, 23rd Structures, Structural Dynamics and Materials Conference, April 1982, p. 56.

14. M.S. Misra and P.D. LaGreca: *Vibration Damping 1984 Workshop Proceedings*, AFWAL-TR-84-3069, Nov. 1984, p. u-1.

15. N.E. Baker, W.E. Wollam and D. Young: *International Journal of Mechanical Science*. 9,743, 1967.

16. Z. Hashin: *International Journal of Solids and Structures*, 6(6), p. 797, 1970

17. A.V. Granato and K. Lucke: *Journal of Applied Physics*, 27(6), p. 583, 1956.

18. A.V.Granato and K. Lucke: *Journal of Applied Physics*, 27(7), p. 789, 1956.

19. D.F. Walsh, J.W. Jensen and J. W. Rowland: U.S. Bureau of Mines, Report #6116.

Imploding Krypton Gas Puff Plasmas As A Potential Source For X-Ray Lasers

J. Davis
Naval Research Laboratory

Abstract

An existing technology is finding a new application in the study and development of laboratory x-ray lasers. Capacitively discharged pulsed power generators are being used to drive material loads to produce hot dense plasmas that possibly can be used as a medium for x-ray lasing or as a radiation pump source to photopump a variety of specially designed x-ray targets. The possibilities are considered of using pulsed power generators to drive a configuration of coaxially cylindrically symmetric krypton gas puff plasmas to conditions conducive to achieving gain in several lasing transitions of neonlike krypton. Using a fully self-consistent radiation hydrodynamics model, numerical simulations are performed driving the outer plasma inward where it crashes onto the core plasma establishing highly localized regions in the compressed core plasma. It is shown that in the localized regions it is possible to generate plasma conditions that can support a population inversion leading to gain in excess of unity in several transitions. Contour plots are presented during the collision process illustrating the behavior of the temperature, density, and gain in the core plasma.

Introduction

Since the development and utilization of optical lasers there has been a steady flow of ideas and progress toward the development of lasers with shorter and shorter wavelengths. In the last few years this effort has been rewarded with the successful demonstration of lasing in the soft x-ray region of the spectrum. This accomplishment was achieved by irradiating a specially designed target with a high powered infrared laser to create a hot dense plasma with properties conducive to lasing. The need to create a dense hot plasma as the material medium in which lasing will occur is due to the requirement that x-ray line emission is generally the result of atomic transitions between widely separated energy levels of highly charged ions. This suggests that the material medium cannot be in the solid or even in a neutral gaseous state but must instead be a hot plasma. This, of course, is the more conventional and time honored approach to x-ray lasers. It does not preclude some of the recent and exciting research involving free electron lasers, electron channeling, and multiphoton absorption concepts. However, these innovative approaches are just in their formative stages and need time to mature and reach their full potential.

absorption concepts. However, these innovative approaches are just in their formative stages and need time to mature and reach their full potential.

Since the majority of present day lasing schemes depend on the creation of a hot dense plasma, there are two separate but related issues that must be addressed. The first issue deals with the choice of a lasing scheme and a determination of the plasma conditions required to produce a population inversion and gain in the lasing transitions. The second issue deals with the selection of a power source capable of generating a plasma with the desired conditions. Both issues can be related by designing targets that are tailored to a particular power source in the hopes of producing a plasma with the desired conditions for lasing. Unfortunately, this is often easier said than done and generally requires a vigorous interaction and fine tuning between theory and experiment.

In general, the atomic processes leading to a population inversion and lasing in the x-ray region are the same ones responsible for lasing in optical lasers, only here they involve more energetic electrons in a hotter environment. Lasing generally occurs as the result of the microscopic processes between atoms (meant to include ions, also) and subatomic particles such as electrons and photons. The electrons are initially liberated from the atoms as a result of externally supplying substantial amounts of energy to the system. As the constituents of the system absorb the energy with a corresponding increase in temperature, electrons are freed (ionized) from the atoms. The electrons now gain energy from the source and in their random walk through the medium crash into the more massive slower moving atoms and ions and further ionize the medium. The process avalanches and continues until a kind of quasi-equilibrium is achieved and a balance is reached between energy in and energy out. During this process the average charge state of the plasma is increased and the plasma emits radiation; electrons are being liberated (ionization) and captured (recombination) and photons are being born (spontaneous decay and recombination) and either die (absorption) or escape the plasma carrying information about the environment it came from (in much the same fashion as astronomers learn about the stars). During this cavalcade of events the plasma percolates and its constituent atoms and ions have their levels populated, i.e., excited by the various collisional and radiative processes. A sample energy level or Grotian Diagram (as it is called) is shown in Figure 1 for a heliumlike atom (i.e., with two electrons orbiting the nucleus). A selected number of levels are shown with their spectroscopic labels along with some of the processes involved in populating them. The process describing the evolution of level population is commonly referred to as ionization dynamics. The first step toward theoretically developing a laser is the requirement of creating a population inversion in one or more of the levels. An inversion occurs when the level population "piles up" over and above that normally achieved in most plasmas. The strategy to accomplishing an inversion is to choose an atom

Figure 1

Typical energy level diagram of heliumlike ion illustrating several processes leading to line emission.

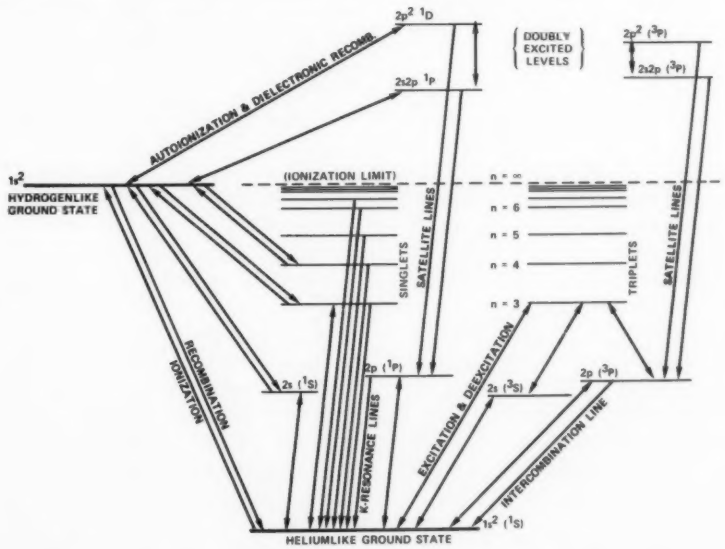

Figure 2

Schematic of Double Gas Puff

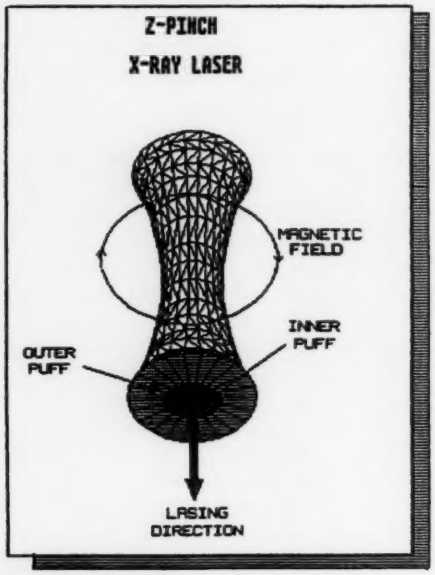

Figure 3

Key energy levels of neonlike krypton.

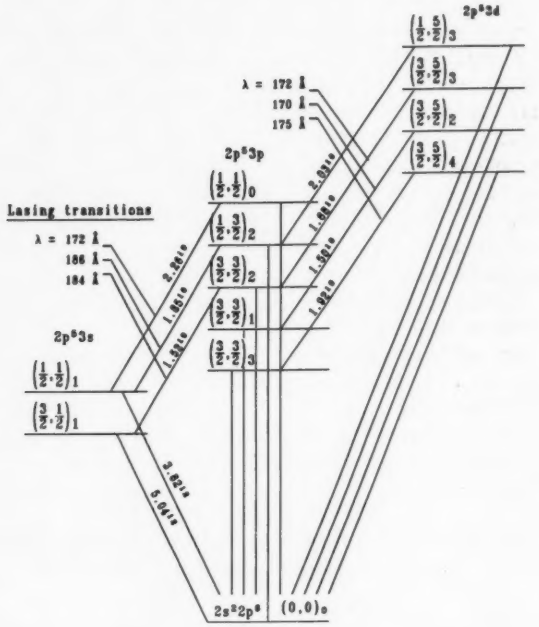

whose atomic level structure, under the right plasma conditions, is conducive to overpopulation with respect to the ground state.

We will focus on the neonlike system of krypton (i.e., krypton in an ionization state with only ten bound electrons remaining) because its unique atomic structure makes it a prime candidate for establishing a population inversion in the manifold of excited states. Once the inversion is obtained, then the competition between the various atomic processes depopulating the inverted states occurs. If radiative decay to selected lower states dominate the de-excitation process, the emission of a monochromatic beam of soft x-rays will follow. Gain in the lasing transitions will occur if the intensity of the x-rays in transit through the material is described simply by the relationship $I = I_o \exp(GI)$ where I is the emitted intensity of the beam at a distance 1 for its origin with intensity I_o.The gain coefficient, G, is positive and depends on the atomic and plasma properties for the medium. Under ordinary circumstances, a beam of light traversing a medium of length 1 is attenuated along its path length and emerges reduced in magnitude, depending on the opaqueness of the medium, i.e., G is negative and represents the absorption coefficient. For gain to occur the wave must be exponentially amplified rather than reduced in magnitude while traversing the medium. In principle, with the appropriate physics models and numerical simulation codes, it is possible to theoretically determine under what conditions inversion and lasing will occur and whether such conditions can be created in the laboratory. We now turn to the issue of generating the plasma.

The power source considered here has been around for some time now and initially was employed extensively in the early days of magnetic fusion research, viz., pulsed power. More recently, pulsed power drivers have been used successfully to generate plasmas for use as intense high brightness sources of x-rays for nuclear weapons effects testing. Conceptually, the simplest of these devices is the so-called z-pinch. The z-pinch in its basic configuration is a cylindrically symmetric plasma carrying an axial current which both heat and confine the plasma by its own induced magnetic field. As the current increases, the magnetic field also increases and compresses the plasma, accelerating it radially inward, causing increased heating by converting the kinetic energy of inward motion to thermal energy; containment and heating occur together. Unfortunately, when driven by very large currents these plasmas exhibit pathological behavior by becoming unstable and ultimately breakup. For both fusion and x-ray laser applications this behavior is obviously undesirable. On the other hand, one of the most attractive features of the z-pinch plasma is its natural elongated shape as a medium in

which to exhibit lasing and gain. Whether it is possible to use these plasmas in an x-ray laser scenario is actively being pursued.

It recently has been suggested that by properly designing material loads it should be possible to delay or deter the growth rate of the instabilities for times longer than the characteristic lasing time.[2] Preliminary experimental results based on concentric gas puffs appear to support this hypothesis.[3] In order to take advantage of these new findings on stability our target is configured as concentric axially symmetric krypton gas puffs. The outer gas puff is a hollow cylindrical annulus while the inner gas puff is uniform and symmetric about the axis. The scheme is conceptually shown on Figure 2. Discharging a megajoule capacitor bank through the gas puffs causes rapid ionization by ohmic heating. As the current continues to flow and increases to a peak value of between 3 to 5 magampers the induced magnetic field stops the plasmas' outward expansion and begins to compress the plasma accelerating it radially inward on a collision course with the inner plasma. The dynamics of the implosion is often characterized as a "slowplow" because it behaves in a similar fashion by scooping up and compresssing more and more mass as it moves along. During the run-in the outer plasma can achieve speeds in excess of a million miles per hour before it crashes and stagnates on the inner plasma. During this phase of the implosion the inductive or magnetic energy is constantly being converted to kinetic, thermal, ion internal, and radiative energy.

Because the plasma evolves through a series of temperatures and densities, its radiation pattern similarly evolves from the infrared to the visible, the ultraviolet, and the x-ray region of the spectrum, becoming a broadband radiator. In order to produce a plasma with just the right temperature and density history for lasing to occur, it is important to match the drivers electrical characteristics with the load design and configuration. Since we are focussing attention on the neonlike ionization stage the electrical parameters must be chosen so as to optimize the plasma conditions for its production. Once into the neonlike stage the level populations are determined by the ionization dynamics. An abbreviated Grotian energy level diagram is shown in Figure 3 along with the level's spectroscopic identification, quantum numbers, and the wavelengths of the lasing transition in Angstrom units (10^{-10} meter). In addition, the spontaneous decay rates of the lasing transitions are also shown on the Figure; the notation, e.g., of the 172 A line between the 3p and 3s states is shown as 2.26^{10} which translates to 2.26×10^{10} sec.$^{-1}$ giving the lifetime of the upper 3p state as $1/2.26 \times 10^{10}$ sec.$^{-1}$ = 4.42×10^{-11} sec.

Figure 4

Schematic of Numerical Simulation Code.

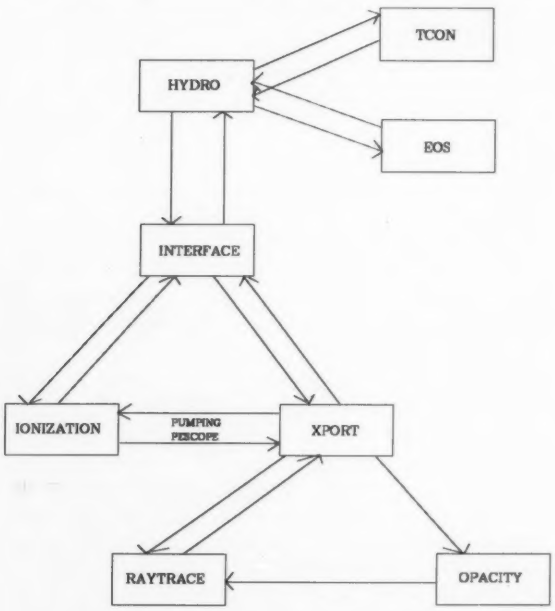

Figure 5

Initial conditions of Gas Puffs.

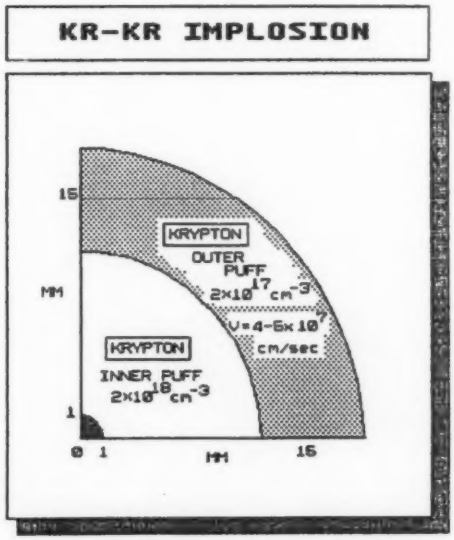

Figure 6

X-ray emission spectra including line and continum components.

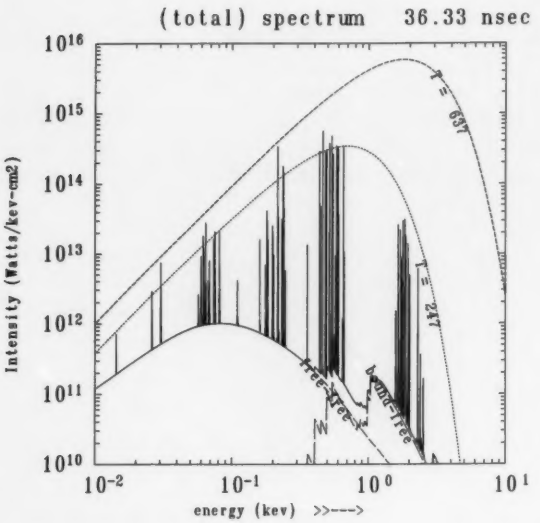

Model

The implosion dynamics of the krypton gas puff plasma is described by the one dimensional equations of radiation hydrodynamics. For simplicity we ignore the magnetic field and replace its effect on the system by assuming the outer plasma has an initial kinetic energy and moves with a constant velocity. This replicates the initial stages of the implosion dynamics but avoids the complex chain of events that occur during the first nanoseconds when the initial surge of current encounters the gas puffs causing phase changes and eventually ionizes them. Also, since there is reasonable evidence from the preliminary analysis of recent experiments and numerical simulations that lasing, if it is to occur, will be achieved well before the onset of the destructive interference caused by the formation of plasma instabilities, we will ignore the problem of plasma instabilities. With these caveats, the model contains enough of the relevant physics to provide a reasonable representation of events describing the behavior of the plasma column as a lasing medium.

The overall morphology of the evolving gas puff plasmas can be schematically represented by appealing to the adjacent flow chart, Figure 4, characterizing the system of equations used to describe the chain of events.

In the diagram the different boxes denote the various physical processes involved in characterizing the implosion dynamics. The arrows entering and leaving each box indicate physical quantities serving as input or output data for each of the subroutines. Although the structure of the flow chart is suggestive of a scaler process, the actual calculation is nonlinear and requires a series of interactive iterations between the various subroutines before a unique solution is converged upon. The actual form of the equations, numerical techniques, and numerical zones are presented elsewhere (for those interested in the details of the simulation see reference 4). The equations of hydrodynamics, denoted as HYDRO, describes the fluid properties of the plasma including shock wave phenomena. TCON and EOS are ancillary subroutines representing thermal conduction processes and equation of state information, respectively. The lower portion of the schematic diagram represents the ionization and radiation physics. Included are the ionization dynamics of nonequilibrium plasmas, radiation absorption and emission processes, and the transport of radiation. All these processes, from above and below, are funneled into a kind of "mixing bowl" labeled Interface. The mixing bowl assimilates all the information and passes the quantities up and down and iterates on them until a converged set of quantities is obtained in each zone of the numerical mesh.

A number of computer simulations were carried out for a variety of gas puff conditions. One of the more interesting simulations resulted from the initial set of conditions shown on Figure 5. Both inner and outer puffs are composed entirely of krypton gas with about seven times more mass contained in the outer puff (140 μgms compared with 20 μgms). The distribution of mass is Gaussian with the bulk of mass located at 15 mm and 1 mm, respectively from the origin. The initial temperature of the outer (inner) gas puff plasma was taken to be 2.5ev (0.5ev). A tenuous background plasma pervades the space between the inner and outer plasmas and has a density of 5×10^{-7} gm/cm^3. This background level was chosen for numerical convenience and is sufficiently low that it has no influence on the results. The outer plasma starts moving inward with a speed reaching upwards of about 1 million miles per hour (actually 4.5×10^7 cm/sec.). The leading edge crashes into and stagnates onto the inner plasma. The "collision" continues in a snowplow-like fashion with more and more mass being accumulated and stacked up on the inner plasma. During this collision process the kinetic energy of run-in is redistributed into thermal, ionization, radiation and kinetic energy associated with the generation and propagation of shock waves and the outward motion of material after the "bounce." This oscillatory motion continues until it is damped by vicious forces. The interface region between interacting plasmas is where most of the interesting phenomenon occurs and where we expect lasing to be observed.

Figure 7

Plasma Temperature as a function of time and radius.

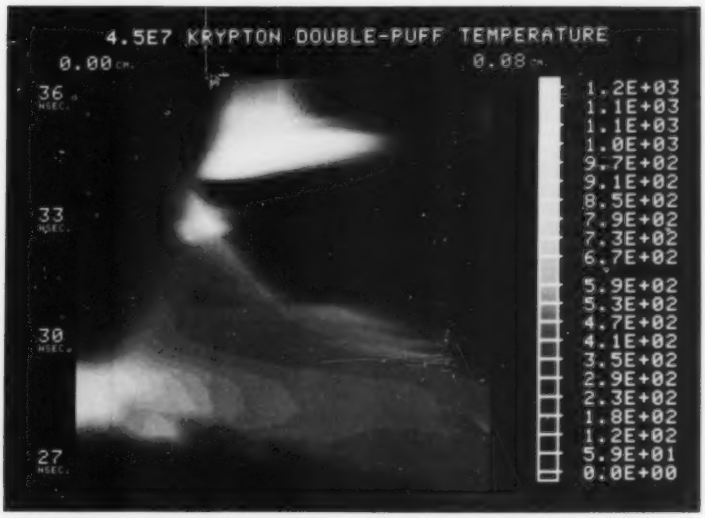

Figure 8

Plasma Ion Density as a function of time and radius.

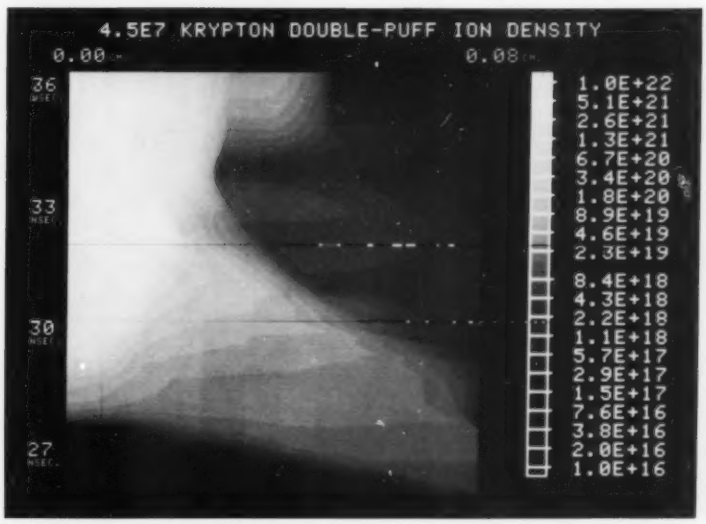

Figure 9

Fraction of neonlike ions as a funtion of time and radius.

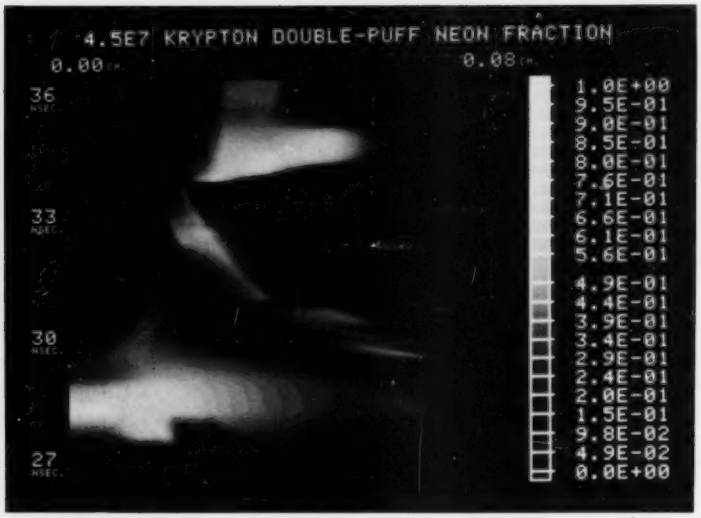

Figure 10

Gain per cm of the 170Å line as a function of time and radius.

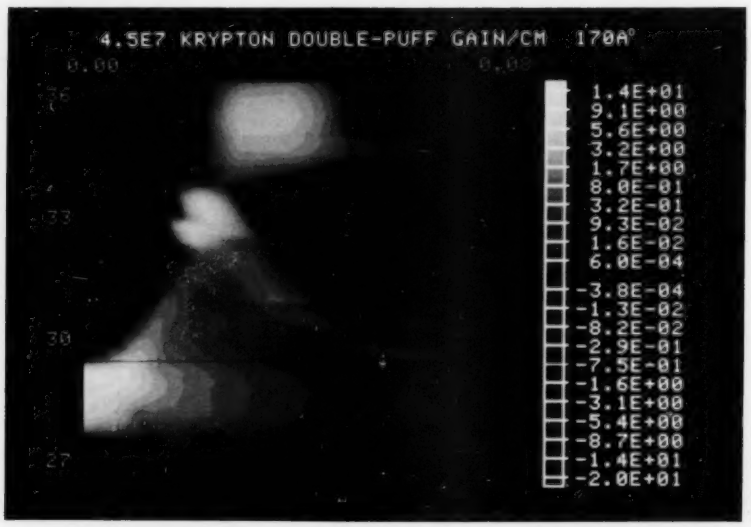

Figure 11

Gain per cm of the 172 Å line as a function of time and radius.

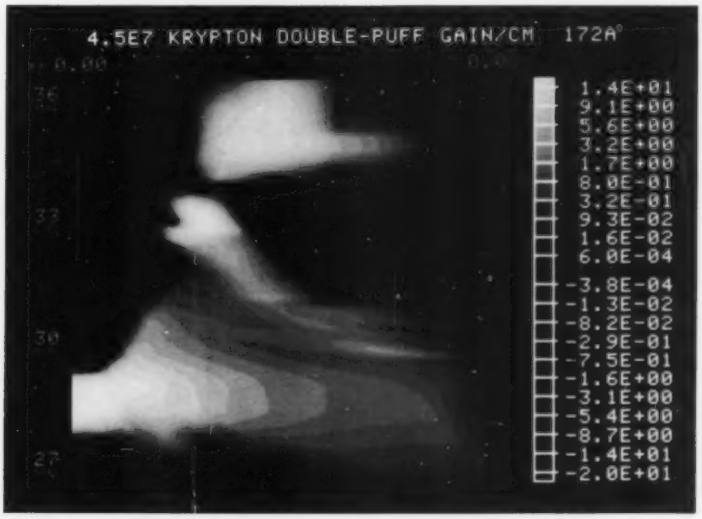

The radiation emitted during this sequence of events not only cools the plasma but is the messenger of conditions within the plasma. The emission spectra is a "fingerprint" that can lead to knowledge about the temperature, density, size, opacity, and velocity of the emitting region. A typical emission spectra is shown in Figure 6 at 36.33 nsec into the implosion. The snapshot picture of the radiation signature shows the intensity of radiation in terms of spectral lines (spike-like structures) sitting on top of a continuum of radiation composed of recombination and bremsstrahlung as a function of photon energy extending from 10 - 10,000 eV. Most of the line radiation from 400 to 2,000 eV originates from neonlike krypton. This is very encouraging because it is in the neonlike system that we expect lasing to occur. The temperature associated with the spectra is several hundred eV and the particle density of neonlike ions is between 10^{18} and 10^{20} ions/cm^3 in the interface region. The curves represented by T=637 and 247 correspond to a plasma radiating as a Blackbody at those temperatures in eV and are simply there to indicate what a blackbody spectrum would look like in comparison with the actual radiated spectrum.

A novel way of presenting the results of the numerical simulations is to illustrate the behavior of the physical parameters such as temperature, density, and gain as a function of time and radius in the region where the two plasmas interact. In the following Figures time runs along the vertical axis from 27 nsec to 36 nsec and displacement or radius runs along the horizontal axis from the origin out to 0.08 cm. In this region the core plasma is being compressed and heated by the incoming outer plasma. Initially, the core plasma is relatively cold but as the outer plasma gets hot it starts radiating with some fraction of the photons impinging on the core plasma causing its temperature to rise. This process continues until the bulk of the outer plasma stagnates onto the core plasma causing further heating. During the collision the core plasma becomes hot and begins to expand, radiate, cool, and recombine. The various shades of light and dark are coded on the Right Hand Side (RHS) of the figures. There are several ways to understand and interpret the results. One of the easiest is to choose a time and then observe how the parameters vary from larger to smaller displacements and simply repeat the process for increasing times. Also, remember that these results extend into the plane of the figure for the length of the cylinder, which is 3 cm, or for a distance over which the quantities are uniform and homogeneous, which appears to be about 1.7 cm^3. The radial temperature history is shown on Figure 7 over distances mainly confined to the compressed core plasma and the interaction region. The brighter regions are primarily the result of compressional wave heating or weak shocks. The expanding darker regions later in time extending from the axis outward reflect the effects of radiative cooling while the brighter regions from 34 nsec on, indicate heating due to weak shocks moving outwards. The temperature peaks around 1 kilovolt (over 11 million degrees) in this region. The ion density is

shown on Figure 8 where it is seen that as time increases the density along the axis increases where the plasma is compressing. These high pressures near the origin slow down the incoming plasma creating velocity gradients at about 33 nsec. Thus, kinetic energy is constantly being thermalized in this region, commencing just after the on-axis assembly. Radiation cooling in this region falls off sharply with radius following the corresponding density falloff. Just after 33 nsec, the plasma near the origin begins to expand in a complicated fashion; parts of the plasma move outwards while other parts continue their inward motion. This produces compressions and rarefactions leading to heating and cooling in localized regions. At just after 34 nsec, the plasma at about 0.008 cm from the origin is expanding radially while elsewhere the plasma is moving radially inwards. From the contour plot of temperature shown on Figure 7, it can be seen that alternating rapid cooling and heating is produced from 33 to about 36 nsec in localized regions. Very large pressure gradients which have been built up at 24 nsec will very quickly be relieved. At 35 nsec relief of the large pressure gradient has caused a virtual stagnation to occur at about 0.035 cm. Plasma is now moving radially outward from this point and colliding with imploding plasma. As a result, a fairly broad shell of hot plasma (about 1 kev) has been produced. Since the ion density is fairly low over much of this region the radiative cooling rate is not excessive.

The fraction of neonlike krypton ions in the ground state is shown on Figure 9. Since the fractional abundance of neonlike ions is strongly temperature dependent and only weakly density dependent, it is not to surprising to observe that the number of neonlike ions tracks the temperature. The greater abundances occur for temperatures in excess of about 400 ev which is about the threshold temperature for the appearance of neonlike krypton. Shown on Figure 9 are a number of localized regions where the fractional abundance of neonlike ions exceed 50% and a few regions where it is upwards of about 70%, i.e., in those regions of the plasma anywhere from 50 to 70 percent of all the ions are in the neonlike ground state. A very propitious situation, indeed, for our proposed x-ray laser scheme!

By way of an introduction to the final gain calculations a few words are in order explaining the relationship between the shape of a spectral line and the gain in the lasing transitions. Whenever a transition between discrete states of an atom in a plasma takes place a spectral line is radiated from the plasma. Contrary to the results presented on Figure 6 spectral lines emitted from plasmas do not appear as infinitely sharp lines or spikes. Under closer scrutiny with good wavelength resolution it is possible to observe a spectral line profile as a function of wavelength is generally distributed symmetrically about its unperturbed wavelength representing the separation of the two atomic energy levels involved in the transition. The line profile or distribution function results from such line broadening effects as the finite lifetime of the upper state of the atom, which is a result of the Uncertainty Principle, collisions and

Figure 12

Gain per cm of the 184 Å line as a function of time and radius.

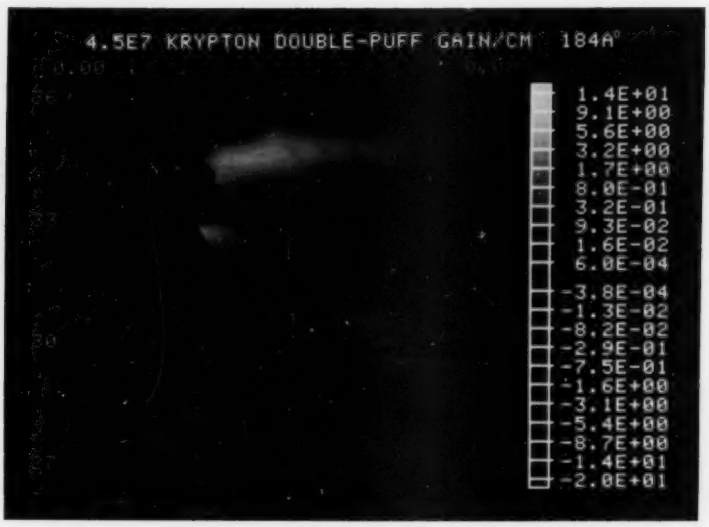

environmental influences which also manifest themselves in broadening the spectral line. Oftentimes it is just these effects on spectral lines that provide valuable information on conditions within the environment. In the gain calculations presented here the line profile functions are represented by Voigt functions, i.e., a convolution of Lorentzian and Doppler width profiles where the damping parameters for the Lorentzian is composed of natural and collision broadened widths and the Doppler includes thermal and motional broadening effects. The transport of radiation in the presence of large velocity gradients is accounted for in the Sobolev approximation developed for the expanding envelopes of stars.[4]

Conditions conducive to a population inversion leading to gain in the lasing transitions were achieved for three of the lines: the 172, 170, and 184Å lines, respectively. These results are shown on Figures 10, 11, and 12, respectively. Reference to Figure 3 shows the wavelengths of the respective transitions. Gains of one or more occur in highly localized regions eventually achieving values in excess of 9/cm for the 172Å line; 5/cm for the 170Å line; and 3/cm for the 184Å. The atomic processes contributing to the gain are predominantly due to recombination and electron impact excitation. The gain 172Å line extends over the largest radial region extending from the origin out to about 0.048 cm from 28 to 29 nsec. A more localized region occurs from 34 to 36 nsec. The gain for the 170Å line occurs at the same time but is confined to smaller regions. Finally, gain for the 184Å line, which is due predominantly to electron collisions, is confined to an even smaller region peaking around 35 nsec. Note, that on the scale on the RHS of the gain profiles some of the values represented are negative numbers and correspond to absorption of radiation. The point to be made is that it is possible to achieve a population inversion and gain in three of the expected lasing lines from our imploding plasma scenario. The final confirmation of whether this approach is feasible is currently unfolding with the analysis of the experimental observations. Preliminary results are very encouraging.

Acknowledgements

The research presented in this paper represents a collaborative effort with Drs. R. Clark, J. Apruzese, and P. Kepple.

This work was supported by the Innovative Science and Technology Office of the Strategic Defense Initiative Organization.

Biography

Dr. Davis is the Branch Head of the Hydrodynamics Radiation Branch at the Naval Research Laboratory. He has a broad background in Atomic and Plasma Physics with special emphasis in Atomic Collision Theory, Plasma Spectroscopy, and Radiation Transport Theory. His present activities include x-ray laser studies, broadband x-ray source development, and the theoretical investigation of dense plasma atomic physics phenomenon. Dr. Davis is a Fellow of the American Physical Society and Associate Editor of the Physics of Fluids and the Journal of Quantitative Spectroscopy and Radiative Transfer.

References

1. An excellent source of some recent advances in x-ray laser research can be found in the Journal De Physique, C6 (1986) which contains the Proceedings of an "International Colloquium on X-Ray Lasers."
2. J. Davis, Invited Talk, APS Annual Plasma Physics Meeting, Los Angeles, 1983.
3. M. Krishnan, T. Nash, P.D. Le Pell and R. Rodenburg, "Krypton on Krypton Z-Pinch, X-Ray Laser Experiments," Physics International Internal Rept. PIT-87-02 (1987).
4. J. Davis, R. Clark, J. Apruzese, and P. Kepple, Phys. Fluids 29, 1971 (1986).

Artifact Diamond
Its Allure and Significance

Max N. Yoder
Office of Naval Research

Abstract

While the preponderance of the mechanical, optical, and electronic properties of natural diamond have been known for over a decade, only recently has artifact diamond in technologically useful form factors become an exciting possibility. The advent of sacrificial, lattice matched crystalline substrates provides the basis not only for semiconducting applications of diamond, but for optical mirrors, lenses, and windows as well.

As a semiconductor, diamond has the highest resistivity, the highest saturated electron velocity, the highest thermal conductivity, the lowest dielectric constant, the highest dielectric strength, the greatest hardness, the largest bandgap and the smallest lattice constant of any material. It also has electron and hole mobilities greater than those of silicon. Its figure of merit as a microwave power amplifier is unexcelled and exceeds that of silicon by a multiplier of 8200. For integrated circuit potential, its thermal conductivity, saturated velocity, and dielectric constant also place it in the premier position (32 times that of silicon, 46 times that of Gas). Although not verified, its radiation hardness should also be unmatched.

Aside from its brilliant sparkle as a gemstone, there has been little use of diamond in the field of optics. Processing of the diamond surface now appears to be as simple as that of any other material — albeit with different techniques. In fact, it may be possible to etch diamond far more controllably (at economically viable rates) than any other material as the product of the etch is gaseous and the etched trough is self-cleaning. Other properties of diamond make it an ideal optical material. Among them are its unmatched thermal conductivity, its extremely low absorption loss above 228 nanometers, and unmatched Young's modulus, Poisson's ratio, tensile strength, hardness, thermal shock, and modulus of elasticity. If the recently-found mechanisms by which erbium impurities in III-V junctions can be made to "lase" are indeed applicable to indirect gap semiconductors, then even efficient diamond lasers at attractive portions of the spectrum become a distinct possibility.

Background

Although diamond has been known for centuries, it was the advent of X-rays that permitted its crystalline structure to become known in the second decade of the present century. The father and son Bragg duo used X-ray diffraction to show that diamond had a cubic structure and a lattice constant of 3.56 Angstroms. With tetrahedral bonding, the nearest neighbor distance is 1.53 Angstroms and at the centerpoint the electron density is approximately 1.59 electrons per square Angstrom! Although the covalently bonded diamond crystal exhibits a very open lattice, the presence of an interstitial impurity atom, a misplaced carbon atom, or a vacancy leads to a considerable change in the electron density and to lattice distortion.

Characterization

With an electronic bandgap of 5.45 electron volts, diamond should exhibit no optical absorptions within the visible spectrum as its absorption edge should be 2250 Angstroms. Although many water clear gemstones are found in nature, there are also those of yellow, blue, green, pink, mauve, and black. Clearly nature has placed electronic absorption levels within the bandgap. It was these in-gap absorption levels that led diamonds to be broadly classified as type 1 or type 2. If the specimens demonstrated a sharp increase in absorption at wavelengths shorter than 2250 Angstroms and there was negligible absorption at wavelengths longer than 3000 Angstroms, they were classified as being type 2. Type 2 diamonds exhibit very little visible fluorescence under moderate ultra violet or ionizing illumination. Under intense ionizing radiation, even type 2 diamonds, will exhibit luminescence in the blue region. Although ultraviolet emission has been seen, it is very rare. In type 2 diamonds, the response to radiation near to but below the bandgap is generally that of its response to radiation of much longer wavelengths. In this case the dielectric constant throughout the visible spectrum is equal to the static dielectric constant (5.76) or the square of the index of refraction. Type 2 diamonds are further subdivided as A or B with the A group having a very sharp and temperature independent absorption cut off (they are P-type semiconductors) and the B group having a broader and temperature dependent absorption cut off. Type 1 diamonds exhibit significant absorption at wavelengths of 3000 Angstroms or longer. Exception for their tribological use as abrasives or cutting tools, they have little commercial usefulness. Although diamond is monatomic and non-polar, even the best of natural diamonds exhibit some infrared absorption centered at 7.8 micrometers. Even then, its absorption is approximately 4 order of magnitude less than that of competing materials as shown in Figure 1.[1]

Figure 1

Optical absorption in diamond and other materials.

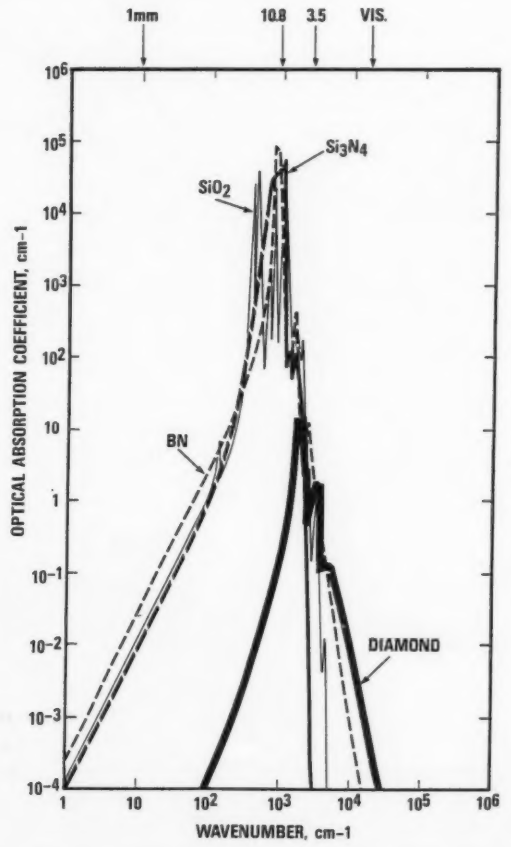

Mirrors, Lenses, and Coatings

Figure 1 compares the optical absorption of diamond with several competing materials for optical lenses and windows. Although not shown in the figure, diamond also exhibits approximately four orders of magnitude less peak absorption than do magnesium difluoride, yttrium oxide, and zinc selenide. For use with high intensity optical beams such as generated by free electron lasers, diamond has another unmatched attribute; its thermal conductivity is unexcelled. Thus even if appreciable energy is absorbed, the absorbed energy can be readily dissipated to the edge of the diamond. As such, optical beams exhibiting power densities greater than 10^6 Watts/cm^2 can be transmitted by diamond windows.[2]

Liquid etches, even at high temperatures, are well known to be ineffective in etching diamond. While atomic oxygen is known to attack diamond, it is not an efficient etch. Using a combination of energetic ions and a physisorbed, oxygen-containing gas, Geis has shown that the diamond surface can be etched as easily as that of any other semiconductor.[3] Not only has he been able to create etch troughs ten time deeper than the remaining diamond pillars are wide, the residual effluent is gaseous and the trough bottoms are self-cleaning! The feasibility of a diamond Fresnel lens is thus established. Using special high power laser processing techniques, Geis has also demonstrated that diamond windows can be fabricated as optical polarizers giving extinction ratios in excess of 15:1 at temperatures as high as 1400 Celsius.[4]

While it is difficult to conceive of the use of natural diamonds to protect optical mirrors, lenses, and windows made of other materials, the advent of synthetic diamond engenders the optical engineer with better approaches to sys-

tems design. Not only can the underlying optical material be protected against microparticle abrasion by virtue of the unmatched hardness of diamond (9000 kG/mm^2), but its extremely high surface energy (as high as 9400 ergs/cm^2) protects it from many (including biological) adherents — virtually nothing (excepting hydrogen) wets diamond. To improve the threshold of high power optical damage to silicon windows, a consortium of investigators from Crystallume, NASA Langley Research Center, and Old Dominion University investigated synthetic diamond overcoatings.[5] They used the thermal stress parameter to motivate their work. It is proportional to tensile fracture strength, thermal conductivity, thermal coefficient of expansion, and elastic modulus — in each of which the properties of diamond are unexceeded. The measured threshold of single pulse 1.06 micrometer illuminating damage ranged from a low of 5.97 J/cm^2 to a high of 12.43 J/cm^2. Comparisons of the thermal stress parameter of diamond with that of other optical materials is shown in Figure 2.

Electronically Active Diamond

Virtually all of the electronics properties of diamond are unexcelled excepting that of electron mobility. Even then, its mobility exceeds that of silicon. With very high charge carrier mobilities and velocities, diamond is expected to exhibit extremely fast electronic devices capable of operating with very large voltage excursions, at very high temperatures, and with high immunity to radiation damage.[6] Unfortunately, diamond is an indirect bandgap semiconductor and it is well known that injection lasers fabricated with indirect bandgap materials have not been successful. Diamond, however, affords a new approach. With its extremely large forbidden bandgap, there exists the possibility that many elements of the periodic table may have optical transition energies therein, as blue emission and even externally pumped lasing is well known in diamond.[7] In recent years, charge carrier pumping of impurities in more common semiconductors has produced emission and even single mode lasing.[8,9] Using similar techniques it is feasible that diamond can be internally pumped by forward biasing a diamond junction or, more plausibly, a heterojunction of boron nitride on diamond. Since diamond is a column IV semiconductor, a valence 3 rare earth impurity could serve as the acceptor material immediately inside the P side of such a junction and possess a very large capture cross section of "pump" electrons. Figure 3a illustrates such a rare earth atoms shown as A3+ before forward bias while figure 3B illustrates a possible electron and optical transition after application of the forward bias. In this illustration 4f transitions of rare earth atoms are shown, but 2d transitions of the transition metals impurity atoms may also be considered. Figure 4 illustrates transition levels from impurity atoms having energy levels just within the conduction and valence bands. While less probably than those transition shown in Figure 3, they are possible. Finally, optical transitions from impurity levels just within the conduction band to energy levels within the same ion, but within the diamond bandgap can not be ignored. Thus it is conceivable that a diamond injection laser could be engineered to emit at virtually any wavelength from the infrared to the ultra violet.

Summary

The combination of this tensile strength, unexcelled thermal conductivity, low optical absorption, very large bandgap, appropriate Young's modulus and Poisson's ratio, and recent advances in its synthesis render it an ideal candidate for many optical applications.

Figure 2

Thermal stress parameters of diamond and other materials.

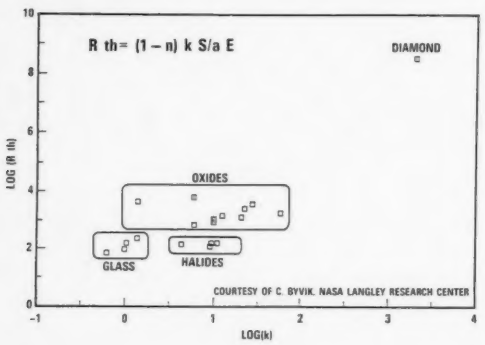

Figure 3

Intra ion energy level transitions in diamond. (a) before forward bias, (b) after bias pulse

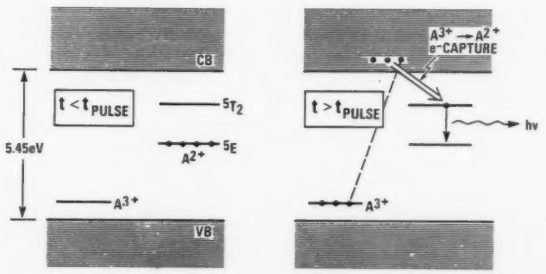

Biography

Mr. Max Yoder is an electronics engineer with the Solid State Electronics Branch of the Office of Naval Research where he supervises programs in semiconductor materials, monolithic microwave integrated circuits, gigabit logic, new electronic device structures, and electromagnetic system applications. He has published and presented many papers in these fields of solid state materials. He is a pioneer in the development of research programs for monolithic microwave devices in the U.S. Currently he manages at ONR the new research program in diamond semiconductor technology.

Figure 4

Bandgap magnitude intra ion energy transitions

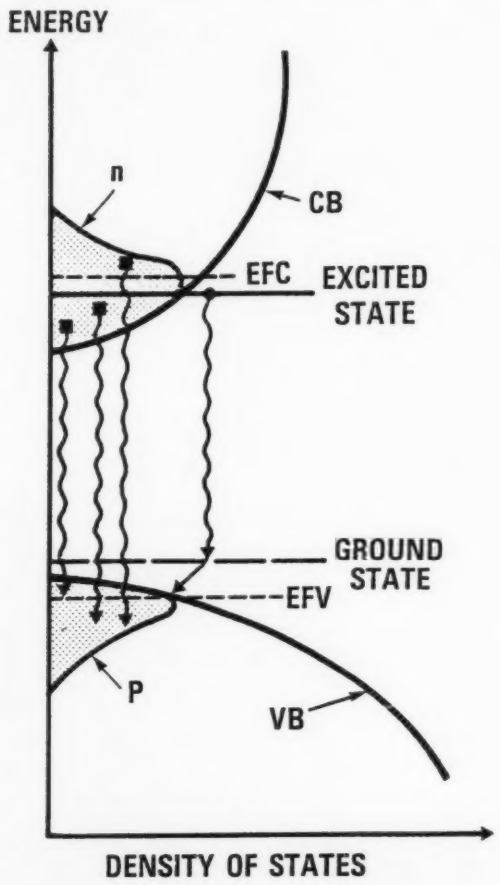

References

1. Data for Figure 1 supplied by R. Schwartz of the Naval Weapons Center.

2. J. R. Seitz, "Laser systems with diamond optical elements", U. S. Patent 3,895,313 15 July 1975

3. M. W. Geis, presented at the 1986 S.D.I.O./IST – ONR Diamond Technology Initiative Seminar, Durham, N.C. 17 July 1986 (unpublished).

4. M. W. Geis, "Electrical and optical properties of diamond interfaces", Proceedings, Third Annual SDIO/IST-ONR Diamond Technology Symposium, Crystal City, VA 12-14 July (1988), Paper W15

5. S. Albin, A. Cropper, L. Watkins, C. Byvik, A. Buoncristiani, K.Ravi, and S. Yokota, "Diamond films for laser optics", Paper Th4 Book of Abstracts, SDIO/IST-ONR Diamond Technology Symposium, 12-14 July 1988, Crystal City, VA

6. M. N. Yoder, "Synthetic diamond, its properties and synthesis", Mat. Res. Soc. Symp. Proc. 97, 315-326 (1987)

7. S. Rand and L. DeShazer, "Visible color-centered laser in diamond", Optics Lett. 10(10) 481-483 (1985)

8. P. Klein, J. Furneaux, and R. Henry, "Time-dependant photoluminescence of InP:Fe", Phys. Rev. B 29(4), 1947-1961 (1984)

9. W. Tsang and R. Logan, "Observation of enhanced single longitudinal mode operation in 1.5 micron GaInAsP erbium-doped semiconductor injection lasters", Appl. Phys. Lett. 49(25) 1686-1688 (1986).

The Oxygen Heat Engine Based On Solid Electrolytes

A. V. Joshi, N. Weber, & J. Nachlas
Ceramatec Inc.
Salt Lake City, Utah

Abstract

The oxygen heat engine, based on solid state ceramic oxygen ion conductors like ZrO_2 and Bi_2O_3, is a promising thermoelectric energy conversion concept being developed at Ceramatec, Inc. The device converts heat to electricity directly, at high efficiency. The device utilizes thermal energy from sources such as solar concentrators, and expands oxygen gas across a ZrO_2 ceramic membrane at 900°C or greater and compresses the gas through Bi_2O_3 membrane at about 500°C; electricity is generated electrochemically across the ceramic membranes. The actual efficiency under load is expected to exceed 20. Several unique features such as the absence of moving parts, low mass, compactness and modularity, high efficiency, and simplicity of the system make this concept very attractive for space platform and satellite applications.

In a preliminary research and development effort sponsored by ONR/SDIO, the feasibility of this novel concept has been established and a bench scale heat engine has been successfully built and tested. For realistic commercial development of such a device, additional engineering is required. Such an effort would involve further development in the area of electrode/electrolyte systems that are durable, efficient, and withstand the operating temperatures. Additionally, work towards integrating sub-systems to provide a multi mega-watt power system capable of delivering useful power, with the high integrity necessary for critical mission requirements, is required. Such improvements have been made in recent technology developments of high power solid oxide fuel cells.

This article describes the concept of the oxygen heat engine. Recently acquired experimental data that demonstrates "proof of concept" are described. The advantages over present state-of-the-art technologies are pointed out. Future directions for research and development are discussed.

Introduction

Current space vehicles and platforms are generally powered by solar photo-voltaic generation systems coupled with storage batteries. These systems offer adequate power for satellites requiring relatively low power levels; typically about 10KWe/- operation. Future space power applications, however, demand much greater power due to different mission requirements.Tomorrow's space platforms are envisioned to require 300 KWe or greater by the mid to late 1990s; some will periodically consume many megawatt-hours of energy.[1] Such space platforms will include manned space stations, communication stations, surveillance platforms and defensive weapons. Clearly future space power needs are several orders of magnitude greater than what can be effectively delivered by current technologies. The challenge is to explore new power technologies that will meet the projected power needs. A potential solution is the use of solar or nuclear power based heat engine systems.

About twenty years ago, scientists at the Ford Motor Company Scientific Laboratory conceived the idea of producing electric power from a thermally regenerative electrochemical system called the sodium heat engine (SHE), based on a sodium ion conducting solid electrolyte.[2] This invention generated a lot of interest in the scientific community due to the significant advantage offered by solid electrolyte technology. The advantages, over current state-of-the-art technology, are no moving parts, modularity, compactness and light weight, and high system efficiency.

In pursuit of these advantages, Ceramatec scientists conceived of a solid electrolyte energy conversion device based on an oxygen ion conducting solid electrolyte. This device, an oxygen heat engine (OHE), offers some advantages over the SHE. In the following sections, the working principle of the oxygen heat engine is explained. The projected performance of this device is compared to the SHE, and preliminary

Figure 1

Ceramatec's oxygen generators based on zirconia tubular design are shown in the photograph. Ceramatec demonstrated over 5,000 hrs. of continuous high efficiency performance through these generators. Model A is 15 liters/hr. capacity unit, while Model B is 3 liters/hr. capacity unit.

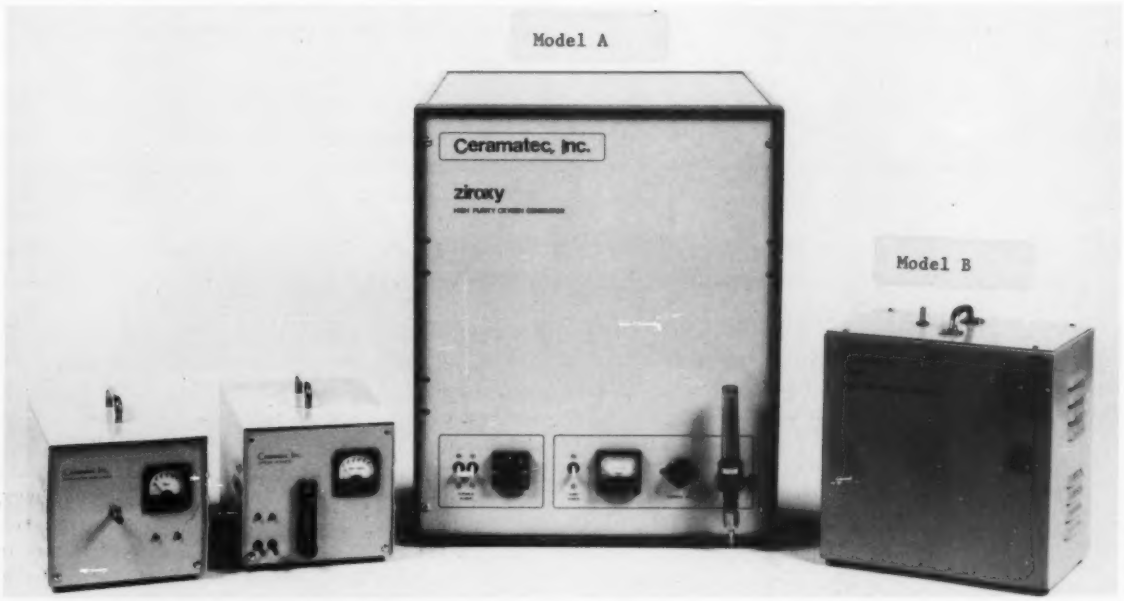

laboratory performance data are described. Finally the applicability of the oxygen heat engine as a potential power source for future space power applications is discussed.

The Oxygen Heat Engine

Basic Concept

The critical materials that make the operation of this novel technology possible belong to a class of materials called solid electrolytes. These materials have the unique property of being able to transport ions rather than electrons through their crystal structure. Zirconia (ZrO_2), and bismuth oxide (Bi_2O_3) are examples of oxygen ion conducting solid electrolytes.

Although the concept of using a ZrO_2 based solid electrolyte ceramic for pumping oxygen and for an oxygen heat engine has been around over a decade[3,6] the first practical small prototype, using single tube cells, was built and tested by Ceramatec in 1982 to develop and evaluate an efficient electrolyte/electrode system. The initial experiments in 1982 at Ceramatec on ZrO_2-based tubular configurations demonstrated the concept but unfortunately excessive power losses were experienced due to electrode/-electrolyte deficiencies. In 1984, Ceramatec developed a novel type of electrode/electrolyte system which resulted in an order of magnitude lower power consumption for the zirconia oxygen generator. With this development, the oxygen ion conducting solid electrolyte process became attractive in terms of commercially viable oxygen pumping devices.

In 1985 Ceramatec built many small prototype tubular oxygen generators with capacities ranging between 1/2 liter and 10 liters/h of oxygen flow. These prototypes demonstrated over 5,000 hours of continuous, efficient performance under current densities exceeding 100 mA/cm^2. A photograph showing these devices is given in Figure 1.

In Ceramatec's oxygen heat engine, gaseous oxygen is expanded at a high temperature across a ZrO_2 membrane and compressed at a lower temperature across a Bi_2O_3 membrane, much like a conventional heat engine. The use of ZrO_2 for electrochemical compression at low temperature is not appropriate because the conductivity of ZrO_2 at 500-600°C is too low to achieve any useful power density. This fact was recognized by Ruka & Weissbart[6] who patented the use of a ZrO_2 membrane only for the high temperature expander in an oxygen heat engine. They did not recommend the use of a ZrO_2 membrane for the low temperature compressor but instead suggested that the compressor might be "any of the well known mechanical devices for compressing gases". It would appear that an all electrochemical device without any moving parts using oxygen as the working fluid has been undeveloped for want of an efficient oxygen ion conductive electrolyte/electrode to serve as an electrochemical compressor at temperatures low enough so that (T_2-T_1) is sufficiently large. The recent developments of high oxygen ion conductivity in modified Bi_2O_3 electrolyte materials.[7-12] at temperatures as low as 500°C presented an opportunity to use these materials for an electrochemical compressor. Ceramatec scientists proposed this concept to SDIO and it is illustrated in Figure 2. As shown in Figure 2, oxygen gas is expanded through a ZrO_2 membrane at perhaps 1000-1200°C (T_1) and compressed through a modified Bi_2O_33 membrane at 500-600°C (T_1). During operation, oxygen at a high pressure P_2 is expanded electrochemically and isothermally to pressure P_1. This EMF at zero current can be expressed in terms of Nernst equation.

Figure 2

Schematic diagram of electromechanical heat engine based on solid oxygen ion conductors.

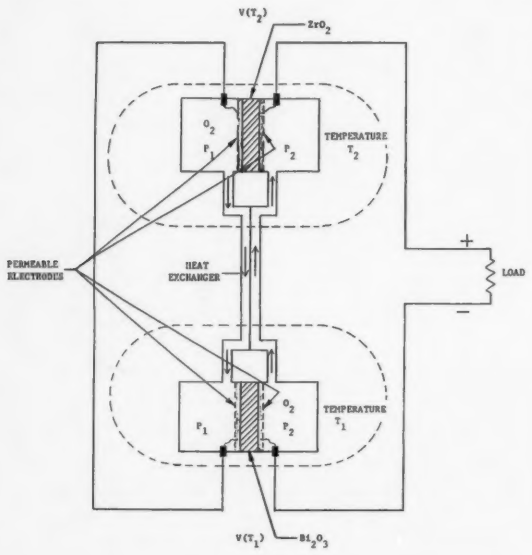

$$V = \frac{RT}{4F} \ln\left(\frac{P_2}{P_1}\right) \qquad (1)$$

where R = gas constant

F = Faraday constant

Part of this output voltage from this cell is used to drive an electrochemically similar isothermal Bi_2O_3 based membrane compressor cell at a lower temperature. The net output voltage V_o is the difference, in the Nernst potentials at T_2 and T_1 i.e.

$$V_o = (RT_2/4F) \ln (P_2/P_1) - (RT_1/4F) \ln (P_2/P_1)$$
$$= [R (T_20-T_201)/4F] \ln (P_2/P_1)$$

Figure 3

Heat engine cycle comparison

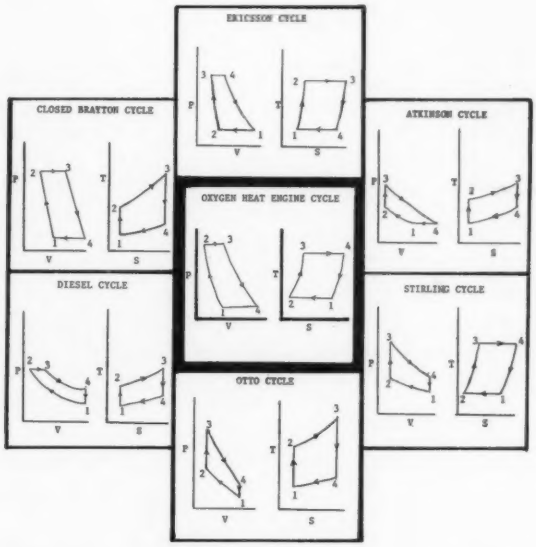

The molar heat of expansion, q, abstracted from the reservoir at T_2 is $(RT_2)\ lnP_2/P_1$. The theoretical maximum efficiency E is just the ratio of net work out (4 FV)/heat in at T_2 per mole of fluid transferred.

$$E = 4FV_o/q = (T_2-T_1)/T_2 \qquad (2)$$

The cycle also includes the sensible heat absorbed and given up as oxygen circulates between the two thermal reservoirs. If we imagine a perfectly efficient gas-gas heat exchanger for the two fluid streams, then the two terms of equal magnitude and opposite sign cancel out in the expression for efficiency.

As with any heat engine, the larger the T_2-T_1, the larger is the efficiency. The upper practical temperature limit for this oxygen based device is governed by electrode stability. The practical lower temperature is governed primarily by electrolyte conductivity, but also by other thermally activated processes associated with mass and charge transfer at interfaces. In Figure 3, P-V and T-S diagrams are shown for the oxygen heat engine cycle. Shown also for comparison are corresponding diagrams for several other gas cycles. The similarity between the OHE cycle and the Ericsson cycle is evident. According to Karlekar[12] a gas turbine plant with reheat, intercooling and regeneration executes a cycle that is close to the Ericsson cycle.

How Does Oxygen Heat Engine Compare With Sodium Heat Engine?

The oxygen thermoelectric generator has many attractive features in common with the sodium heat engine for SDI applications. One of the clearest potential advantages of this solid electrolyte based electrochemical device is that it can be very small and light weight. There are no moving parts except for slowly circulating fluid. Modular designs are possible allowing for system expansion without major redesign or scrapping of existing hardware. Smaller generators will be equally economically feasible. The cell is simple, rugged and may be insensitive to ionizing radiations. Efficiency will be virtually independent of size. The nature of this electrochemical technology allows significant design flexibility to meet any specific end use requirements.

Compared to the sodium heat engine (SHE) for example, the oxygen heat engine has some advantages. A heat exchange between input and output legs of the high temperature reservoir is easier to accomplish. Because the working fluid is an insulator, achieving an electrical series system to minimize lead thermal conduction and resistive losses will be much easier. A gaseous fluid system will also be less sensitive to thermal shock and acceleration forces. Finally, the relative ease of working with oxygen over sodium may reflect in capital and maintenance cost advantages. The comparison also reveals some disadvantages. Two membranes are required in the cycle instead of one, and the oxygen solid electrolytes, even at high temperature, are inferior in conductivity to sodium beta"-alumina. The working fluid cannot serve as a conducting lead, and four permeable electrodes are required instead of one. The output voltage of the expander cell is smaller by a factor of four for a given pressure ratio since four electrons are required to transfer one mole of fluid compared to one in the case of sodium.

An analysis of the oxygen fluid device will undoubtedly show maximum efficiencies at a lower electrolyte area for specific power levels than are found for the SHE. Available from previous studies on the SHE, the analytical and theoretical machinery for a detailed calculation of thermal conversion efficiencies in the oxygen system is ready to be put in motion.

Experimental Results

The program at Ceramatec has focussed upon materials development, fabrication process development, device set up and assembly, and performance testing and evaluation.

The major thrust of our initial efforts was directed towards the understanding, synthesis and development of low temperature Bi_2O_3 based membranes, as well as efficient high

Figure 4

Oxygen ion conducting solid electrolyte tubes with various compositions.

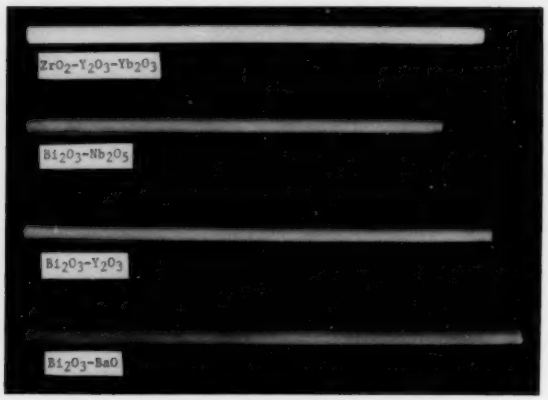

temperature and low temperature electrode systems. While the high temperature electrolyte membrane has been widely studied, the low temperature bismuth oxide membrane needed development especially due to the thermodynamic instability exhibited by these electrolytes under actual operating conditions.

As pointed out by several investigators[7-12] Bi_2O_33 has four polymorphs α, ρ, γ, & δ Bi_2O_3. The δ phase exists between 1000 K and 1097 K. This phase has an FCC defect fluorite structure and was found to have the highest oxygen ion conductivity with a low activation energy. Attempts to stabilize the δ phase at lower temperatures, under non-electrochemical conditions, were successfully made by various scientists and are well documented in the literature.[6-11] A successful oxygen heat engine device must not only contain a high conductivity phase Bi_2O_3 electrolyte membrane for the efficient compressing of O_2 at low temperatures, but it must exhibit exceptional durability and phase stability in an oxygen/vacuum environment and under an oxygen pumping mode. We have carried out stability studies on these materials under actual pumping modes. We will now describe the

Figure 5

Schematic of bielement cell Bench Scale Apparatus

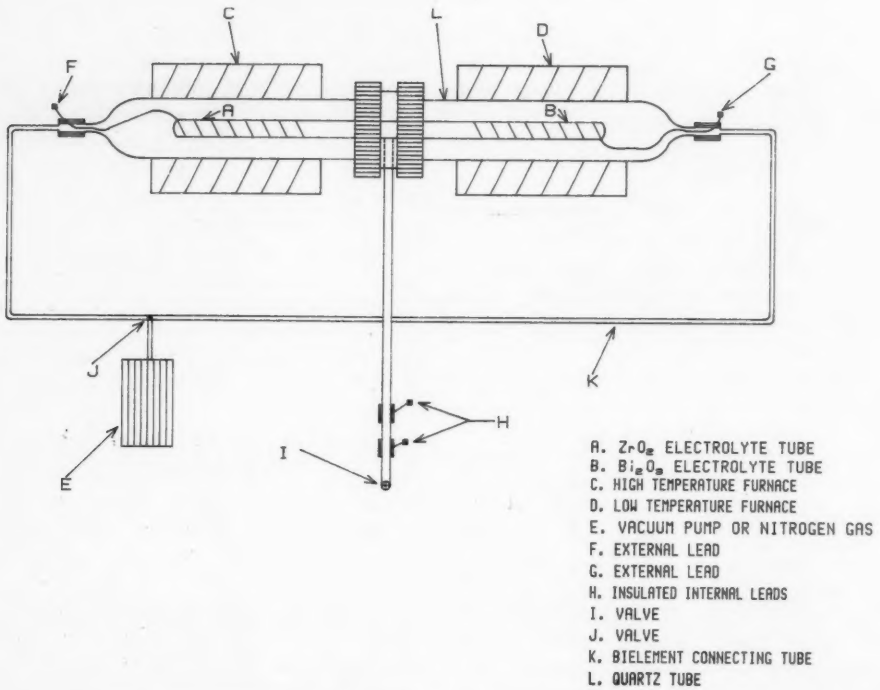

Figure 6

Stability Studies for 2 Electrolyte Systems Current Decay as a Function of Time Under a Constant Applied Potential of 0.2 Volts at 700 C

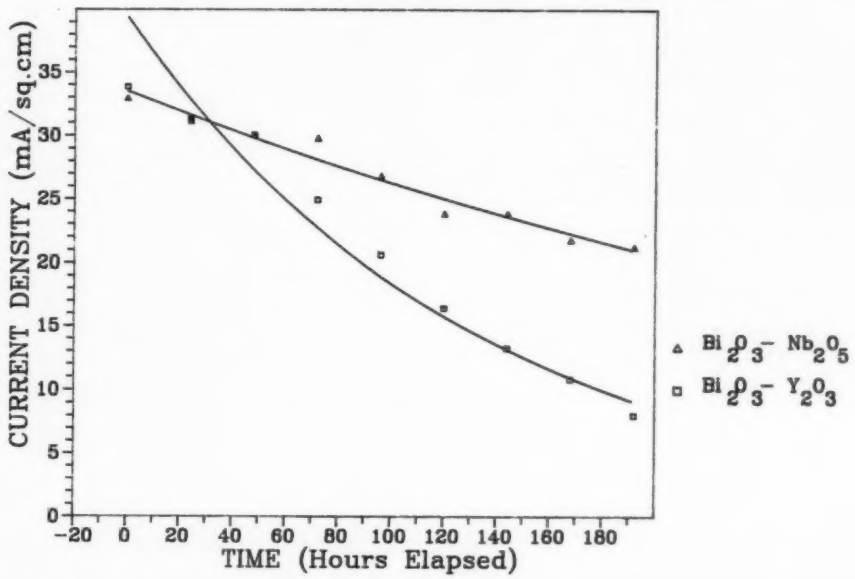

fabrication of components, test apparatus as well as experimental results obtained on a bench scale bi-element heat engine device.

Fabrication.

Bi_2O_3 Electrolytes: Bi_2O_3 electrolyte tubes stabilized with various aliovalent dopants such as Ba, Pb, Y, and Nb nominally 12mm dia, 25cm long and 1.1mm wall were fabricated at Ceramatec by cold isostatic pressing followed by high temperature sintering. The processing conditions were studied to achieve concentric, straight axis, low porosity (95 theoretical density) gas impermeable tubes. These tubes are shown in Figure 4. The processing conditions were optimized to produce these tubes.

ZrO_2 electrolytes: Stabilized zirconia tubes nominally 25cm long and 1cm dia were fabricated by the usual procedure of cold isostatic pressing followed by sintering at high temperature of 1600°C for 2 hours.

Electrodes: For initial experiments, various noble metals as well as Ceramatec's proprietary electrodes were used with Bi_2O_3 electrolyte based on our prior extensive experience with electrochemical devices such as oxygen pumps. These materials are good electrodes for feasibility testing of the concept for operation up to 500 hours at temperatures below 700°C. These electrodes were applied by painting the electrolyte tubes (both ZrO_2 as well as Bi_2O_3) using a nylon brush, followed by baking at 700°C to 900°C to drive off the organic binders in the electrode slurries.

Bench Scale Device: A simple tubular bench scale bi-element device (Figure 5) containing a ZrO_2 ceramic expander and a Bi_2O_3 based electrochemical compressor was fabricated and used for feasibility demonstration- Parametric experiments varying the composition of the Bi_2O_33 compressor cell and its temperature, while keeping the high temperature ZrO_2 cell at a constant temperature of 900°C were conducted using this bench scale apparatus. Stability and device performance characteristics were studied and are reported below.

Stability of Bi_2O_3 Electrolytes

As pointed out previously, building a successful oxygen heat engine device depends critically on utilizing the high conductivity phase of Bi_2O_3 electrolyte that must be stable under operating conditions. Stability tests under dynamic electrochemical conditions were carried out on Bi_2O_3 tubes with the various dopants as outlined below. Experiments consisted of applying 0.2 volts D.C. on the respective electrolyte tube fitted with electronically conducting electrodes which were kept heated at 700°C. The current resulting from the

applied potential is directly related to amount of oxygen being pumped through the solid electrolyte membrane. As an example, 1 ampere of current corresponds to 3.5 cm^3/min. of oxygen gas transport through the electrolyte. The current was monitored as a function of time over two hundred hours. Our experiments indicate that certain compositions of Bi_2O_3, although possessing high conductivity, were unstable under (oxygen pumping) testing conditions. For example, despite the fact that the ionic conductivity of $Bi_2O_3(Y_2O_3)$ compositions is high at temperatures as low as 600°C our experiments indicate that these materials are not useful as solid electrolytes under the application of voltage in air environment. We have found that Y_2O_3 doped Bi_2O_3 composition decomposes into the lower conductivity rhombohedral and monoclinic phases. Furthermore, it was found that significant grain growth occurred in these solid electrolyte tubes under applied potential conditions. It appears from our experiments that the phase diagram of $Bi_2O_3.Y_2O_3$ as given by Datta and Mahan[14] is insufficient to interpret the behavior under applied D.C. current conditions. Some doped Bi_2O_3 compositions (such as Group II element doped compositions) exhibit a rapid decay in current carrying capacity within 24 hours. No further investigations were carried out on such compositions due to the severe degradation of these electrolytes. The aim of our detailed investigations was to identify those Bi_2O_3 compositions that underwent negligible degradation and hence led to stable device performance. To illustrate device performance decay, two compositions of doped Bi_2O_3 were investigated for current density measurements as a function of time under an applied potential of 0.2V. The current decay curves are shown in Figure 6. Preliminary analysis indicated that the current decay in these materials may have occurred due to degradation in electrode/electrolyte interface as well as electrolyte instability. Further experiments are in progress to characterize the electrode/electrolyte interface and identify electrochemically stable Bi_2O_3 electrolyte materials. Our recent laboratory findings show promise for the development of such stable materials.

Bench Scale Test Results

As described previously, the high temperature element consisted of a stabilized ZrO_2 tube with electronically conducting electrodes, while the low temperature cell was a circular shape of stabilized Bi_2O_3 material. In order to simplify the analysis of the data, the high temperature cell was always

Figure 7

Power -vs- Load Characteristics for Thermoelectric Devices Utilizing Various Bismuth Oxide Compositions (High Temperature Zirconia Expander cell is Maintained at 900 C)

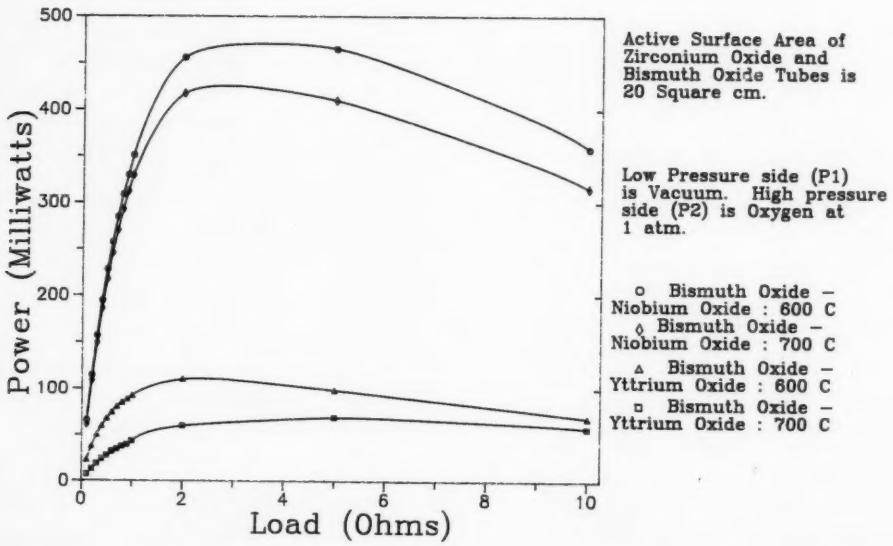
Power (Milliwatts)
Load (Ohms)
0
100
200
300
400
500
0
2
4
6
8
10
Active Surface Area of Zirconium Oxide and Bismuth Oxide Tubes is 20 Square cm.
Low Pressure side (P1) is Vacuum. High pressure side (P2) is Oxygen at 1 atm.
o Bismuth Oxide – Niobium Oxide : 600 C
◊ Bismuth Oxide – Niobium Oxide : 700 C
Δ Bismuth Oxide – Yttrium Oxide : 600 C
□ Bismuth Oxide – Yttrium Oxide : 700 C

kept at 900°C and the temperature of the low temperature cell was varied. Two compositions of Bi_2O_3 solid electrolyte were studied, namely $Bi_2O_3(Y_2O_3)$ and $Bi_2O_3(Nb_2O_5)$.

Figure 7 shows the power v. load characteristics for Y_2O_3 stabilized as well as Nb_2O_5 stabilized electrolytes at two different temperatures. These data clearly indicate that $Bi_2O_3.Nb_2O_5$ solid electrolyte is superior to $Bi_2O_3.Y_2O_3$ solid electrolyte in terms of power density. The voltage vs. current curves for both the electrolytes are shown in Figure 8. Further studies are underway to characterize other stabilized Bi_2O_3 based materials for use in the low temperature compressor in terms of their stability and influence on the power output of the heat engine.

Future Developments

The current program has clearly demonstrated the concept of oxygen based thermoelectric electrochemical conversion utilizing zirconia as a high temperature expander and Bi_2O_3 as a low temperature compressor. However, for achieving the high power densities, the performance characteristics have to be optimized. This will be achieved through improvements in understanding of the electrode and electrolyte materials as well as the fundamental charge transfer processes that occur at the electrode/electrolyte interface. Theoretical analysis of the heat engine with attention given to mass transport considerations will be conducted to further assess the performance characteristics.

Further development can also be made via design and fabrication technology refinements. Virtually all rapid advances occurring in the Solid Oxide Fuel Cells (SOFC) technology (Ceramatec's Planar Geometry SOFC and Argonne National Laboratory's Monolithic SOFC design) can be applied to oxygen heat engine. With such thin film designs and efficient electrodes, power densities of over 1000 mW/cm^2 are possible.

The program has also demonstrated that for commercial viability of this device, further effort in the development of efficient, durable & stable electrode/electrolyte systems is required. For an electrochemical system based on ZrO_2 and Bi_2O_3 solid electrolytes, this entails safe, reliable, and efficient operation for a period of time in excess of 40,000 hrs at operating temperatures of 500-700°C for Bi_2O_3 and 1000-1200°C for ZrO_2 based electrochemical cells under 1 atmosphere of oxygen pressure and lower. When a durable and efficient electrode/electrolyte system is demonstrated, advanced engineering will be required. Efforts will then focus on design and economic issues to allow more complete and realistic assessment of the oxide ion solid electrolyte concept for thermoelectric power generation.

Figure 8

Voltage -vs- Current for various Low Temperature Solid Electrolyte Elements

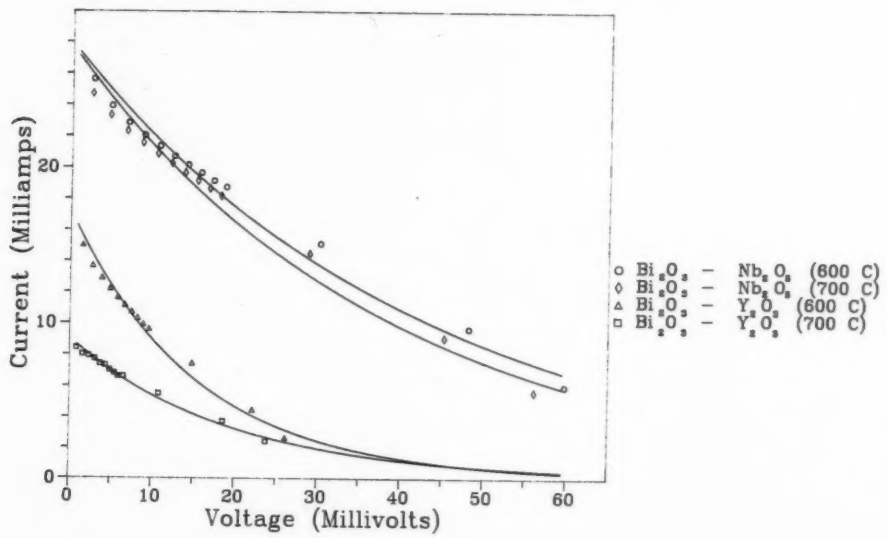

With the capability and experimental results acquired in the present program, we believe that oxygen ion conducting solid electrolyte approach offers unique opportunities and exciting possibilities for space power generation systems.

Acknowledgements

This work was funded by the Office of Naval Research under Contract N00014-86-C-0827. We are grateful to professor A. V. Virkar of the University of Utah, Dr. James Auborn of AT&T, and Mr. Jordan Diamond for their technical assistance and support.

Biographies

Dr. Ashok Joshi is Vice President of Cerion Systems Division at Ceramatec. He currently is directing the programs at Ceramatec on electrochemical systems including zirconia and Bi_2O_3-based oxygen heat engine, solid state battery electrolytes and several proprietary systems. Dr. Joshi is the author or co-author of over 15 technical papers and holds 10 US patents. He is a recognized expert in the technology and design of electrochemical systems.

Dr. Neill Weber is Corporate Fellow at Ceramatec. Prior to joining Ceramatec, he had a distinguished career for over 20 years at Ford Motor Company where he led technical efforts on designs and materials research on Alkali metal thermoelectric converter (AMTEC) cells. Recent activities included design and evaluation of experimental cells, analyses of system component design and selection of materials and experimental verification of electrode performance. Co-inventor of stabilized beta"-alumina, the AMTEC, and the Sodium Sulfur battery, he has conducted research in all aspects beta"-alumina of AMTEC materials, including the ionic and electromagnetic pump design, AMTEC electrode deposition and current collection systems. Dr. Weber is intentionally recognized as an expert in solid electrolyte processes and novel energy conversion and storage systems.

Mr. Jesse A. Nachlas joined Ceramatec in 1983 as a research scientist. He has carried out research and development work for commercial applications of solid state ionic conductors. His efforts have concentrated primarily on zirconia-based devices such as oxygen concentrators, oxygen sensors, and electrochemical decomposition of flue gas constituents. Other research activities have include crystal growth and ion exchange of beta"-alumina for phosphor applications. He also has experience in ceramic processing and fabrication of ionic and electronic conducing oxides.

References

1. J.G. Slaby, Transactions of Fourth Symposium on Space Nuclear Power Systems, Page 1, Jan. 12-16, 1987. Editors M.S. Elgenk M.D. Hoover.

2. J.T. Kummer and N. Weber, U.S. Patent 3,458,35 (1968).

3. D. Yuan & F. Kroger, J. Electrochem. Soc. 110, 594-600 (1969)

4. T.H. Etsell and S.N. Flengas, Chem. Revs. 70 339 (1970).

5. E.C. Subbarao & H.S. Maiti, Solid Electrolytes with Oxygen Ion Conduction, Solid State Ionics, 11 317-338 (1984).

6. R.J. Ruka & J. Weissbart, U.S. Patent 28, 792.

7. T. Takahashi and H. Iwahara, Mat. Res. Bull, 13, (1978) 1447.

8. J. A. Kilner and R.J. Brook, "A Study of Oxygen ION Conductivity in Doped Non-Stoichiometric Oxides". Solid State Ionics 237-252 (1982).

9. M.J. Verkerk, G.M.H. Van DeVelde and A.J. Bjurggreaf, "Structure and Ionic conductivity o Bi_2O_3 substituted with Lanthanide Oxides", J. Phys. Chem. Solids 43 1129-1136 (1982).

10. F. Honnart, J.C. Boivin, D. Thomas, an K.J. DeVries,"BismuthLead Oxide, A New Highly Conductive Oxygen Material", Solid State Ionics 9&10 921-924, (1983).

11. Wang Changzhen, Xu Xiuguang, and Li Baozheu, "Ionic and Electronic conduction of Oxygen Ion Conductors in the $Bi_2O_3HY_2O_3$ System", Solid State Ionics 13 135-140 (1984).

12. T. Suzuki, K. Kaka, S. Ukawa and Y. Dansui, "Low Temperature Performance of Thin Solid Electrolyte Cell Based on M_0O_3 doped Bi_2O_3", Solid State Ionics 1 237-239 (1984).

13. B.V. Karlekar, Thermodynamics for Engineers, Prentice-Hall Inc. N.J., (1983).

14. R.K. Datta and J. P. Mahan, Z. Anorg, Altg. Chem. 383 (3) 328 (1971).

Research Notes

A New Optoelectronic Semiconductor Switch – Optoelectronic semiconductor switches have received considerable attention, for use in high power switching. However a drawback of this device is that it requires a high power laser source operating for the entire duration of the current flow through the switch. A new concept being researched by Profs. K. Schoenbach and K. Lakdawala at Old Dominion University, offers promise to overcome this problem. The material used for switching is GaAs doped with deep level impurities such as copper. The switching mechanism utilizes the deep levels as intermediate energy levels for charge storage. The increase in conductivity is accomplished by electron ionization from deep centers and bound holes. The reduction in conductivity is obtained by hole ionization from excited centers and subsequent recombination of free electrons and holes. The entirely new and unique capability of this switch is that it uses photons to turn-on and turn-off the conductivity on command, but there is no radiation required to sustain it during the on-state. (Dr. Gabriel D. Roy, ONR)

Radiation-Hardened Non-Volatile Semiconductor Memory – Transistors with Silicon-Oxide-Nitride-Oxide-Silicon (SONOS) gate structures that can act as the memory elements for a Non-Volatile Semiconductor Memory (NVSM) have been demonstrated by Lehigh's Prof. Marvin White. The work, which was done under a contract entitled "Reliability of Small Geometry VLSI Devices for Microelectronics", is funded by SDIO and managed by ONR. The devices are rad-hard to at least 5 MRad total dose, and are capable of greater than 10^7 Write/erase cycles, greater than 10^{12} read cycles, and retention time greater than 1 year. The trapping kinetics must still be studied and modeled, but the results obtained thus far suggest that near term development is warranted. The potential impact lies in the use of these devices in large scale, reliable, rad-hard, NVSM arrays that are needed for a variety of DOD applications. The first use of this technology could be in the SDIO Boost Surveillance and Tracking System (BSTS) program. (Dr. A. Goodman, ONR)

Direction-Of-Arrival of Signals Using Radon Transforms – Professor R. L. Kashyap, an ONR contractor at Purdue, supported through SDI funds, has proposed a new procedure to estimate the directions-of-arrival of emitters. The procedure helps to locate the emitters from signals received by an array of sensors in an electronically disturbed and noisy environment. The two dimensional data is transformed into a set of one dimensional sequences by the Radon Transform and processed to locate the peaks of the two dimensional spatial spectrum by a robust technique. The procedure does not require any prior information about the source emitters and does not assume any model structure for the unknown colored noise. The algorithm is highly suitable for parallel processing. (Dr. R. N. Madan, ONR)

Reliability Predictions of VLSI Circuits – During a recent SDI/IST program review, Professor Hu of the University of California at Berkeley presented his latest research results on VLSI reliability. Since metal electromigration is one of the primary causes of failures for next generation VLSI devices, he has developed a model to predict the lifetime reliability based on AC stress testing. The model predicted that AC stress lifetime would be 10,000 times longer than DC stress lifetime. This prediction has recently been verified by laboratory experiments. The model improves the accuracy of prediction on the lifetime of VLSI thin-line metals by several orders of magnitude over the present predictions. He also presented some results on charge trapping and oxide breakdown in submicron VLSI devices, which are also reliability concerns. His research is a very important part of trying to improve the reliability of VLSI chips and systems, which are widely used in many Navy systems. (Dr. C. Lau, ONR)

Radiation-Harden Nonvolatile Computer Memory – One of the requirements for space-based electronic systems is radiation-harden nonvolatile memories. Professor M. White of Lehigh, under ONR/SDI/IST funding, is developing such in reliable, small VLSI devices. The new device called SONOS (Silicon Oxide Nitride Oxide Semiconductor), with a gate dielectric consisting of very thin multilayers of silicon oxide, silicon nitride, and silicon oxide. These SONOS devices have been shown to be resistant to radiation of over 1 Megrad, and can be used in nonvolatile memory applications with retention time well over 10 years. Together with radiation harden VHSIC technology, this SONOS technology when fully developed may prove to be extremely important to Navy's space-based memory-intensive satellite systems. (Dr. C. Lau, ONR)

New Compiler for Rapid Antenna Array Weight Design – Professor Steven Boyd, recipient of an ONR Young Investigator award (1985-88) at Stanford, has been investigating linerization of nonlinear circuits and systems. He has recently applied his techniques to computer aided design of antenna array weights. Antenna array weights are variable signal amplitude and phase angles assigned to each array

element that give an improved array beam pattern. Variable antenna element weights improves antenna performance in terms of desired mainlobe width, maximum side-lobe constraints, position of nulls, and percentage of bandwidth coverage.

His compiler translates these antenna specifications into a non-differentiable convex optimization problem and determines the feasibility of the specifications. If feasible, a computer program calculates the optimal weights needed to provide the desired antenna pattern. Many examples have been worked for planar, circular and parabolic antenna array geometries of up to 30 elements. The results have been substantially better than other computational methods. Dr. Boyd's work has generated considerable interest in the Navy with a NWC, China Lake collaborative effort in progress. (Dr. R. Madan, ONR)

ONR Scientific Officer is invited Speaker at IEE Conference in London – Dr. Gabriel D. Roy was an invited speaker at the Pulsed Power Conference sponsored by the Institution of Electrical Engineers, UK. The conference was held at the Savoy Place in London. Dr. Roy presented his paper on "High Power, High Repetition Rate Switches: An Overview", which was then published in the IEE Proceedings. While at UK, he visited the universities where US (SDIO/ONR) supported research programs are carried out. These were Aston University in Birmingham, Univ. of Kent in Canterbury, Univ. of Strathclyde in Glasgow and Univ. of St. Andrews in St. Andrews. The UK research focusses on surface breakdown phenomena in dielectrics and insulators, diagnostic development of surface breakdown and the impact of meteorites in space. He attended the annual program review of the SKI supported pulse power programs conducted at the ministry of Defence, London and was a special guest at Imperial College, London at the Executive Committee meeting of the UK Space Power Group.

Diamond Growth Speeds Up – Research Triangle Institute (RTI) with SDIO/ONR support, has demonstrated a method of growing diamond at very fast rates without the expenditure of excessive amounts of energy. The new method parallels one recently advanced by a group at AT&T Bell Laboratories and uses alternate cycle epitaxy wherein pure methane and molecular hydrogen are alternately applied to the growth surface — both in the presence of excited state helium. In this method it would appear that during the hydrogen portion of the cycle, the diamond copiously absorbs atomic hydrogen and effusively releases it to the growth surface during the methane portion of the cycle. In this manner there is effectively no boundary layer to inhibit the arrival of atomic hydrogen to the surface and growth rates of 50 to 100 times those of conventional low energy approaches are experienced.

While this method is expected to be applicable to the growth of single crystalline diamond for electronics use, the preliminary studies have all been conducted on polycrystalline material where it has a near term application in optics. Lenses, windows, and mirrors made of these films are expected to operate in the infra-rad, visible, and ultra violet portions of the spectrum where their optical losses are lower than those of competing materials and their ability to resist microparticle abrasion and scratching is unsurpassed.

With a coefficient of friction similar to that of Teflon, extremely hard diamond films are expected to provide durable and friction-resistant bearings. As a semiconductor material, diamond is superior to silicon or gallium arsenide for high power electronics applications. Workers within this field anticipate that within six years diamond films will be available for use as semiconductors at a cost equivalent to present gallium arsenide materials. As a semiconductor, diamond is unexcelled in virtually all of the properties which characterize semiconductors. Only in electron mobility is diamond inferior to gallium arsenide; however, it remains superior to silicon. Mobility is represented by the slope of the lines in the figure. The properties illustrated translate to a figure of merit for microwave power amplifiers that is 900 times that of gallium arsenide and 8000 times that of silicon. The ability of semiconducting diamond to operate at very high temperatures makes it an ideal candidate for use in monitoring jet engines and nuclear reactors. **(Dr. Max Yoder, ONR)**

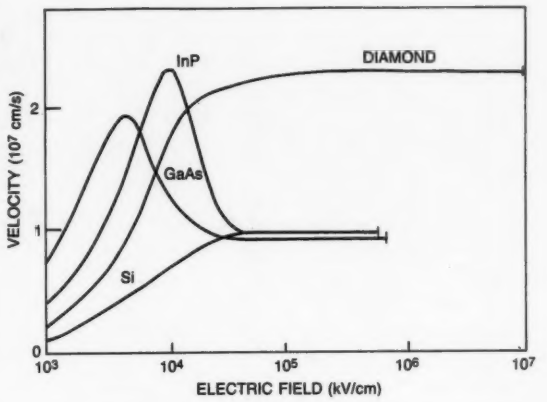

10 μm OF DIAMOND GROWTH ON (111) TEXTURED DIAMOND SEED

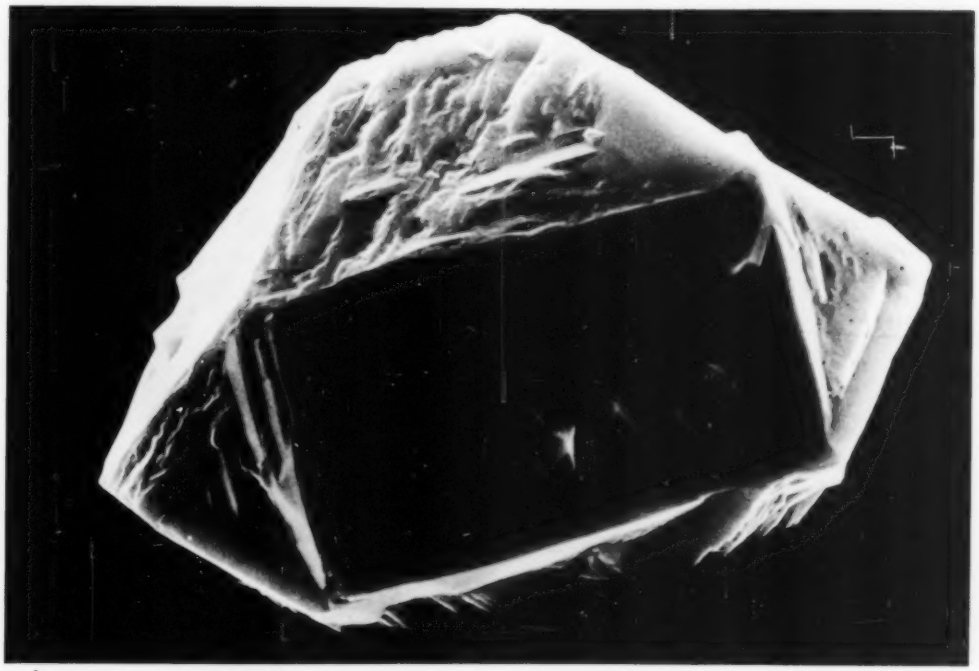

10 μm

DEPARTMENT OF THE NAVY
OFFICE OF NAVAL RESEARCH
ARLINGTON, VA 22217

OFFICIAL BUSINESS
PENALTY FOR PRIVATE USE, $300